SYNTHESIS, CHARACTERIZATION AND PHOTOPHYSICAL STUDY OF LOW DIMENSIONAL INORGANIC/ORGANIC MATERIALS

BY

SADHAN SAMANTA

A Thesis submitted to

VIDYASAGAR UNIVERSITY

For the Award of the degree of

DOCTOR OF PHILOSOPHY

(SCIENCE)

Department of Chemistry & Chemical Technology

Vidyasagar University

Paschim Medinipur

West Bengal

Pin-721102

2016

Dedicated

To

MY TEACHERS
&
FAMILY MEMBERS

Prof. Ajay Kumar Misra
Professor of Chemistry
Dept. of Chemistry & Chemical Tech.
Vidyasagar University
Midnapore (w) - 721102
ajaymsr@yahoo.co.in

CERTIFICATE

This is to certify that the research work presented in this thesis entitled, *"**SYNTHESIS, CHARACTERIZATION AND PHOTOPHYSICAL STUDY OF LOW DIMENSIONAL INORGANIC/ORGANIC MATERIALS**"* was carried out under my supervision in the Department of Chemistry & Chemical Technology, Vidyasagar University, Midnapore, W.B and is the bonafide record of work done by **Mr. Sadhan Samanta**. This work is original and has not been submitted for any other degree or diploma of this or any other University.

Date:

(Prof. Ajay Kumar Misra)
Research Guide

Department of Chemistry and Chemical Technology, Vidyasagar University, Midnapore-721102, INDIA
Phone: +91-3222-276554/276555/276557/276558 Extn. 437, Fax: +91-3222-275329

DECLARATION

*The research work embodied in this thesis entitled "**SYNTHESIS, CHARACTERIZATION AND PHOTOPHYSICAL STUDY OF LOW DIMENSIONAL INORGANIC/ORGANIC MATERIALS**" has been carried out by me under the supervision of Prof. Ajay Kumar Misra in the Department of Chemistry & Chemical Technology, Vidyasagar University, Midnapore, W.B. This work is original and no portion of the work has been submitted at this University or anywhere by me or any other person in part or full for any degree.*

Date: *(Sadhan Samanta)*

Acknowledgement

It is a great pleasure to express my gratitude to the persons who have provided me guidance, advice, support, accompany, inspiration etc. in the journey of my Ph.D life. The first person I would like to express my cordial gratitude is my Ph.D guide **Prof. Ajay Kumar Misra**, for his splendid guidance, authentic supervision, advice, technical discussion, clarification, support, constant encouragement and affection throughout my Ph.D life. I owe him lots of gratitude and respect for introducing me to such an interesting and advanced field of research. It was a worthy experience to work with and learn various things from him both as a scientist and as a human being. He is an excellent and ideal teacher. It was a great honour for me to work with him.

I express my deep sense of gratitude to Hon'ble Vice chancellor, Prof. Ranjan Chakraborty and Registrar, Dr. Jayanta Kishore Nandi for providing various facilities. I convey my deep regards to my teachers Prof. Bhudeb Ranjan De, Prof. Sayed Sirajul Islam, Prof. Braja Gopal Bag, Dr. Sudipta Dalai, Dr. Sumita Roy, Dr. Subal Chandra Manna, Dr. Moidul Hossain, and Prof. Amiya Kumar Panda for their moral support, affection and encouragement throughout my research life.

I would like to thank my lab mates Dr. Harekrishna Bar, Dr. Priyanka Sarkar, Dr. Sankar Prasad De, Dr. Gobinda Prasad Sahoo, Dr. Dipak Kumar Bhui, Dr. Sankarlal Ash, Dr. Hasibul Beg, Dr. Santanu Pyne, Mr. Ashim Maity, Mr. Debasish Das, Mr. Partha Sarathi Sheet, Mrs. Prativa Mazumdar, Mr. Milan Shyamal, Mr. Samir Maity, Mr. Debkumar Mandal and Mr. Rakesh Maity for their generous assistance in each moment. I wish to thank my senior scholars of the department for their very helpful behaviour throughout my research career.

I am also thankful to Mr. Bibhas Panda, Mr. Subrata Hazra and Mr. Ranjit Majhi in our department for their cooperation.

Above all I feel a deep sense of gratitude for my loving father, Sri Purna Chandra Samanta, and my sweet mother, Smt. Arati Samanta, who are always proud of me. Especially, I owe my

success to my beloved wife Mrs. Sujata Karan (Samanta). I am also thankful to all of my family members and relatives. Without their constant support and inspiration it would have been impossible for me to be where I am at present.

I also wish to express special thanks to colleagues and the authority of Dibakarpur High School (H.S.) for encouragement and official support to complete this work.

I greatly acknowledge to the Central Research Facility (CRF), IIT Kharagpur, India for TEM study. I am also thankful to the Department of Physics, Vidyasagar University for XRD study and also grateful to University Scientific Instrumentation Centre (USIC), Vidyasagar University for other instrumental facilities. I also acknowledge to the Departmental Instrument Facility, Dept. of Chemistry and Chemical Technology, Vidyasagar University.

Finally, I am thankful to Council of Scientific and Industrial Research (CSIR), Department of Science and technology (DST), University Grand Commission (UGC), New Delhi and Government of India, for financial assistance.

Date:
Place: Midnapore, India *(Sadhan Samanta)*

Abbreviations

AgNPs	Silver nanoparticles
CVD	Chemical vapour deposition
CTAB	Cetyl trimethyl ammonium bromide
CCD	Close circuit camera
DFT	Density Function Theory
DMF	Dimethyl formamide
DNA	Deoxy ribonucleic acid
EDX	Energy dispersive X-ray analysis
FCC	Face centred cubic
FETs	Organic field-effect transistors
FESEM	Field emission scanning electron microscope
FTIR	Fourier transform infrared spectroscopy
HRTEM	High resolution transmission electron microscope
HPMC	Hydroxy propyl methyl cellulose
JCPDS	Joint Committee on Powder Diffraction Standards
keV	Kilo electron volt
LRD	Local reactivity descriptors
LSPR	Localized surface plasmon resonance
LSP	Localized surface Plasmon
MWCNT	Multi walled carbon nanotubes
MBE	Molecular beam epitaxy
MC	Methyl cellulose
MPA	Mercapto propionic acid
NLO	Nonlinear optical properties

$NaBH_4$	Sodium borohydride
Na-AOT	Sodium di-(ethyl hexyl sulfosuccinate)
NMR	Nuclear Magnetic Resonance
OLED	Organic light emitting diodes
PVD	Physical vapour deposition
PVA	Poly vinyl alcohol
PVP	Poly vinyl pyrrolidine
PEG	Poly ethylene glycol
PMT	Photomultiplier tube
ppm	Parts-per-million
PLM	Polarizing Microscopes
SPR	Surface plasmon resonance
SPPs	Surface plasmon polaritons
SPs	Surface plasmons
SDS	Sodium dodecyl sulphate
SEM	Scanning electron microscope
SAED	Selected area electron diffraction
SERS	Surface enhanced Raman scattering
TSC	Tri sodium citrate
TEM	Transmission electron microscope
TCSPC	Time correlated single photon counting
THF	Tetra Hydro Furan
UV	Ultra violet
UV-VIS-NIR	Ultraviolet-Visible-Near Infrared
XPS	X-ray Photoelectron Spectroscopy
XRD	X-ray diffraction

An Overview of thesis

This thesis entitled *"**SYNTHESIS, CHARACTERIZATION AND PHOTOPHYSICAL STUDY OF LOW DIMENSIONAL INORGANIC/ORGANIC MATERIALS**"* contains the work carried out in the Department of Chemistry and Chemical Technology, Vidyasagar University, Midnapore, Paschim Medinipur, W.B., PIN-721102, India under the supervision of Prof. Ajay Kumar Misra. This thesis comprises seven chapters.

Chapter I:

This chapter incorporates general introduction on low dimensional materials. This chapter discusses briefly the comparison between bulk and low dimensional materials, classification of low dimensional materials dimension wise and composition wise including nanoparticles and microparticles, various examples of nanoparticles and microparticles, their properties including optical, magnetic, electrical, thermal, mechanical and structural properties. Surface plasmon resonance (SPR) of metal nanoparticles, quantum size effect, Mie theory, luminescent properties, non-linear optical (NLO) properties are intricately discussed in the optical properties section. This chapter also depicts the applications of low dimensional materials in several fields including catalysis, sensor, medical, optical, electronics, information storage, energy, magnetic, thermal and waste water treatment fields.

Chapter II:

This chapter describes various methods for the synthesis of low dimensional materials, including both bottom-up and top-down approaches. Mechanism of particle formation in the bottom-up approach has been discussed. Four different stabilization processes viz. electrostatic stabilization, steric stabilization, electrosteric stabilization and stabilization by ligand or solvent

are described in this chapter. This chapter also accounts the various methods for the synthesis of organic low dimensional materials.

Chapter III:

This chapter concisely discusses various characterization techniques of the synthesized low dimensional materials such as UV-Vis spectroscopy, Fluorescence spectroscopy, transmission electron microscopy (TEM), selected area electron diffraction (SAED), scanning electron microscopy (SEM), X-ray diffraction (XRD) spectroscopy, Fourier transform infrared spectroscopy (FTIR).

Chapter IV:

This chapter describes the synthesis of silver nanostructures of varying morphologies through a simple seed mediated growth approach. Seeds are prepared by reducing silver nitrate with sodium borohydride, and trisodium citrate is used as capping agent. This citrate capped seed sol is mixed to the growth solution containing ascorbic acid, sodium dodecyl sulphate (SDS) and sodium hydroxide. Colour of the growth solution changes from colourless to pink and the surface plasmon resonance (SPR) shows two distinct bands, indicating the formation of anisotropically grown silver nanostructures. Synthesized silver nanoparticles are characterized by UV-vis spectroscopy, transmission electron microscopy (TEM) & X-ray diffraction (XRD) techniques. Silver nanoseeds are spherical in shape with diameter ranges from 8-16 nm. On the other hand, a mixture of morphologies with shapes like triangular and hexagonal nanoplates, nanorods are obtained in the growth solution. XRD results suggest that the particles are crystalline in nature with face centered cubic (fcc) geometry.

Chapter V:

This chapter presents synthesis of silver nanodiscs and triangular nanoplates in aqueous PVP matrix, their photophysical study and simulation of UV-vis extinction spectra using DDA

method. Circular silver nanodiscs and truncated triangular shaped silver nanoplates have been synthesized through a seeding growth approach in polyvinyl pyrrolidone (PVP) matrix at room temperature. Seeds are prepared on reduction of silver nitrate ($AgNO_3$) by sodium borohydride ($NaBH_4$) and methyl cellulose (MC) is used as encapsulating matrix. Coloured silver sols are obtained as variable amounts of seeds are added to the growth solution containing silver nitrate, polyvinyl pyrrolidone (PVP) and ascorbic acid. Silver nanostructures are characterized using UV-vis spectroscopic and transmission electron microscopic (TEM) study. TEM studies reveal that particles are mostly circular disc and truncated triangular plate like as different amount of seeds are used in the growth solution. Simulation of UV-vis extinction spectra using discrete dipole approximation (DDA) method nicely explain the observed localized surface Plasmon resonance (LSPR) band of spherical and circular disc like silver nanoparticle.

Chapter VI:

This chapter describes synthesis of ZnO microcrystals with hexagonal morphologies via a fast and facile hydrothermal route using hexamethylene tetramine (HMTA) as reducing and hydroxylpropyl methyl cellulose (HPMC) as morphology directing agent. In the absence of HPMC, hexagonal rod shaped ZnO microcrystals are formed where as hexagonal bar and both end open hexagonal bar shaped structures are obtained in the presence of different amount of HPMC. Synthesized ZnO microstructures are characterized using XRD, SEM and fluorescence spectroscopic study. The strong asymmetric blue emission band from ZnO micro rod has been explained due to the presence of extended Zn_i states within the microcrystals. Photo catalytic activities of the microcrystals are investigated by monitoring the photochemical degradation of Methylene Blue. It has been observed that the catalytic efficiency of hexagonal both end open bar shaped ZnO microcrystals is higher than the other ZnO structures.

Chapter VII:

This chapter presents synthesis of N-doped carbon nanodots through a fast and facile microwave assisted synthesis method using polyethylene glycol (PEG-200) as carbon source and urea as nitrogen precursor. The prepared N-doped carbon nanodots exhibit bright blue emission under UV-light (365 nm) and excellent stability in aq. solution. Factors affecting the FL emission intensity have been analyzed and nanodots are prepared at optimized conditions. The prepared nanodots are characterized by UV-Vis absorption spectroscopy, Fluorescence emission spectroscopy and FT-IR study. We find that the synthesized N-doped carbon dots can be used as fluorescence turn-off sensors for Fe^{3+} ions.

Table of Contents

Contents	Pages
Chapter I: Introduction	**1-45**
1.1. Low dimensional materials	2
1.2. Comparison between bulk and low dimensional materials	3
1.3. Types of low dimensional materials	5
1.3.1. Dimension wise classification	5
1.3.2. Size wise classification	5
1.3.2.1. Nanoparticles	5
1.3.2.1.1. Inorganic nanoparticles	6
1.3.2.1.2. Organic nanoparticles	8
1.3.2.2. Microparticles	9
1.3.2.2.1. Inorganic microparticles	9
1.3.2.2.2. Organic microparticles	10
1.4. Properties of low dimensional materials	11
1.4.1. Optical properties	11
1.4.1.1. Surface plasmon resonance (SPR)	12
1.4.1.2. Quantum size effect	16
1.4.1.3. Mie theory	17
1.4.1.4. Luminescent properties	18
1.4.1.5. Non-linear optical (NLO) properties	19
1.4.2. Magnetic properties	19
1.4.3. Electrical properties	20
1.4.4. Thermal properties	21
1.4.5. Mechanical properties	23
1.4.6. Structural properties	23
1.5. Application of low dimensional materials	24
1.5.1. Catalysis	25
1.5.2. Sensor	25
1.5.2.1. Chemical sensor	26
1.5.2.2. Biological sensor	26
1.5.3. Medical field	27

1.5.4. Optical field 28
1.5.4.1. Light emitting materials 28
1.5.4.2. Development of non-linear optical materials 29
1.5.4.3. Lasing Action 29
1.5.5. Electronics field 30
1.5.6. Information Storage field 31
1.5.7. Energy field 31
1.5.8. Magnetic field 31
1.5.9. Thermal field 32
1.5.10. Waste water treatment field 32
References 33
Chapter II: Synthesis of low dimensional materials **46-78**
2.1. Top down approach 47
2.1.1. Physical Methods 48
2.2.Bottom up approach 52
2.2.1. Mechanism of bottom-up approch 53
2.2.2. Stabilization of low dimensional materials 55
2.2.2.1. Electrostatic stabilization 56
2.2.2.2. Steric stabilization 57
2.2.2.3. Electrosteric stabilization 58
2.2.2.4. Stabilization by ligand or solvent 59
2.2.3 Synthetic methodology of low dimensional materials by bottom up approach 59
2.2.3.1. Chemical methods 59
2.2.3.2. Biosynthesis methods 64
2.2.3.3. Synthesis of organic low dimensional materials 68
References 70
Chapter III: Characterization Techniques **79-98**
3.1. UV-Vis spectroscopy 80
3.2. Fluorescence spectroscopy 83
3.3. Transmission electron microscopy (TEM) 86
3.3.1. Selected Area Electron Diffraction (SAED) 90
3.4. Scanning Electron Microscopy (SEM) 90

3.5. X-ray diffraction (XRD) 93
3.6. Fourier transform infrared spectroscopy (FTIR) 96
References 98
Chapter IV: Synthesis of silver nanostructures of varying morphologies through seed mediated growth approach **99-111**
4.1. Introduction 100
4.2. Experimental 101
4.2.1. Chemicals 101
4.2.2. Preparation of Silver Seed 102
4.2.3. Preparation of silver nanostructures of varying morphologies 102
4.2.4. Instrumentations and measurements 102
4.3. Results and discussion 103
4.3.1: TEM Study 103
4.3.2: UV-vis spectroscopic study 104
4.3.3: Role of sodium hydroxide in growth solution 106
4.3.4: XRD analysis 108
4.4. Conclusions 109
References 110
Chapter V: Synthesis of silver nanodiscs and triangular nanoplates in PVP matrix: Photophysical study and simulation of UV-vis extinction spectra using DDA method **112-131**
5.1. Introduction 113
5.2. Materials and Methods 115
5.2.1. Chemicals 115
5.2.2. Preparation of methyl cellulose (MC) solution 115
5.2.3. Preparation of silver seed nanoparticles 116
5.2.4. Preparation of silver nanodiscs and triangular nanoplates 116
5.2.5. Instrumentations and measurements 116
5.2.6. Discrete Dipole Approximation (DDA) 117
5.3. Results and Discussion 119
5.3.1. UV-vis spectroscopic study 119
5.3.2. TEM and SAED study 121

5.3.3. Simulation of UV-vis extinction spectra using DDA method 125
5.4. Conclusions 127
References 129
Chapter VI: Hydrothermal synthesis of hexagonal ZnO micro structures in HPMC polymer matrix and their catalytic activities **132-148**
6.1. Introduction 133
6.2. Experimental Section 135
6.2.1. Reagents and Instruments 135
6.2.1.1. Reagents 135
6.2.1.2. Instruments 135
6.2.2. Synthesis 136
6.2.2.1. Synthesis of hexagonal rod, bar and both end open bar like ZnO microstructures 136
6.2.2.2. Photocatalytic Tests 136
6.3. Result and Discussion 137
6.3.1. SEM study 137
6.3.2. XRD study 139
6.3.3. Role of Hexamethylene tetramine (HMTA) 140
6.3.4. Emission Study 141
6.3.5. UV light driven Photocatalysis and Photocatalytic Mechanism 143
6.4. Conclusions 145
References 146
Chapter VII: Microwave-assisted synthesis of fluorescent N-doped carbon nanodots and its potential use as sensor for Fe(III) ions **149-167**
7.1. Introduction 150
7.2. Experimental 151
7.2.1. Chemicals and Materials 151
7.2.2. Synthesis of N-CDs 152
7.2.3. Instrumentation and Characterization 152
7.3. Results and Discussions 153
7.3.1. Optimization of synthetic conditions 153
7.3.2. FL Emission spectroscopy study 156
7.3.3. UV-Vis absorption spectroscopy study 158

7.3.4. Determination of Quantum Yield (QY) 159
7.3.5. FT-IR spectroscopy study 160
7.3.6. Fluorescence detection of Fe^{3+} 161
7.4. Conclusions 165
References 166
List of Publications **168-170**

Chapter I

Introduction

Introduction

"A biological system can be exceedingly small. Many of the cells are very tiny, but they are very active; they manufacture various substances; they walk around; they wiggle; and they do all kinds of marvellous things—all on a very small scale. Also, they store information. Consider the possibility that we too can make a thing very small that does what we want—that we can manufacture an object that manoeuvres at that level."

- Richard P. Feynman

(From the talk entitled ***"There's plenty of Room at the Bottom"***)

1.1. Low dimensional materials

The materials or structures of metal, metal oxide, metal alloy, composite, crystalline form of inorganic or organic materials having either dimension from one nm to thousand micrometer are generally called as low dimensional materials. These materials belong to the intermediate state between bulk materials and single molecules and therefore consist of a huge number of very small particles. The very small particles are named as nanoparticles or microparticles by taking into account the scaling parameter. The word 'nano' is derived from Greek word 'dwarf' which means one billionth (10^{-9}) in dimension. Thus, a nanometer (nm) is 10^{-9} m. One nanometer is approximately the length equivalent to 10 hydrogen or 5 silicon atoms aligned in a line. To put this into perspective, think of a material with dimensions approximately 75000 times smaller than the diameter of a human hair follicle!

Nobel Laureate Richard P. Feynman gave the first lecture regarding the applications for nanoscale materials. His talk, entitled "There's Plenty of Room at the Bottom", was delivered on 29 December 1959 at the annual American Physical Society meeting in the campus of Caltech. Feynman pointed out

that designing materials atom-by-atom is a real possibility as it would not violet any physical laws. He also predicted such sci-fi accomplishments as writing 24 volumes of the Encyclopedia Britannica on the head of a pin.

The interest of chemists in low dimensional materials is being due to several reasons. The chief reason is the fact that studying nanoparticles and microparticles of various elements and compounds opens up new directions in chemistry that cannot be described in terms of already known relationships and properties of the bulk materials. Many years ago, the earliest civilizations used nanoscale materials for a variety of applications without knowing its scientific aspects. For example, the Mayans used magnesium aluminium silicate clay called palygorskite, which contained nanosized channels that were filled with water. The Mesopotamian civilization used coloured glass for decorative applications that contained embedded metallic nanoparticles. As time forwarded, the secret science revealed and a new branch of science developed.

The first use of of the term "nanotechnology" was by Norio Taniguchi in 1974 at the international conference on precision engineering (ICPE). His definition of ‘‘nanotechnology’’ referred to "production technology to get extra high accuracy and ultra fine dimensions, i.e., the preciseness and fineness on the order of 1nm (nanometer), 10^{-9} m in length".

1.2. Comparison between Bulk and Low dimensional materials

As the dimensions of bulk materials are reduced to low they demonstrate unique physical, chemical and optoelectronic properties which are strikingly different from those of their bulk counterparts. Micrometer scale materials may demonstrate physical properties the same as that of

bulk form; however, materials in the nanometer scale certainly exhibit physical properties distinctively different from that of bulk. Materials in this size limit show some remarkable specific properties. As for example, crystals in the nanometer scale have a low melting point (the difference may be as large as 1000°C) and reduced lattice constants. Crystal structures of bulk materials which are stable at elevated temperatures, found to be stable at much lower temperatures in nanometer dimensions. Ferroelectrics and ferromagnetics may lose their ferroelectricity and ferromagnetism when the materials are reduced to the nanometer scale. Bulk semiconductors become insulators when the dimensions are reduced to ultra small (a few nanometers only). Au nanocrystal demonstrates to be an excellent low temperature catalyst whereas bulk gold does not exhibit catalytic properties.

The behaviour of low dimensional materials can better be explained from their surface and interface properties. In bulk materials, only a small percentage of atoms are present near or at the surface or interface whereas in case of low dimensional materials, the small size feature ensures that a huge number of atoms perhaps half or more, will be present near or at the surface or interface. The nature of an atom residing at the surface is dissimilar compared to that of an atom situated inside of the same material. In addition to this, an atom at the smooth surface of a single crystal is different from an atom at the surface of a small cluster of the same element. Moreover, the properties of a surface atom of a small metal cluster is dependent on the type of support on which it is situated and whether the cluster is doped with even a few atoms of a different element. Due to this reason, surface properties such as energy levels, electronic structures and reactivity of low dimensional materials can be quite different from their bulk counterpart.

Because of the unsatisfied bonds on the surface, surface atoms or molecules are under an inwardly

directed force and the bond distance between the surface atoms or molecules and the sub-surface atoms or molecules, is smaller than that between interior atoms or molecules. When solid particles are very small, such a decrease in bond length between the surface atoms and interior atoms becomes significant and the lattice constants of the entire solid particles show an appreciable reduction. This can result in a noticeable reduction of bond length in nanoparticles.

1.3. Types of Low dimensional materials

Low dimensional materials are mainly classified into two heads: one is dimension wise and another is size wise.

1.3.1. Dimension wise Classification:

Low dimensional materials are classified dimension wise according to the number of dimensions of the constructing elementary units of the material and named as 0D, 1D, 2D and 3D structures. Quantum dots are the best examples of 0D low materials. Rods, wires, tubes etc. are the examples of 1D structure. Plates, discs, triangles, hexagons, sheets etc. are the examples of 2D structures. 3D structure includes octahedra, icosahedra, pyramid, tripod etc. where nucleation and growth occurs in three directions (X, Y and Z) simultaneously

1.3.2. Size wise Classification:

Low dimensional materials can be classified into two main types viz. a) nanoparticles and b) microparticles based on the size of the particles.

1.3.2.1. Nanoparticles

Nanoparticles are very small particles which constitute a bridge between isolated molecules and microparticles, having at least one dimension in the nanometer range (1-100 nm). Nanotechnology is the design, production, characterization, and application of functional materials, devices and systems by controlling shape and size at nanometer scale (1-100 nm). Nanoparticles can be classified into two main groups viz. inorganic nanoparticles and organic nanoparticles based on the composition.

1.3.2.1.1. Inorganic nanoparticles

Inorganic nanomaterials are composed of pure elements, inorganic compounds, metal alloy or composite of elements etc. Owing to different structural design and wide range of applications in various fields, inorganic nanomaterials have been explored vigorously in the last few years. Elemental metal nanostructures like Ag, Au, Cu, Pt, Ru, Rh, Ir etc., metal oxide nanocrystals like CuO, ZnO, CdO, MnO, Mn_3O_4, Fe_2O_3, CoO, NiO etc., metal sulfide nanostructures such as PbS, MnS, CuS, ZnS, CdS etc., nanocrystals of metal nitrides like AlN, GaN, InN, metal nanoalloy cluster like Ag-Au, Cu-Au, Ni-Cu, Cu-Zn, Ni-Ag, Ni-Pt, Ni-Pd, Pt-Pd, Fe-Co, Co-Ni etc. have been synthesized with different shapes and sizes. Core@shell nanoparticles involving metal, semiconductor or oxide nanocrystals in the core, with shells composed of different materials have been investigated widely. Examples of core@shell nanoparticles are Au@Ag, Ag@Au, Au@Pd, Fe@Au, Fe_3O_4@Au, Au@TiO_2, Au@SiO_2, CdSe@ZnS CdSe@CdS, CdSe@ZnSe etc.

Nanostructures can be further classified into four types such as 0D, 1D, 2D and 3D structures according to the number of dimensions of elementary constructing units. Example of zero dimensional (0D) nanoparticles is quantum dots. In general, quantum dots have diameter below 10 nm but actual

diameter of the quantum dots is dependent on the material used to prepare such dots. Definitely low dimensional materials are termed as quantum dots when the quantum confinement effect occurs i.e. when particle radius is lower than one of the magnitude among Bohr radius of electron, hole and exciton. It is worthy to mention that Bohr radius is dependent on the material. Quantum dot usually consists of few hundreds to a few millions of atoms, but only a small number of free electrons ($\leq$100) [1]. Typical quantum dots are C-dots [2], Si-dots [3], Ge-dots [4], Si-Ge dots [5], PbS dots [6], PbSe dots [7], CdS dots [8], CdSe dots [9], ZnS dots [10], InAs dots [11], InP dots [12] etc. Nanorods, nanowires, nanotubes and nanobelts are examples of one dimensional (1D) nanoparticles. Different types of nanorods like Ag nanorods [13], gold nanorods [14], Cu nanorods [15], Pt nanorods [16], Fe nanorods [17], ZnS nanorods [18], CdS nanorods [19], ZnO nanorods [20], Fe_2O_3 nanorods [21], Mn_3O_4 nanorods [22], V_2O_5 nanorods [23] and nanowires including metallic nanowires like Cu [24], Ag [25] and Au [26], Ni [27], Pt [28], metal oxide nanowire like CuO nanowire [29], semiconductor nanowires like ZnO nanowire [30], CdS nanowire [31], metalloid nanowires like Te nanowires [32], non-metallic nanowires like Se nanowires [33] and insulating nanowires like SiO_2 [34], nanotubes of carbon [35], manganese oxide [36], MoS and WS_2 [37] etc. exist. Remarkable two dimensional (2D) nanostructures are nanoplates [38], nanotriangle [39], nanostar [40] etc. Three dimensional (3D) nanoparticles are nanoparticles in which growth occurs in three dimensions (X, Y and Z) concurrently. There are various 3D nanoparticles. Besides very common spherical nanoparticles, some of the interesting examples of three dimensional nanostructures are nanoprisms of Ag [41], N-doped TiO_2 [42], ZnO [43], nanooctahedra of Cu [44], Co_3O_4 [45] and Cu_2O [46], nanopyramids of Au [47], Cu_2O [48], Ag-Au [49], nanocubes of Pt [50], Ag [51], Pd [52], Au [53], PbS [54], nanotripods of Au [55], Pt

[56], nanoicosahedra of Zr–Pd and Zr–Pt binary alloy [57] etc.

1.3.2.1.2. Organic nanoparticles

Synthesis of nanoparticles from organic molecules has been paid little attention compared to the inorganic metal and semiconductor nanoparticles. However in recent years, the number of studies of organic nanoparticles has been increasing as their special properties lie between the properties of molecules and those of bulk materials [58] and as these nanocrystals allow much increased variability and flexibility in the synthesis of materials, preparation of nanoparticles, and investigation of their physicochemical properties. The electronic properties of organic nanoparticles differ fundamentally from those of inorganic ones because of weak intermolecular forces accompanying interactions of van der Waals type or hydrogen bonding. From a fundamental point of view, organic nanoparticles are fascinating because their optical properties on absorption and emission depend on size [59]. Recently, development of low dimensional structures from small organic molecule have attracted a great interest due to their low production cost and unique, tunable electronic and optical properties [60] and their potential applications in fabricating nano devices, such as optoelectronic and field-effect transistors. Organic nanoparticles were successfully synthesized by reprecipitation, microemulsion, ultra-sonication, self-organization, physical vapour deposition, thermal evaporation, laser ablation, template method etc. Organic nanostructures of various shapes have been synthesized like nanodots [61], nanorods [62], nanowire [63], nanotubes [64], nanobelts [65], nanoplates [66] etc.

1.3.2.2. Microparticles

One of the dimensions of these low dimensional materials lies in the micrometer (0.1 to 100 μm) range. Microparticles constitute a bridge between nanoparticles and bulk materials. Flour, powdered

sugar, sand, pollen, dust etc. are the examples of microoparticles used in daily life. Ceramics, glass, polymers, and metals provide a wide variety of these materials which are commercially available. A much larger surface-to-volume ratio of these particles compared to the bulk materials enables them to possess a behavior quite different from the bulk. Spherical microparticles are called microspheres, and these are used where consistent and predictable particle surface area is important. In biological systems, microparticles are small membrane bound vesicles circulating in the blood derived from cells that are in contact with the bloodstream such as platelets and endothelial cells. Microparticles carry useful information and can be detected and characterized by flow cytometry as they retain the signature of membrane protein composition of the parent cell.

1.3.2.2.1. Inorganic microparticles

The number of studies to synthesize inorganic microparticles is found much less compared to the inorganic nanoparticles in the literature. However, studies on functionalized inorganic microparticles constitute an interesting topic in the present materials science as their applications in the field of electronics, photonics, catalysis etc. are increasing.

Various inorganic microparticles have been synthesized like metallic microparticles such as Ag microparticles [67], Au microparticles [68], Cu microparticles [69], Pt microparticles [70], Pd microparticles [71], semiconductor and metal oxide microparticles such as Si microparticles [72], CuO microparticles [73], ZnO microparticles [74], CdS microparticles [75], Fe_3O_4 microparticles [76], In_2O_3 microparticles [77], metal carbonate microparticles such as $FeCO_3$ microparticles [78], $CaCO_3$ microparticles [79]. Hollow inorganic microparticles [80-82] have attracted increasing interest due to

their potential applications in catalysis, chemical storage, drug delivery carriers, ionic intercalation, surface functionalization, as light weight fillers, battery electrodes, photonic crystals etc. as they possess features of having high surface area, large interior spaces, low density, and good permeability properties. Gold microparticles can be used in diagnostic tests as well as conjugation studies of proteins and antibodies. Highly dispersed metal microparticles (e.g. Ag, Au, Pt, Pd, Cu etc.) may be synthesized by various methods, among which direct electrochemical reduction of metal ion on electrode surface is one [83]. Various types of micro alloy clusters like Ag-Au, Cu-Au, Pt- Ru and Ni-Al oxide have been successfully prepared and widely applied in the field of electronics and catalytic applications [84]. Structured composite microparticles such as Fe_2O_3-Al_2O_3 [85], core@shell microparticle such as Fe_3O_4@SiO_2 [86] etc. have been prepared.

1.3.2.2.2. Organic microparticles

Synthesis of organic microparticles have some advantages over inorganic one like unlimited choice of molecules, easy to modify, flexible for processing, cheap for manufacturing etc. Physical, chemical and optoelectronic properties of these particles differ widely from that of the isolated molecules and bulk materials. The electronic properties of organic microparticles differ fundamentally from those of inorganic ones because of weak intermolecular interaction forces like van der Waals force, hydrogen bond, π-π stacking, charge transfer interactions etc. These particles are of considerable interest for various potential applications in the field of photocatalyst, sensor, OLEDs, optical devices, drug delivery devices etc. [87-89]. Researchers devoted many efforts to synthesize organic microparticles having various size and shapes. This includes zero dimensional (0-D) spherical or

tetrahedral quantum dots [90, 91], one-dimensional (1-D) microrods [92-94] and microwires [95, 96] from various organic compounds and two-dimensional (2-D) microplates [97], microcapsule [98], microribbon [99], microtube [100], sub-microtube [101], microflower [102], etc. Following are the some examples of organic microparticles synthesized from various organic compounds: from anthracene [103], from Diphenylalanine [92, 93] from perylene diimide [93] from glycopolymer [104], from azobenzene containing polymer [105], from Chitosan [106], from 4-mercapto ethyl pyridine [107], polystyrene core and poly (methyl methacrylate) shell microparticles [108].

1.4. Properties of Low dimensional materials

Low dimensional materials exhibit fascinating properties that are notably different from both of the single molecules and bulk materials. Origin of the properties of these materials is related to the large fraction of surface atoms, high surface energy, spatial confinement, size, shape and reduced imperfections. These properties are- (i) Optical properties, (ii) Magnetic properties, (iii) Electrical properties, (iv) Thermal properties, (v) Mechanical properties and (vi) Structural Properties.

1.4.1. Optical Properties

Low dimensional materials have attracted much interest for their novel optical properties which have great aesthetic, intellectual and technological values. Fundamentally, optical absorption spectra of a particle provide information on the electronic structure of the particle which depends on the particle's size, shape and dielectric function of media [109]. Colloidal solutions of the noble metals such as silver and gold show a very intense colour and exhibit a strong absorption band, which is remarkably different from the bulk material as well as from the individual atoms. The change in optical properties

of low dimensional materials is mainly guided by two phenomena viz. quantum size effect and surface plasmon resonance (SPR). Due to quantum size effect, efficient energy and charge transfer over nanoscale distance occur. The colour of metal nanoparticles develops due to surface plasmon resonance.

1.4.1.1. Surface Plasmon Resonance

The term Plasmon refers to the plasma-like behaviour of the free electrons in a metal under the influence of electromagnetic radiation. For a bulk metal having infinite size, the frequency of oscillation of free charges, 'ω_p' can be described by $\omega_p = (Ne^2/\varepsilon_0 m_e)^{1/2}$, where 'N' is the number density of conduction electrons, 'e' is the charge of an electron, 'ε_0' is the dielectric constant of vacuum, and 'm_e' is the effective mass of an electron [110]. Thus, the bulk plasmon frequency of a particular metal depends only on its free electron density. The plasmon frequencies for most metals occur in the UV region, with alkali metals and some transition metals such as Cu, Ag, and Au exhibiting plasmon frequencies in the visible region.

Surface Plasmons (SPs) are coherent oscillations of conduction electrons on a metal surface stimulated by electromagnetic radiation at a metal-dielectric interface. Surface plasmon is important in case of metal nanoparticles, as the penetration depth of an electromagnetic radiation on the metal surface is limited. The resonance condition is established when the frequency of incident photons matches the natural frequency of surface electrons oscillating against the restoring force of positive nuclei and it is termed as surface plasmon resonance (SPR). There are two types of SPRs that can be generated: *surface plasmon polaritons* (SPPs) and *localized surface plasmon resonance* (LSPR). Often

the term SPR is applied to the both cases to denote the general phenomenon of confined plasma oscillations. SPPs originate from propagating waves along the interface of metal and dielectric. In other words, SPPs are generated when light becomes trapped at a metal-dielectric interface (Fig.1.1.A).

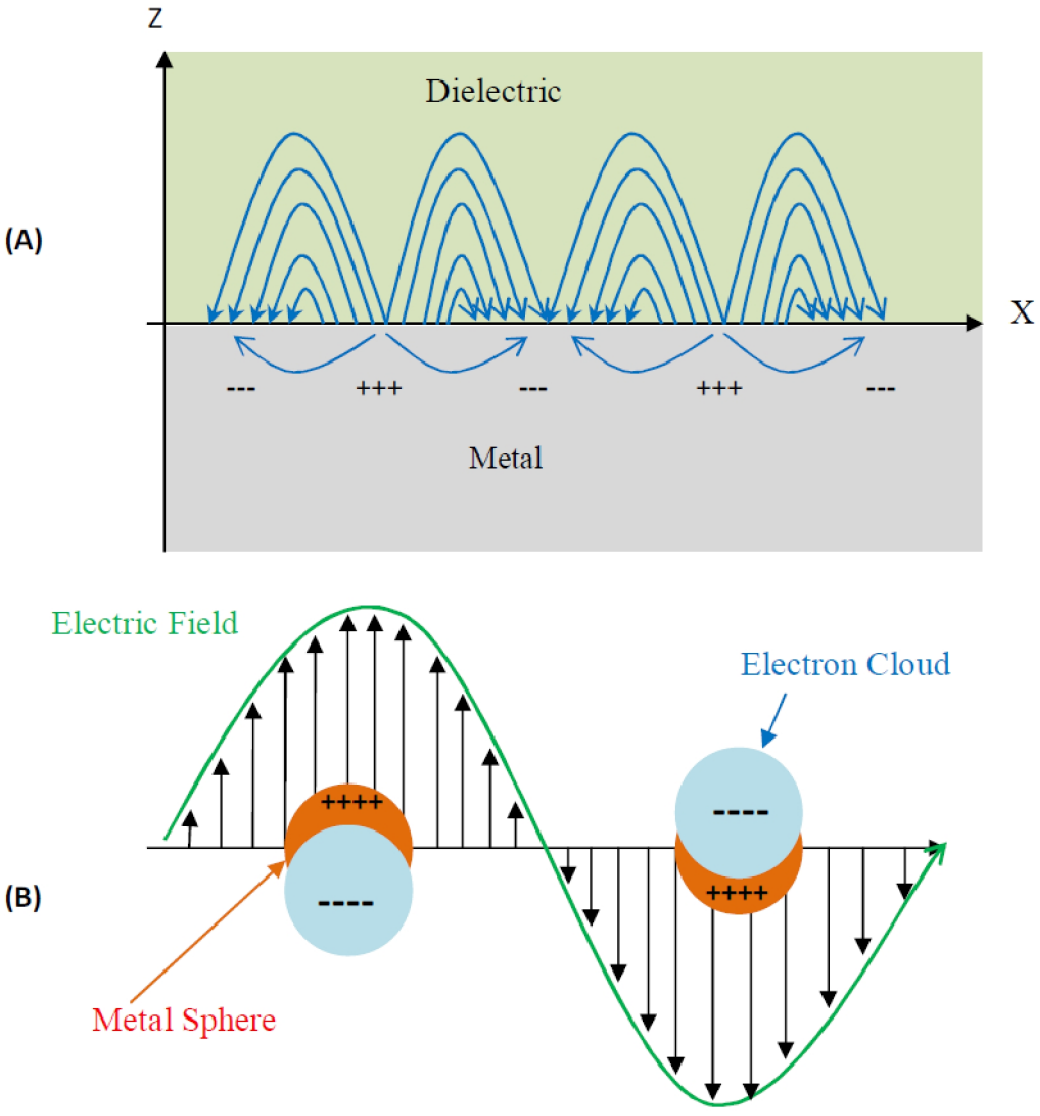

Figure 1.1: Schematic diagrams illustrating (A) surface Plasmon polariton and (B) localized surface plasmon resonance.

Incoming electromagnetic radiation can be coupled into the free conduction electrons at the surface of a metal. After coupling, the resulting charge density waves propagate along all directions in the plane (x- and y-directions) of the interface, reaching distances in the order of micrometers. The electromagnetic radiation also extends in the direction normal to the interface (z-direction), with the field decaying exponentially away from the surface, reaching roughly 200 nm into the dielectric environment [111]. When light is coupled into an appropriate metal-dielectric interface, it will continue to propagate until either the interface is interrupted or the propagation distance becomes too great and the SPP decays away. On the other hand, if the collective oscillations of the surface electrons are confined to a finite volume (i.e. the non-propagating counterpart of SPPs) with dimensions smaller than the wavelength of the incident light as in a metal nanoparticle, the corresponding plasmon is called a *localized surface plasmon* (Fig. 1.1.B) and theoretical frequency of such a plasmon is $\omega_p/\sqrt{3}$ for a metal sphere placed in vacuum. In order for the terms that describe the electronic surface plasmon to exist, the real part of the dielectric constant of the conductor must be negative and its magnitude must be greater than that of the dielectric. This condition is met in the infrared-visible wavelength region for air/metal and water/metal interfaces (where the real dielectric constant of a metal is negative and that of air or water is positive). In such a case, the electric field of incident electromagnetic radiation can cause the free electrons to move away from the metal particle in one direction, creating a dipole that can switch direction with the change in electric field. When the frequency of the dipole plasmon is exactly the same as the incident light, a resonance condition is reached, leading to constructive interference and the strongest signal for the plasmon. Such a condition is referred to as *localized surface plasmon resonance* (LSPR) mentioned above. The confinement of the *localized surface plasmon* to a small

volume results in an oscillating electromagnetic field that resides very close to the particle surface, extending only nanometers into the dielectric environment. Consequently, LSPR can generate much higher local field enhancements (100-10000 times the incident field) as compared to those of an SPP (10-100 times the incident field) [112].

For a qualitative understanding of a *surface plasmon resonance* (SPR), the analogy to a mechanical oscillator can be made. When a simple harmonic oscillator is displaced from its equilibrium position, it experiences a restoring force that brings the oscillator back to its initial position or equilibrium position. A simple oscillator, once perturbed from equilibrium, will undergo a continuous sinusoidal type motion until damping forces or restoring forces bring the system back to rest. The effects of damping can be overcome if an additional (external) force is applied to the oscillator. In the case of a sinusoidal applied external force, there exists at least one frequency at which the force applied will result in the oscillator achieving maximum amplitude. This particular frequency is called the resonant frequency: a frequency either above or below the resonant frequency yields lower amplitudes of oscillation. This phenomenon arises when the external force is applied "in phase" with the natural frequency of the oscillator, resulting in the oscillator absorbing a maximum amount of energy from the driving force.

The shape and frequency of SPR depends on the material composition, size, shape and dielectric environment [113]. For nanoparticle, having much smaller diameter than λ, the electromagnetic field is uniform across a particle, as a result all the conduction electrons move in phase producing only dipole-type oscillations manifested by a single, narrow peak in the SPR spectrum. As the size increases, the field across the particle becomes non-uniform, and this phase retardation broadens the dipole

resonance and excites higher multipole resonances, such as the quadraupole, octupole, etc. leading to several peaks in the spectra (Fig.1.2) [114]. On the other hand for anisotropic nanoparticles the dipole plasmon resonance split into transverse and longitudinal modes due to different dimensions along the width and length of the particles respectively. The position of both transverse and longitudinal bands depends on the aspect ratio and the absolute dimensions of the particle [115].

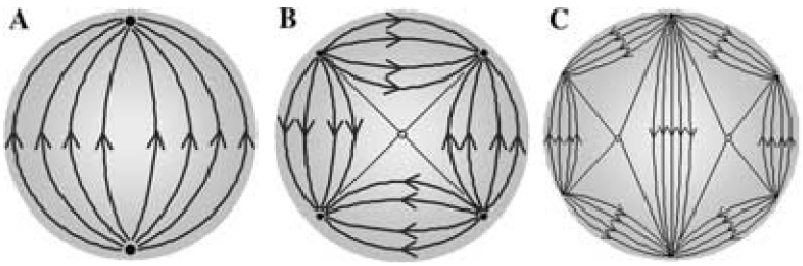

Figure 1.2: Diagrams depicting the electric field lines of the (a) dipole, (b) quadrupole, and (c) octupole resonances.

1.4.1.2. Quantum Size Effect:

Unusual property of extremely small crystals that arise from confinement of electrons to small region of space in one, two or three dimensions are known as quantum size effect. Unique optical property of nanomaterials may arise from this effect. When the size of a nanocrystal is smaller than the de-Broglie wavelength, electrons and holes are spatially confined and electric dipoles are formed and discrete electronic energy levels would be formed in the material. Similar to a particle in a box, the energy separation between adjacent levels increases with decreasing dimensions. The quantum size effect is most pronounced for the semiconductor nano and microparticles [116], where the band gap increases with decreasing size resulting in the interband transition shifting to higher frequencies [117]. In a semiconductor, the energy difference between the completely filled valence band and the empty

conduction band is of the order of a few electron volts and increases rapidly with a decreasing size [118].

1.4.1.3. The Mie's theory:

In 1908 Gustav Mie provided an analytical solution to the Maxwell's equations for a sphere of arbitrary size [119]. Mie was able to calculate the extinction (sum of absorption and scattering) spectra for metal colloids containing spherical particles of any size. Many of the experimental observations of his day, including the red colour of Faraday's gold were explained by applying his theory and now an inter-disciplinary field known as plasmonics has been evolved which is related to the understanding of how light interacts with metals on the nanometer scale length.

The main assumptions of Mie's theory is that the particle and its surrounding medium are each homogeneous and describable by their bulk optical dielectric functions [120]. The solution of the electrodynamic calculation with appropriate boundary conditions for a spherical object yields an expression for the extinction cross section, which is a sum over electric and magnetic multipoles. When the size of a particle is much smaller than the wavelength of the exciting radiation ($2R << \lambda$), the extinction is dominated by the dipole term (dipole approximation), with a cross section $\sigma(\omega)$ given by,

$$\sigma(\omega) = 9\varepsilon_m^{3/2} V_0 \frac{\omega}{c} \frac{\varepsilon_2(\omega)}{[\varepsilon_1(\omega) + 2\varepsilon_m]^2 + \varepsilon_2^2(\omega)} \quad \text{.....(1)}$$

where, ω is the frequency and c the velocity of light, V_0 is the volume of the absorbing particle, ε_m and $\varepsilon(\omega) = \varepsilon_1(\omega) + i\varepsilon_2(\omega)$ are the dielectric constant of the embedding medium (assuming frequency-independent over the spectral range of interest) and the absorbing solid respectively. It is to be noted that $\varepsilon(\omega)$ is a function of energy and $\varepsilon_1(\omega)$ and $\varepsilon_2(\omega)$ are the real and imaginary parts of the

frequency-dependent dielectric constant of the absorbing solid describing polarizability and energy dissipation respectively. For small particles, the dielectric function of the metal nanoparticles itself is assumed to become size dependent [$\varepsilon = \varepsilon(\omega, R)$] and this renders a size-dependent extinction cross section even within the dipole approximation (intrinsic size effects). For larger nanoparticles ($2R > 25$ nm for gold) the dipole approximation is no longer valid and the plasmon resonance explicitly depends on the particle size. The larger the particles become, the more important are the higher order modes as the light can no longer polarize the nanoparticle homogeneously. These higher order multipole modes explicitly depend on the particle size and peak at lower energies. Thus, with increasing size the plasmon absorption maximum is shifted to longer wavelength and the bandwidth increases, this is thus regarded as an extrinsic size effects.

1.4.1.4. Luminescent properties

Luminescence is the emission of electromagnetic radiation in the visible or near visible region of the spectrum by a substance not resulting from heat; it is thus a form of cold body radiation. It can be caused by chemical reactions, electrical energy, subatomic motions, or stress on a crystal. The luminescence involves at least two steps, excitation of electron of the material and the subsequent emission of photons. There are mainly four types of luminescence properties e.g. (i) photoluminescence - a result of absorption of photons which includes fluorescence and phosphorescence, (ii) electroluminescence – a result of an electric current passed through the material, (iii) cathode luminescence – a result of the luminescent material being struck by electrons and (iv) thermoluminescence – the re-emission of absorbed energy when the substance is heated. The

luminescence wavelength, luminescence efficiency and lifetime of luminescence depend upon the nature of the material. Additionally, the size of the material plays an important role in case of the low dimensional materials. As for example, the doping of ZnS nanoparticles with manganese can be considered. ZnS which has a wide direct band gap, shows bulk band gap luminescence at ~ 344nm [121]. But if Mn is introduced in small quantity (~ 0.1 atom %) it produces discrete energy levels in the band gap and emits luminescence at ~ 590 nm. Cathodoluminescence in ZnO nanoparticles [122] has been investigated. It has been observed that nanoparticles are better luminescence materials than microparticles [123].

1.4.1.5. Nonlinear Optical (NLO) Properties

The linear and nonlinear optical properties of semiconductors are the subject of much current theoretical and experimental interest. Nonlinear optical materials have a nonlinear response to the electric field associated with the light having very high intensity such as a laser beam, leading to a variety of optical phenomena such as the generation of new light frequencies or the alteration of the material's optical properties [96]. There are some reports on NLO properties e.g. of gold nanocubes and nano-octahedra [124] of organic nanocrystals [125] in the literature.

1.4.2. Magnetic properties

A very important property of materials is magnetism because it has various applications in information storage, electronic circuits, motors, transformers, sensors, medical diagnosis and treatment, actuators etc. Magnetism in bulk material arises due to the presence of magnetic moments on constituting atoms, ions or molecules of the materials. Low dimensional magnetic materials are

attracting considerable interest as their magnetic properties found different from their bulk counterpart. It is found that ferromagnetic bulk materials lose their ferromagnetism and converted to superparamagnetic material when they are reduced to nanometer scale owing to the high surface energy [126]. Nanometer sized ferromagnetic particles of up to $N = 10^5$ atoms ferromagnetically coupled by exchange forces, form a single domain [127], with a large single magnetic moment with up to 10^5 Bohr magnetons. These clusters or particles can be analogously described as paramagnetic atoms or molecules with much larger magnetic moments at elevated temperatures [128]. Magnetic nanoparticles, nanowires, thin films and some metal oxide films, doped semiconductor nanoparticles have become the focus of attention due to their interesting magneto resistive properties. As low dimensional materials have large surface to volume ratio, surfaces and interfaces play an important role in their magnetic properties. At the surface of low dimensional materials symmetry breaking of the bulk crystal structure occurs in addition to a change in the lattice constant and coordination number. Due to this effect magnetic properties of low dimensional materials are quite different from their counterpart.

1.4.3. Electrical Properties

Conductivity is defined in terms of the properties of electrons in the solids and is given by

$$\sigma = \frac{Ne^2\tau}{m}$$

where σ=electrical conductivity, N= Number of electrons, e=electron charge, τ= relaxation time, m=mass of electron. It is found that due to increased surface scattering electrical conductivity decreases with a reduced dimension. However, electrical conductivity of low dimensional materials could also be increased significantly, due to the better ordering in microstructure, e.g. in polymeric

microfibrils. The effects of size on electrical conductivity of low dimensional materials are complex, since they are based on distinct mechanisms. These mechanisms can be generally grouped into four categories: surface scattering including grain boundary scattering, quantized conduction including ballistic conduction, Coulomb charging and tunneling, and widening and discrete of band gap, and change of microstructures. For inelastic scattering of electron, the scattered electron loses its velocity along the direction parallel to the surface or the conduction direction, and the electrical conductivity decreases whereas for elastic collision momentum or velocity along the direction parallel to the surface is preserved and hence the electrical conductivity remains the same as in the bulk. In nanowires and thin films, the surface scattering of electrons results in the reduction of electrical conductivity. When the critical dimension of thin films and nanowires is smaller than the electron mean-free path, the motion of electrons will be interrupted through collision with the surface. In contrast, increased perfection, such as reduced impurity, structural defects and dislocations, would increase the electrical conductivity of nano/microstructures since increased perfection results a reduction in defect scattering and hence lowering in resistivity. Thin films attached to metal nanoparticles have been shown to change their electrical conductivity rapidly and reproducibly in the presence of organic vapors, and this has been exploited for the development of novel gas sensor [129].

1.4.4. Thermal Properties

The thermal stability of low dimensional materials is of critical importance for their implementation as building blocks in nano/micro scale electronic and photonic devices. Due to the large surface area-to-volume ratio in nanowires and other nanoparticles, the thermal stability of

nanowires is anticipated to differ significantly from that of the bulk material. Thermal stability of various low dimensional materials has been studied. It is well documented that melting point of a bulk solid material is significantly lowered as compared to that of the bulk material when it is processed as nanomaterial [130]. Theoretical studies of materials in confined geometries show that the melting point of the material is reduced in nanostructures. The lowering of the melting points is in general explained by the fact that the surface energy increases with a decreasing size. The decrease in the phase transition temperature can be attributed to the changes in the ratio of surface energy to volume energy as a function of particle size.

It is not always easy to determine or define the melting temperature of nanoparticles. Increased surface reactivity may promote oxidation of the surface layer and, thus, change the chemical composition on the particle surface through reactions with surrounding chemical species, leading to a change of melting temperature. However, it is possible to make an experimental determination of the size dependence of melting temperature of nanoparticles. Three different criteria have been explored for this determination: (i) the disappearance of the state of order in the solid, (ii) the sharp variation of some physical properties, such as evaporation rate, and (iii) the sudden change in the particle shape [131]. The melting point of bulk gold is of 1337 K and decreases rapidly for nanoparticles with sizes below 5 nm [131] Such size dependence has also been found in other materials such as copper [132], tin [133], indium [134] lead and bismuth [135] in the forms of particles and films.

1.4.5. Mechanical Properties

Many studies have been focused on the mechanical properties of low dimensional materials. Mechanical properties of nanomaterials may reach the theoretical strength, which are one or two orders of magnitude higher than that of single crystals in the bulk form. The enhancement in mechanical strength is simply due to the reduced probability of defects. It has been long known that the calculated strength of perfect crystals exceeds that of real ones by two or three orders of magnitude. Two possible mechanisms have been proposed to explain the enhanced strength of nanowires or nanorods (in reality with diameters less than 10 microns). One is to ascribe the increase of strength to the high internal perfection of the nanowires. The smaller the cross-section of a nanowire, the less is the probability of finding in it any imperfections such as dislocations, micro-twins, impurity precipitates etc [136]. In addition, some imperfections in bulk materials, such as dislocations are often created to accommodate stresses generated in the synthesis and processing due to temperature gradient and other inhomogeneities. Another mechanism is the perfection of the side faces of nanowires. In general, smaller structures have less surface defects. It is particularly true when the materials are made through a bottom-up approach. It is a great scientific challenge to develop nano/micro materials with novel mechanical properties. Many of the mechanical properties such as hardness, elastic modulus, fracture toughness, scratch resistance, fatigue strength etc. are modified due to the nano/micro size dimension of the materials.

1.4.6. Structural Properties

The change of crystal structure may occur when the dimension of materials is sufficiently small.

For example, Arlt *et al* found that the crystal structure of $BaTiO_3$ changes with particle size at room temperature [137]. It is very interesting to observe that a phase change from tetragonal to pseudo cubic structure of $BaTiO_3$ gradually takes place with increasing particle size from 0.5 μm to 1.5 μm. Temperature and pressure also plays their significant effect on crystal structures. As for example, it has been shown that ZnS nanoparticles having diameter 1.4 nm exhibit liquid like disordered structure by careful analysis of XRD patterns. Nevertheless, larger nanostructures of ZnS indeed show same cubic structure as that found in the bulk. Effect of pressure on structural properties has also been well explored for some nanoparticles. For example, bulk CdSe needs just 2 GPa pressure to transform it from wurtzite to rock salt structure whereas for the said transformation CdSe nanoparticles of 2 to 4 nm size require 3 GPa to 4.9 GPa pressure.

1.5. Applications of low dimensional materials

The low dimensional materials offer an extremely broad range of potential applications in all disciplines. Various possible applications have been explored and a large number of systems, devices have been studied. Researchers are engaged in devising more potential applications and new device using various low dimensional materials. Applications of nanostructures are based on (i) the peculiar physical properties of nanosized materials, (ii) the huge surface area, such as mesoporous titania for photoelectrochemical cells, and (iii) the small size that offers extra possibilities for manipulation of multiple functionalities. For many applications, new materials and new properties are introduced. Following are the some examples of applications of low dimensional materials.

1.5.1. Catalysis

The catalytic reactivity of the low dimensional materials depends on their size, shape, composition and surface atomic arrangement. Nanomaterials show better catalytic performance compared to microparticles in various chemical reactions. Bulk gold is chemically inert and thus considered to be not active or useful as a catalyst. But gold nanoparticles can have excellent catalytic properties. For example, gold nanoparticles including nanospheres, nanoprisms and nanorods show catalysis for selective chemical reduction of different aromatic nitro compounds to the corresponding amino derivative at room temperature [138]. Redox Catalytic Properties of Palladium Nanoparticles has been studied by N.R. Jana et al [139]. Pd nanoparticles catalyzed the selective hydrogenation reaction of unsaturated alcohols like allyl or crotyl alcohol [140]. Photo-degradation of organic dyes catalyzed by TiO_2 nanoparticles has been reported [141]. C.Wang et al reported reduction of 4-nitrophenol catalysed by gold nanoparticles [142].

1.5.2. Sensor

Low dimensional materials can be applied for sensing purpose. Sensors can be of two types viz. chemical sensors and biological sensors. As a chemical sensor these materials can be used to detect selectively various inorganic ions and organic molecules. The unique physicochemical properties of such materials at the nanoscale have led to the development of a wide variety of biosensors, such as: (i) nanobiosensors for point of care disease diagnosis, (ii) nanoprobes for *in vivo* sensing/imaging, cell tracking and monitoring disease pathogenesis or therapy monitoring and (iii) other nanotechnology-based tools that benefit scientific research on basic biology [143].

1.5.2. 1. Chemical Sensor

Various metal ions and molecules can be detected with the help of nano/microparticles. For example, S.Maiti et al showed detection of heavy metal ions like Cu^{2+}, Hg^{2+} using silver nanoparticles [144]. Pb^{2+} and Cu^{2+} ions detection by the use of gold nanoparticles has been reported [145]. A CO_2 sensor system has been developed very recently by Y.Ma et al [146] using CO_2 responsive polymer functionalised Au-nanoparticles. Development of gold nanoparticle-based colorimetric sensor for cysteine detection has been reported by S. Jongjinakool et al [147]. A highly selective Hg^{2+} colorimetric sensor using green synthesized and unmodified silver nanoparticles has been developed by K.Farhadi et al [148].

1.5.2.2. Biological Sensor

To meet the increasing demands, more sensitive sensors are developed by the guidance of nanotechnology. To monitor global environmental health, food inspection, medical diagnostic etc. nanostructures materials such as nanofiber or nanowebs are performing as acoustic wave sensor, resistive sensor, photoelectric sensor, optical sensor, amperometric sensor [149]. Gold nanoparticles shows a wide range of applications as biological sensor such as detection of mutations in epidermal growth factor receptor [150], detection of mutagenic DNA photodimers [151] , detection of unamplified hepatitis C virus RNA [152], detection of melamine in whole milk [153], detection of Mycobacterium tuberculosis DNA in clinical samples [154]. Various nanoparticles have been used as biological sensor like DNA sensor for the simultaneous detection of multiple pathogens [155], ultrasensitive electrochemiluminescence immunosensor [156], foodborne pathogens on a piezoelectric

biosensor [157].

1.5.3. Medical field

There is a wide range of medical applications including diagnostic, therapeutic and pharmaceutical applications which utilize low dimensional materials. Silver and gold nanoparticles show potential application in antibacterial and antifungal activities against even multidrug registrant pathogenic microbes [158]. Gold nanoparticles exhibit strong anti angiogenic activity over angiogenesis of ovarian cancer. It also possesses strong effect on proliferation of multiple myeloma cells and angiogenesis in (B-CLL) B-Chronic Lymphocytic Leukemia [159] where silver nanoparticles interact with HIV-1 with size dependency [160]. There are some recent reports on specific bio-application for noble metal NPs, such as molecular diagnostics and therapy [161] or cancer applications [162]. Water dispersed supermagnetic iron oxide nanoparticles have been used in magnetic resonance imaging (MRI) for cancer infected cell detection. Titanium nanoparticles, nanocrystalline / helical rosette nanotubes (HA/HRN) hydrogel scaffold, HA hydroxyl apatite coated titanium, multiwall carbon nanotube (MWCNT) promise that boan, cartilage, vascular tissue will be repaired and grown without risk [163]. Lipid based nanostructures that have been developed for drug delivery applications include lipid nanotubes, lipid nanosphere, and lipid nanoparticles [164]. Functionalized carbon nanotubes can be used for drug design and discovery [165]. Folic acid, aptamers, lectins etc. can be attached to the magnetic nanoparticle surface. This enables targeting of magnetic nanoparticles to specific tissues or cells [166]. This strategy is applied in cancer research to target and treat tumors in combination with magnetic hyperthermia or nanoparticle-delivered cancer drugs.

Another potential treatment of cancer includes attaching magnetic nanoparticles to free-floating cancer cells, allowing them to be captured and carried out of the body. The treatment has been tested in the laboratory on mice and will be looked at in survival studies [167]. Magnetic CoPt nanoparticles are being used as a contrast agent in magnetic resonance imaging (MRI) for transplanted neural stem cell detection [168].

1.5.4. Optical field

Low dimensional materials are used for various purposes in optical field such as light emitting materials, for the development of non-linear optical materials, in lasing action etc.

1.5.4.1. Light Emitting materials

A new branch of optical engineering named 'nanophotonics' deals with light emitters including light emitting diods (LED) based on nanomaterials. CdSe/ZnS hybrid semiconductor nanomaterials are often used in different colour emitting optical purpose [169]. In 1987, a double layer organic light emitting diode (OLED) using thin films of 1,1-bis(4-(dip-tolylamino)phenyl)cyclohexane (TAPC) as a hole-transporting material and tris(8-quinolinolato)aluminum (Alq_3) as the emitter material sandwiched between transparent indium tin oxide (ITO) and an alloy of magnesium and silver was reported which exhibited a luminance of over 1000 cd m^{-2} at a operating voltage of 10V [170]. Subsequently, a single-layer OLED using a thin film of poly(p-phenylenevinylene), ITO/polymer/Ca, was reported in1990 [171]. These two reports have inspired researchers for extensive research and development of OLEDs from the standpoints of both fundamental science and potential technological applications for full color, flat-panel displays and lighting [172].

1.5.4.2. Development of nonlinear optical (NLO) materials

Nonlinear optics deals with the interaction of applied electromagnetic fields in various materials, which generates new electromagnetic fields altered in frequency, phase, or other physical properties. Future generations of optoelectronic devices for telecommunications, information storage, optical switching and signal processing are predicted to a large degree on the development of materials with exceptional NLO responses. A large number of organic π-conjugated molecules have been investigated in the last 30 years for suitability to function as components in hypothetical NLO materials [173]. Coherent NLO phenomena, such as second- and third-harmonic generations (SHG and THG respectively), depend explicitly on the crystallographic structure of a medium, as well as the polarization scheme. ZnO is a material of particular interest since studies of microcrystalline ZnO thin films have revealed large second-order nonlinearity, χ^2, a parameter that determines the efficiency of a material as a non-linear optical converter at optical frequencies. This indicates that low dimensionl ZnO structures are potentially useful as an effective frequency converter in the UV region. This might also find use as logic components in nanoscale optoelectronics.

1.5.4.3. Lasing Action

Nanowires with flat ends can be exploited as optical resonance cavities to generate coherent light on the nanoscale. To this end, Yang et al have observed room temperature UV-lasing from arrays of ZnO nanorods grown on sapphire substrates using the VLS method [174]. ZnO is a wide band band-gap (3.37 eV) compound semiconductor that is suitable for blue optoelectronic applications with ultraviolet lasing action already been reported in disordered particles and thin films [175]. Yang and

co-workers also observed lasing effects in GaN nanowires [176]. By creating p-n junctions in these individual nanowires, it might be possible to test the possibility of making electrically pumped UV and blue lasers out of individual nanowires. The chemical flexibility and one-dimensionality of these nanowires should make them ideal candidates for fabricating miniaturized laser light sources. These miniaturized nanolasers will find applications in nanophotonics and microanalysis.

1.5.5. Electronics field

Potential application of low dimensional materials is found in the electronics industry. Silicon based micro-device are replaced by nanomaterials. Silicon nanoparticles are being used in optoelectronic devices [177] whereas amorphous 'Si' and crystalline 'Si' based semiconductor nanoparticles are used to design modern molecular electronics. Many nanoscale electronic devices have been demonstrated such as tunnelling junctions, [178] devices with negative differential resistance [179] electrically configurable switches [180]. Devices have also been connected together to form circuits capable of performing single functions such as basic memory [181] logic function [182]. Semiconductor nanocrystals with controlled size, shape and chemical composition have been explored as the building blocks for thin film transistors. Organic field-effect transistors (OFETs) are expected to be a promising technology for low cost, flexible and large-area electronics for applications in displays, sensors, and memories. In addition to this, they have an advantage over silicon FETs for having lower processing temperature. The high charge carrier transporting ability of pyrene has also attracted attention for the fabrication of OFET devices. Thus, pyrene has found application as a semiconducting material for p-type OFETs fabricated via vacuum sublimation as well as ambipolar OFETs using a

single crystal of a pyrene derivative and also in organic light-emitting field-effect transistors (OLEFETs) [183].

1.5.6. Information storage field

Research is going on for information storage using magnetic nanoparticles. The most promising candidate for high-density information storage is the face-centred tetragonal FePt alloy. The grain sizes can be as small as 3 nm. If it is possible to modify the magnetic nanoparticles at this small scale, the information density that can be achieved with this media could easily surpass 1 TB (Terabyte) per square inch [184].

1.5.7. Energy field

Scientists are trying to manufacture different nanomaterials to improve energy harvesting, storage and utilization. Low dimensional materials are being commercially used in solar cell for energy harvesting exhibiting higher efficiencies [185]. Indium doped ZnO nanoparticles are incorporated in the buffer layers of organic solar cell [186]. ZnO, TiO_2, CdSe, CdS etc. nanoparticle based solar cell system is important for energy harvesting and storage [187]. RuO_2 nanoparticles have synthesized for energy storage application [188]. Nanotechnology provides LED which offers strong reduction of energy consumption for illumination i.e. maximum utilization of energy.

1.5.8. Magnetic field

Magnetic low dimensional materials can be widely used in magnetosensor, magnetoelctronics, data storage, computer devices, magnetic semiconductor, single electron devices etc. Hematite (Fe_2O_3)

and magnetite (Fe_3O_4) nano/micro materials in their different forms, especially α and γ forms, are predominant in the field of magnetic nanotechnology [189].

1.5.9. Thermal field

A new class of heat transfer fluid can be engineered by suspending metallic nanoparticles in conventional heat transfer fluids. Improvement of thermal properties like thermal conductivity, thermal diffusivity have been developed by using nanomaterials like Au, Al_2O_3, CuO in the form of nanofluids of Au/toluene, Al_2O_3/water, CuO/water [190]. It is found that Au nanoparticles can enhance the thermal transport into culture media nano fluid [191]. One of the benefits of nanofluids will be dramatic reductions in heat exchanger pumping power.

1.5.10. Waste water treatment

Owing to the presence of very large surface to volume ratio magnetic nanoparticles have a good potential for treatment of contaminated water [192]. For this purpose EDTA-like chelators are attached to carbon coated metal nanomagnets which results in a magnetic reagent for the rapid removal of heavy metals from contaminated water by three orders of magnitude to concentrations as low as micrograms per litre. Super-magnetic oxide nanoparticles (like meghemite, magnetite) hold much potential for waste water treatment since they have excellent biocompatibility.

References:

[1] P. Matagne, J.-P. Leburton, *Quantum Dots: Artificial Atoms and Molecules (Quantum Dots and Nanowires*), American Scientific Publishers , California, **2003**

[2] C.-W. Lai, Y.-H. Hsiao, Y.-K. Peng, P.-T. Chou, *J. Mater. Chem.,* 22, **2012,** 14403

[3] X. D. Pi, T. Yu, D. Yang, *Part. Part. Syst. Charact.,* 31**, 2014**, 751

[4] Y. Itoh, S. Hatakeyama, T. Kawashima, K. Washio, *J. Crystal Growth*, 426, **2015**, 61

[5] E. Tevaarwerk, P. Rugheimer, O.M. Castellini, D.G. Keppel, S.T. Utley, D.E. Savage, M.G. Lagally, M.A. Eriksson, *Appl. Phys. Lett*. 80 ,**2002**, 4626

[6] Y. Jiao, X. Gao, J. Lu, Y. Chen, J. Zhou, X. Li, *Mat. Letters,* 72, **2012**, 116

[7] J. Zhang, J. Gao, E.M. Miller, J.M. Luther, M.C. Beard, *ACS Nano*, 8, **2014**, 614

[8] Y.-m. Mo, Y. Tang, F. Gao, J. Yang, Y.-m. Zhang, *Ind. Eng. Chem. Res* 51, **2012**, 5995

[9] M.L. Landry, T.E. Morrell, T.K. Karagounis, C.-H. Hsia, C.-Y. Wang, *J. Chem. Edu.,* 91, **2014**, 274

[10] C. Li, D. Jiang, L. Zhang, J. Xia, Q. Li, *Langmuir,* 28, **2012**, 9729

[11] H. Uesugi, M. Kita, T. Omata, *J. Crystal Growth,* 416, **2015**, 134

[12] O.I. Micic, C.J. Curtis, K.M. Jones, J.R. Sprague, A.J. Nozik, *J. Phys. Chem.,* 98, **1994**, 4966

[13] Y. Yang, L. Xiong, J. Shi, M. Nogami, *Nanotechnology,* 17, **2006**, 2670–2674

[14] X. Bai, Y. Gao, H. Liu, L. Zheng, *J. Phys. Chem. C, 113,* **2009**, 17730

[15] A.K. Patra, A. Dutta, A.Bhuamik, *Catalysis Comm.* 11, **2010**, 651-655

[16] R. Nirmala, R. Navamathavan, J.J. Won, K.S. Jeon, A. Yousef, H.Y. Kim, *Mat. Sci. Engg. B,* 177, **2012**, 826

[17] D. Zhang, X. Ni, H. Zheng, *J. Colloid and Interface Science,* 292, **2005**, 410

[18] J.H. Yu, J. Joo, H.M. Park, S. Baik, Y.W. Kim, S.C. Kim, T. Hyeon, J. Am. Chem. Soc. 127, **2005**, 5662

[19] T. Shanmugapriya, R. Vinayakan, K. G. Thomas, P. Ramamurthy, *Crys. Engg. Comm.,* 13, **2011**, 2340

[20] H. Wei, Y. Wu, *Mat. Sci. and Engg.A,* 393, **2005**, 80

[21] S.Mandal, A.H.E. Müller, *Mat. Chem. and Phys.* 111, **2008**, 438

[22] D. Li, F. Meng, X. Yan, L.Yang, H. Heng, Y. Zhou, *Nanoscale Research Letters,* 8, **2013**, 535

[23] Y. Wang, Z.Li, X.Sheng, Z.Zhang, *The Journal of Chem. Phys*.126, **2007**, 16470

[24] Z. Liu, Y. Yang, J. Liang, Z. Hu, S. Li, S. Peng, Y. Qian, *J. Phys. Chem. B,* 107, **2003**, 12658

[25] R.-L. Zong, J. Zhou, Q. Li, B. Du, B. Li, M. Fu, X.-W. Qi, L.-T. Li, S. Buddhudu, *J. Phys. Chem. B*, 108, **2004**, 16713

[26] C. Wang, Y. Hu, C. M. Lieber, S. Sun, *J. Am. Chem. Soc.*, 130, **2008**, 8902

[27] F. Tian, Z.P. Huang, L. Whitmore, *Phys. Chem. Chem. Phys.,* 14, **2012**, 8537-8541

[28] Y. Lu, S. Du, R. Steinberger-Wilchens, *Applied Catalysis B: Environmental*, 164, **2015**, 389

[29] A.S. Ethiraj, D.J. Kang, *Nanoscale Research Letters*, 7, **2012**, 70

[30] S. Ramanathan, S. Patibandla, S. Bondyopadhyay, J.D. Edwards, J. Anderson, *J. Mat. Science,* 17, **2006**, 651

[31] S. Yan, L. Sun, Y. Sheng, N. Huang, Z. Xiao, *New J. Chem.,* 35, **2011**, 299

[32] B. Mayers, Y. Xia, *J. Mater. Chem.* **2002**, 12, 1875

[33] B. Gates, B. Mayers, B. Cattle, Y. Xia, *Adv. Func. Mater.,* 12, **2002**, 219

[34] Z. Xiao, L. Zhang, G. Meng, X. Tian, H. Zeng, M. Fang, *J. Phys. Chem. B*, 110, **2006**, 15724

[35] S. Iijima, T. Ichihasi, *Nature*, 363, **1993**, 603-605

[36] Q. Feng, *Inorg. and Metallallic Nanotubular Mat.* (*Topics in applied Physics),* Springer, Berlin, 117, **2010**, 73

[37] M. Nath, A. Govindaraj, C.N.R. Rao, *Adv. Mat.,* 13, **2001**, 283

[38] J. Yang, H. Wang, H. Zhang, *J. Phys. Chem. C,* 112, **2008**, 13065

[39] L. Scarabelli, M. Coronado-Puchau, J. Giner-Casares, L.M. Liz-Marzan, *ACS Nano*, 8, **2014**, 5833

[40] G. K. Christopher, T. Vo-Dinh, *J. Phys. Chem. C*, 112, **2008**, 18849

[41] A. Sarkar, S. Kapoor, T. Mukherjee, *J. Colloid and Interface Sc.,* 287, **2005**, 496

[42] J. Du, G. JhaO, Y. Shi, H. Yang, Y. Li, G. Zhu, Y. Mao, R. Sa, W. Wang, *Apl. Surf. Sc.,* 273, **2013**, 278

[43] D. Yuan, G.S. Wang, Y. Xiang, Y. Chen, X.Q. Gao, G. Lin, *J. Alloys Compd.* 478, **2009**, 489.

[44] S.-C. Lu, M.-C. Hsiao, M. Yorulmaz, L.-Y. Wang, P.-Y. Yang, S. Link, W.-S. Chang, H.-Y. Tuan, *Chem. Mat.* 27, **2015**, 8185

[45] G.-L. Xu, J.-T. Li, L. Huang, S.-G. Sun, *Nano Energy*, 2, **2013**, 394

[46] A. Ahmed, N.S. Gajbhiye, G. Joshi, *J. Solid State Chem.* 184, **2011**, 2209

[47] W. Hasan, J. Lee, J. Henzie, T.W. Odom, *J. Phys. Chem. C,* 111, **2007**, 17176

[48] C.Iida, M.Sato, M. Nakayama, A. Sanada, *Int. J. Electrochem. Sci,* 6, **2011**, 4730

[49] M. Tabatabaei, N.K. Zanjani, P. Torchio, A. Merlen, F.L. Labarthet, *J. Phys. Chem. C,* 117, **2013**, 14778

[50] M.N. Mankin, V. Mazumdar, S. Sun, *Chem. Mater.* 23, **2011**, 132

[51] Q. Zhang, C. Cobley, L. Au, M. McKiernan, A. Schwartz, L.-P. Wen, J. Chen, Y. Xia, *ACS Appl. Mater. Interfaces,* 1, **2009**, 2044

[52] W. Niu, Z.-Y. Li, L. Shi, X. Liu, H. Li, S. Han, J. Chen, G. Xu, Crystal Growth & Design, 8, **2008,** 4440

[53] R. Jin, S. Egusa, N. F. Scherer, *J.Am.Chem.Soc.,*126, **2004**, 9900

[54] W.-k. Koh, S.R. Saudari, A.T. Fafarman, C.R. Kagan, C.B. Murray, *Nano Lett.* 11, **2011**, 4764

[55] A.A. Umar, M. Oyama, *Crys. Growth Des*. 9, **2009**, 1146

[56] X. Teng, H. Yang, *Nano Lett.* 5, **2005**, 885

[57] J. Saida, M. Matsushita, A. Inoue, *J. Alloys Compd.* 342, **2002**, 18

[58] D. Horn, J. Rieger, *Angew. Chem., Int. Ed. 40*, **2001,** 4330

[59] H.-B. Fu, J.-N. Yao, *J. Am. Chem. Soc.* 123, **2001**, 1434

[60] X. Zhang, X. Zhang, W. Shi, X. Meng, C. Lee, S. Lee, *J. Phys. Chem. B,* 109, **2005**, 18777

[61] F. Pi, P. Dillard, R. Alameddine, E. Benard, A. Wahl, I. Ozerov, A. Charrier, L. Limozin, K. Sengupta, *Nano Lett.* 15, **2015**, 5178

[62] M. Lan, J. Zhang, X. Zhu, P. Wang, X. Chen, C.-S. Lee, W. Zhang, *Nano Research*, 8, **2015**, 2380

[63] J.J. ArmaoIV, Y. Domoto, T. Umehara, M. Maaloum, C. Contal, G. Fuks, E. Moulin, G. Decher, N. Javahiraly, N. Giuseppone, *ACS Nano,* 10, **2016**, 2082-2090

[64] M.R. Ghadiri, J.R. Granja, R.A. Milligan, D.E. McRee, N. Khazanovich, *Nature,* 366, **1993**, 324

[65] J. Y.Zheng, C. Zhang, Y.S. Zhao, J. Yao, *Phys. Chem. Chem. Phys.* 12, **2010**, 12935

[66] D.E. Martinez-Tong, G. Gbabode, C. Ruzié, B. Chattopadhyay, G. Schweicher, A.R. Kennedy, Y.H. Geerts, M. Sferrazza, *RSC Adv.*, 6, **2016**, 44921

[67] C. Zhang, P. Chen, J. Liu, Y. Zhang, W. Shen, H. Xu, Y. Tang, *Chem. Comm.,* 28, **2008**, 3290

[68] H. Yang, T.H. Lu, K.H. Xue, S.G. Sun, S.P. Chen, *J. Appl. Electrochem.* 27, **1997**, 428

[69] Z. Zhang, H. Che, Y. Wang, X. She, J. Sun, P. Gunawan, Z. Zhong, F. Su, *ACS Appl. Mater. Interfaces*, 4, **2012**, 1295

[70] K. Shimazu, D. Weisshaar, T. Kuwana, *J. Electroanal. Chem. and Interfacial Electrochem*., 223, **1987**, 223

[71] A. Mouraro, S.M. Wong, H. Seigenthaler, L.M. Abrantees, *J. Solid State Electrochem.*, 10, **2006**, 140

[72] J. Wu, H. Jheng, H. Cheng, L. Zhou, K.C. Leong, R. Rajagopalan, H.P. Too, W.K. Choi, *Langmuir,* 30, **2014**, 2206

[73] L. Si, L. Yue, D. Jin, *Cryst. Res. and Tech.,* 46, **2011**, 986

[74] P. Li, Y. Wei, H. Liu, X.-k. Wang, *J. Solid State Chem.* 178, **2005**, 855

[75] A. Phuruangrat, N. Ekthammathat, T. Thongtem, S. Thongtem, *J. Alloys and Compounds,* 509, **2011**, 10150

[76] S. Xuan, Y.-X.J. Wang, J.C. Yu, K.C.-F. Leung, *Chem. Mater*, 21, **2009**, 5079

[77] M. Meng, X. Wu, X. Zhu, L. Yang, Z. Gan, X. Zhu, L. Liu, P.K. Chu, J. Phys. Chem. Lett. 5, **2014**, 4298

[78] M. Chirita, A. Leta, *Crystal Growth and Design,* 12, **2012**, 883

[79] M. Mihai, S. Schwarz, P. Doroftei, B.C. Simionescu, *Crystal Growth and Design,* 14, **2014**, 6073

[80] T. Nomura, Y. Morimoto, M. Ishikawa, H. Tokumoto, Y. Konishi, *Adv. Powder Tech.* 21, **2010**, 8

[81] E. Toorisaka, S. Nagamatsu, Y. Saruwatari, M. Hirata, T. Hano, *J. Encapsulation and Adsorption Sciences,* 4, **2014**,114

[82] M. Fujiwara, K. Shiokawa, Y. Tanaka, Y. Nakahara, *Chem. Mat.* 16, **2004**, 5420

[83] K. Shimazu, K. Uosaki, H. Kita, Y. Nodasaka, *J. Electroanalytical Chem. and Interfacial Electrochem.* 256, **1998**, 481

[84] M. Watanabe, M. Uchida, S. Motoo, *J. Electroanalytical Chem. and Interfacial Electrochem.* 229, **1987**, 395

[85] M.A. Karakassides, D. Gournis, A.B. Bourlinos, P.N. Trikalitis, T. Bakas, *J. Mat .Chem.* 13, **2003**, 871

[86] Y. Deng, D. Qi, C. Deng, X. Zhang, D. Zhao, *J. Am. Chem. Soc.,* 130, **2008**, 28

[87] A. Jana, K.S.P. Devi, T.K. Maiti, N.D. Pradeep Singh, *J. Am. Chem. Soc.*,134, **2012**, 7656

[88] T.M. Figueira-Duarte, K. Mullen, *Chem. Rev.,* 111, **2011**, 7260

[89] C. Sanchez, P. Belleville, M. Popall, L. Nicole, *Chem. Soc. Rev.* 40, **2011**, 696

[90] B.K. An, S.K. Kwon, S.D. Jung, S.Y. Park, *J. Am. Chem. Soc.* 124, **2002**, 14410.

[91] K. Panthi, R.M. Adhikari, T. H. Kinstle, *J. Phys. Chem. A*, 114, **2010**, 4550

[92] Q. Li, Y. Jia, L. Dai, Y. Yang, J. Li, *ACS Nano,* 9, **2015**, 2689-2695

[93] B. Muthuraj, S.R. Chowdhury, P.K. Lyer, *ACS Appl. Mater. Interfaces,* 7, **2015**, 21226

[94] R.G. Alargova, V.N. Paunov, O.D. Velev, *Langmuir,* 22, **2006**, 7765

[95] H. Wang, W. Deng, L. Huang, X. Zhang, J. Jie, *ACS Appl. Mater. Interfaces*, 8, **2016**, 7912

[96] J. Lambrecht, T.P.I. Saragi, K. Onken, J. Salbeck, *ACS Appl. Mater. Interfaces,* 3, **2011**, 1809

[97] Y.-W. Chen, Y. Chang, R.-H. Lee, W.-T. Li, A. Chinnathambi, S.A. Alharbi, G.-H. Hsiue, *Langmuir,* 30, **2014**, 9139

[98] W. Xu, I. Choi, F.A. Plamper, C.V. Synatschke, A.H.E. Müller, V.V. Tsukruk, *ACS Nano*, 7, **2013**, 598

[99] S. Wang, P. Gao, I. Liebewirth, K. Kirchhoff, S. Pang, X. Feng, W. Pisula, K. Müllen, *Chem. Mater.* 23, 2011, 4960

[100] H. Xia, Y. Chen, G. Yang, G. Zou, Q. Zhang, D. Zhang, P. Wang, H. Ming, *ACS Appl. Mater, Interfaces,* 6, **2014**, 15466

[101] C. Zhou, J. Han, R. Guo, *J. Phys. Chem. B,* 112, **2008**, 5014

[102] Y. S. Zhao, W. Yang, G. Zhang,Y. Ma, J. Yao, *Colloids Surf. A,* 277, **2006**, 111

[103] H. Yoshikawa, K. Sasaki, H. Masuhara, *J.Phys.Chem.B,* 104, **2000**, 3429

[104] K.T. Petrova, S.S. Dey, M.T. Barros, *Carbohydrate Polymers,* 125, **2015**, 281

[105] J. Li, L. Chen, J. Xu, K. Wang, X. Wang, X. He, H. Dong, S. Lin, J. Zhu, *Langmuir* 31, **2015**, 13094

[106] E. Reverchon, A. Antonacci, *Ind. Eng. Chem. Res.,* 45, **2006**, 5722

[107] H.W. Ooi, B. Ketterer, V. Tronillet, M. Franzreb, C. Barner-Kowollik, *Biomacromolecules*, 17, **2016**, 280

[108] M.K. Klein, N.R. Saenger, S. Schuetter, P. Pfleiderer, A. Zumbusch, *Langmuir,* 30, **2014**, 12457

[109] K. L. Kelly, E. Coronado, L. L. Zhao, G. C. Schatz, *J. Phys. Chem. B*, 107, **2003**, 668

[110] Y. Xia, N.J. Halas, *MRS Bull* 30, **2005**, 338

[111] A. W. Wark, H.J. Lee, R.M. Corn, *Anal. Chem.* 77, **2005**, 3904

[112] A.J. Haes, C.L. Haynes, A.D. McFarland, G.C. Schatz, R.P. Van Duyne, S.L. Zou, *MRS Bull.* 30, **2005**, 368.

[113] K.S. Lee, M.A. El-Sayed, *J. Phys. Chem. B* 110, **2006**, 19220

[114] E. J. Shelley, D. Ryan, S. R. Johnson, M. Couillard, D. Fitzmaurice, P. D. Nellist, Y.Chen, R. E. Palmer, J. A. Preece, *Langmuir* 18, **2002**, 1791

[115] C. Novo, D. Gomez, J. Perez-Juste, Z.Y. Zhang, H. Petrova, M. Reismann, P. Mulvaney, G. V. Hartland, *Phys. Chem. Chem. Phys.* 8, **2006**, 3540.

[116] A.I. Ekimov, Al.L. Efros, A.A. Onushchenko, *Solid State Comm.* 56, **1985**, 921

[117] A.J. Nozik and R. Memming, *Phys. Chem.* 100, **1996**, 13061

[118] W.A. de Heer, A. Chltelain, D. Ugarte, *Science***,** 270, **1995**, 1179

[119] G. Mie, *Ann. Phys.* 25, **1908**, 377

[120] M.M. Alvarez, J.T. Khoury, T.G. Schaff, M.M. Shafigullin, I. Vezmar, R.L. Whetten, *J. Phys. Chem. B,* 101, **1997**, 3706.

[121] L. Jankovic, K. Dimos, J. Bujdak, I. Koutselas, J. Madejova, D. Gournis, M.A. Karakassides, P. Komadel, *Phys. Chem. Chem. Phys.* 12, **2010**, 14236.

[122] M.R. Phillips, O. Gelhausen, E.M. Goldys, *Solid State Physics,* 201, **2004**, 229-234

[123] B. Dierre, X.L. Yuan, N. Ohashi, T. Sekiguchi, *J. Appl. Phys.* 103, **2008**, 083551

[124] Y.H. Lee, Y. Yan, L. Polavarapu, Q.-H. Xu, *Appl. Phys. Lett.* 95, **2009**, 023105

[125] S. Rosenne, E. Grinvald, E. Shirman, L. Neeman, S. Dutta, O. Bar-Elli, R. Ben-Zvi, E. Oksenberg, P. Milko, V. Kalchenko, H. Weissman, D. Oron, B. Rybtchinski, *Nano Lett.* 15, **2015**, 7232

[126] Guozhong Cao, *Nanostructures and Nanomaterials: Synthesis, Properties, and Applications,* Imperial College Press, **2004**

[127] J.P. Bucher, D.C. Douglas, L.A. Bloomfield, Phys. *Rev. Lett.* 66, **1991**, 3052

[128] C.P. Bean, J.D. Livingston, *J Appl. Phys.* 30**, 1959**, 120s

[129] H. Wohltien, A.W. Snow, *Anal. Chem.* 70, **1998**, 2856

[130] P. Buffat, J.-P. Borel, *Phys. Rev.,* 13, **1976**, 2287

[131] K.J. Hanszen, *Z. Phys.* 157, **1960**, 523

[132] N.T. Gladkich, R. Niedermayer, K. Spiegel, *Phys. Stat. Sol.* 15, **1966**, 181

[133] M. Blackman, A.E. Curzon, *Structure and Properties of Thin Films,* Wiley, New York, **1959**

[134] B.T. Boiko, A.T. Pugachev, Y.M. Bratsykhin, *Sov. Phys. Sol. State* 10, **1969**, 2832

[135] M. Takagi, *J.Phys. Soc. Jpn.* 9, **1954**, 359

[136] V.G. Lyuttsau, Y.M. Fishman, I.L. Svetlov, *Sov. Phys. – Crystallogr.* 10, **1966**, 707

[137] G. Arlt, D. Hennings, G. de With, *J.Appl. Phys.* 58, **1985**, 1619

[138] S. Kundu, S. Lau, H. Liang, *J. Phys. Chem.C,* 113*,* **2009**, 5150

[139] N. R. Jana, Z. L. Wang, T. Pal, *Langmuir,* 16*,* **2000,** 2457

[140] S. Bhattacharjee, D.M. Dotzauer, M.L. Bruening, *J. Am. Chem. Soc.* 131/10, **2009**, 3601

[141] A. Hosseinnia, M. Keyanpour-Rad, M.Pazouki, *World Appl. Sci. J.,* 8, **2010**, 1327-1332,

[142] C. Wang, L. Salmon, Q. Li, M.E. Igartua, S. Moya, R. Ciganda, J. Ruiz, D. Astruc, *Inorg. Chem.* 55, **2016**, 6776

[143] K.K. Jain, *Clin. Chem*. 53, **2007**, 2002

[144] S. Maiti, G. Barman, J.K. Laha, *Appl. Nanoscience,* 6, **2016**, 529

[145] P. Nath, R.K. Arun, N. Chanda, *RSC Adv.* 5, **2015**, 69024

[146] Y. Ma, K. Promthaveepong, N. Li, **Anal. Chem,** 2016, (in press)

[147] S. Jongjinakool, K. Palasak, N. Bousod, S. Teepoo, *Energy Procedia,* 56, **2014**, 10

[148] K. Farhadi, M. Forough, R. Molaei, S. Hajizadeh, A. Rafipour, *Sensors and Actuators B,* 161, **2012**, 880-885

[149] B. Ding, M. Wang, X. Wang, J. Yu, G. Sun, *Material today,* 13/11, **2010**, 16

[150] H. Lee, T. Kang, K.A. Yoon, S.Y. Lee, S.W. Joo, K. Lee, *Biosens. Bioelectron.* 25, **2010**, 1669

[151] J.H. Kim, B.H. Chung, *Biosens. Bioelectron.,* 26, **2011**, 2805

[152] S.M. Shawky, D. Bald, H.M. Azzazy, *Clin. Biochem.* 43, **2010**, 1163

[153] F. Wei, R. Lam, S. Cheng, S. Lu, D. Ho, N. Li, *Appl. Phys. Lett*. 96, **2010**, 133702

[154] P.V. Baptista, M. Koziol-Montewka, J. Paluch-Oles, G. Doria, R. Franco, *Clin. Chem.* 52, **2006**, 1433

[155] D. Zhang, M.C. Huarng, E.C. Alocilja, *Biosens. Bioelectron,* 26, **2010**, 1736

[156] D. Tian, C. Duan, W. Wang, H. Cui, *Biosens Bioelectron.* 25, **2010**, 2290

[157] S.H. Chen, V.C. Wu, Y.C. Chuang, C.S. Lin, *J. Microbiol. Methods,* 73, **2008**, 7

[158] V. K. Sharma, R.A. Yngard, Y. Lin, *Adv. in Coll. and Intf. Sci,* 145, **2009**, 83

[159] R. Bhattacharya, P. Mukherjee, *Adv. Drug Delivery Review,* 60, **2008**, 1289.

[160] J.L. Elechiguerra, J.L. Burt, J.R. Morones, A. Camacho-Bragado, X. Gao, H.H. Lara, M.J. Yacaman, *J. Nanobiotechnol,* 3, **2005**, 6

[161] P.V. Baptista, G. Doria, P. Quaresma, M. Cavadas, C.S. Neves, I. Gomes, P. Eaton, E. Pereira, R. Franco, *Prog. Mol. Biol. Transl. Sci.* 104, **2011**, 427

[162] J. Conde, G. Doria, P. Baptista, *J. Drug. Deliv.* 2012, **2012**, Article ID 751075, 12 Pages

[163] L. Zhang, T.J. Webster, *Nano today,* 4/1, **2009**, 66.

[164] P. Verma, A. Ram, A.K. Jha, A. Mishra, A.Thakur, *Int. J. of Pharma. Sci. and Res.* 1, **2010**, 1

[165] M. Prato, K. Kostarelos, A. Bianco, Acc. Chem. Res. 41, **2008**, 60

[166] S. Kralj, M. Rojnik, J. Kos, D. Makovec, *J. Nanoparticle Research,* 15, **2013**, 1666

[167] K.E. Scarberry, E.B. Dickerson, J.F. McDonald, Z.J. Zhang, *J. Am. Chem. Soc.* 130, **2008**, 10258

[168] X. Meng, H.C. Seton, L.T. Lu, I.A. Prior, N.T.K. Thanh, B. Song, *Nanoscale*, 3, **2011**, 977

[169] J. Seol, R. Fudala, W.-J. Kim, R. Rich, B. Tabibi, H. Cho, Z. Gryczynski, I. Gryczynski, W. Yu, *Opt. Mater. Express,* 2, **2012**, 1026

[170] C.W. Tang, S.A. VanSlyke, C.H. Chen, *J. Appl. Phys.* 65, **1989**, 3610

[171] J.H. Burroughes, D.D.C. Bradley, A.R. Brown, R.N. Marks, K. Mackay, R.H. Friend, P.L. Burns, A.B. Holmes, *Nature,* 347, **1990**, 539

[172] Z. Liu, J. Qiu, F. Wei, J. Wang, X. Liu, M.G. Helander, S. Rodney, Z. Wang, Z. Bian, Z. Lu, M.E. Thompson, C. Huang, *Chem. Mater.,* 26, **2014**, 2368

[173] P.C. Ray, *Chem. Rev.*110, **2010**, 5332.

[174] M. Huang, S. Mao, H. Feick, H. Yan, Y. Wu, H. Kind, E. Weber, R. Russo, P. Yang, *Science*, 292, **2001**, 1897

[175] Z.K. Tang, G.L. Wong, P. Yu, M. Kawasaki, A. Ohtomo, H. Koinuma, Y. Segawa, *Appl. Phys. Lett.,* 72, **1998**, 3270

[176] J. Johnson, H.J. Choi, K.P. Knutsen, R.D. Schaller, R.J. Saykally, P. Yang, *Nature Mater.*, 1, 2002, 101

[177] E. Trave, V. Bello, F. Enrichi, G. Mattei, E. Borsella, M. Carpanese, M. Falconieri, C. Abate, N. Herlin-Boime, K. Jursiokova, F. Costa, L. Costa, L. Gini, *Opt. Mater.,* 27, **2005**, 6

[178] R. Compano, *Nanotechnology,* 12, **2001**, 85

[179] J. Chen, M.A.Reed, A.M.Rawlett, J.M.Tour, *Science,* 286, **1999**, 1550

[180] C.P. Collier, G. Mattersteig, E.W. Wong, Y. Luo, K. Beverly, J. Sampaio, E.M. Raymo, J.E. Stoddart, J.R. Heath, *Science*, 289, **2000**, 1172

[181] Y. Luo, C.P. Collier, J.O. Jeppesen, K.A. Nielsen, E. DeIonno, G. Ho, J. Perkins, H.R. Tseng, T. Yamamoto, J.E Stoddart, and J.R. Heath, *Chemphyschem.* 3, **2002**, 519

[182] A. Bachtold, P. Hadley, T. Nakanishi, C. Dekker, *Science,* 294, **2001**,1317

[183] M.L. Chabinyc, A. Salleo, *Chem. Mater.* 16, **2004**, 4509

[184] N. A. Frey, S. Sun, *Magnetic Nanoparticle for Information Storage Applications*, CRC Press, **2010**

[185] C.K. Huang, H.H. Lin, J.Y. Chen, K.W. Sun, W.-L. Chang, *Solar Energy Materials and Solar Cell,* 95, **2011**, 2540

[186] A. Puetz, T. Stubhan, M. Reinhard, O. Loesch, E. Hammarberg, S. Wolf, C. Feldmann, H. Kalt, A. Colsmann, U. Lemmer, *Solar Energy Materials and Solar Cell* 95/2, **2011**, 579.

[187] T. Kundu, S.C. Sahoo, R. Banerjee, *Cryst. Growth Des.* 12, **2012**,2572

[188] A. Devadas, S. Baranton, T.W. Napporn, C. Coutanceau, *J. Power Sources,*196, **2011**, 4044

[189] S. Mørup, M.F. Hansen, C. Frandsen, *Comprehen. Nanosci. & Technol.* 1, **2011**, 437.

[190] X. Zhang, H. Gu, M. Fujii, *Experiment. Therm. Fluid Sci.* 31, **2007**, 593

[191] J.L. Jiménez-Pérez, R. Gutierrez Fuentes, E. M. Alvarado, E. Ramón-Gallegos, A. Cruz-Orea, J. Tánori-Cordova, J.G. Mendoza-Alvarez, *Appl. Surf. Sci.* 255, **2008**, 701

[192] F.M. Koehler, M. Rossier, M. Waelle, E.K. Athanassiou, L.K. Limbach, R.N. Grass, D. Günther, W.J. Stark, *Chem. Commun.* 32, **2009**, 4862

Chapter II

Synthesis of low dimensional material

Synthesis of low dimensional material

Synthesis of low dimensional materials with well defined size and shape for various industrial applications is a great challenge to the scientists and researchers. Synthesis of these materials has been intensively followed up over the last few decades, not only for their scientific interest, but also for their many potential applications [1]. The basic principle for the synthesis of low dimensional materials is to produce a large number of particles with controlled size and shape with sufficient stability. There are two different approaches to synthesize low dimensional materials. These are (i) top-down approach, which utilizes physical methods and (ii) bottom-up approach, which applies solution phase chemical methods.

2.1. Top down Approach

The "top-down" approach means from top (larger) to bottom (smaller). This approach involves (Fig. 2.1) the production of the nano/micro particles by breaking larger materials into fine particles, or in other words "top-down" approach begins with a suitable starting material and then slicing or successive cutting of the bulk material to get nano/micro sized particles.

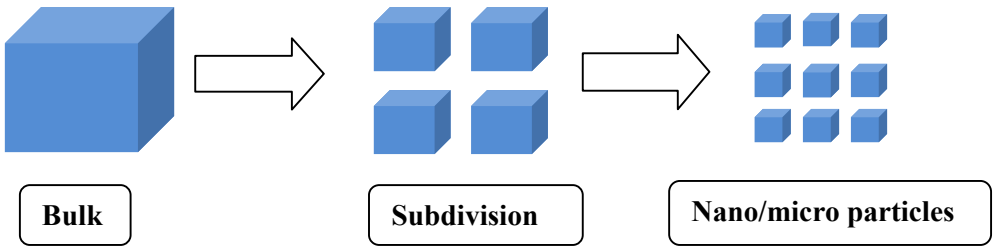

Figure 2.1: Schematic representation of 'top-down' approach.

This approach includes attrition, repeated quenching and lithography. Attrition can produce nanoparticles ranging from a couple of tens to several hundreds of nanometers in diameter. However,

nano/microparticles produced by top down approach have a relatively broad size distribution, contains a lot of impurities and structural defects on surface of the particles.

2.1.1. Physical methods

Top down approach comprises various physical methods like – Chemical vapour deposition (CVD), Physical vapour deposition (PVD), Laser ablation, Molecular beam epitaxy (MBE), Chemical beam epitaxy (CBE), Arc discharge method, Plasma synthesis, Electro-deposition, High energy ball milling, Ion beam techniques etc.

Chemical vapour deposition (CVD)

CVD is the process where a volatile compound of a material to be deposited is chemically reacted with other gases, to produce a non-volatile solid that deposits atomistically on a suitably placed substrate [2]. Non-agglomerated spherical oxide (SiO_2, TiO_2, ZrO_2) nanoparticles having diameters in the range of 10–40 nm has been prepared using an electrospray assisted chemical vapor deposition (ES-CVD) technique [3]. This process is mostly used in semiconductor industry for depositing thin films of various materials. In this process the substrate is exposed to one or more volatile precursors. These precursors decompose on the substrate and produce the desired deposit. In this process, vaporized precursors are made adsorbed onto a substance held at a high temperature. Usually temperature ~ 300 to 1200ºC is used at the substrate [4]. In CVD, Gas phase (homogeneous) reactions and surface (heterogeneous) reactions are intricately mixed. Some researchers have used this method as a means to form nanowires e.g. Ge nanowires were grown by Leon et al [5].

Physical vapour deposition (PVD)

PVD is a process of producing low dimensional materials where transferring growth species from a source and deposition of the species occurs on a substrate to form a thin film. The process proceeds atomistically and mostly involves no chemical reactions. The thickness of the deposits can vary from angstroms to millimetres. In general, those methods can be divided into two groups: evaporation and sputtering. In evaporation, the growth species are removed from the source by thermal means. In sputtering, atoms or molecules are dislodged from solid target through impact of gaseous ions (plasma). There are three main steps involved in this process viz. a) evaporating of a material to vapor phase, b) transportation of the material from source to the substrate, c) formation of the particle and thin film by nucleation and growth.Usually metals or metal oxides are evaporated from filaments of refractory metals like W, Ta, Mo in which the materials to be evaporated are held. Here particle size is small (<5 nm). Size, shape and phase of evaporated particles depend upon the gas and gas pressure of deposited chamber [6].

Laser ablation

Laser ablation is one of the most important physical methods for nanoparticle synthesis where laser beams have been used to evaporate a purified solid target. In this method micro/nanomaterials are deposited on a substrate in vacuum or inert gas phase or in a specified solvent. Absorption characteristics of the material to be evaporated determine the laser wavelength to be used. In order to obtain the high power density which is required in many cases, pulsed laser beams are generally utilized. Laser ablation has proven to be an effective technique for the deposition of complex films including complex metal oxides. One of the great advantages that laser ablation offers is the control of the vapor composition. In principle, the composition of the vapor phase can be controlled as that in

the source. The disadvantages of laser ablation include the complex system design, not always possible to find desired laser wavelength for evaporation, and the low energy conversion efficiency. Various research groups reported synthesis of various low dimensional materials using laser ablation method such as V. Amendola et al [7] reported synthesis of silver nanoparticles, M.Ganjali et al [8] reported synthesis of Ni nanoparticles, D.Jang et al [9] reported synthesis of metal nanoparticles including Cu, Al, Ag using this method.

Molecular beam epitaxy (MBE)

Molecular beam epitaxy can be regarded as a special case of evaporation for single crystal film growth, with highly controlled evaporation of a variety of materials in ultrahigh-vacuum of typically ~ 10^{-10} torr [10]. Besides the ultrahigh vacuum system, MBE mostly consists of realtime structural and chemical characterization capability, X-ray photoelectron spectroscopy (XPS), Auger electron spectroscopy (AES) etc. The main characteristics of MBE include low growth temperature, extremely clean environment, slow growth rate, simple growth mechanism, *in situ* analysis capability etc. which ensure formation of a highly pure epitaxial film having very smooth surface and interface. Synthesis of ZnO nanorods using MBE has been reported by Y.W.Heo et al [11]. A number of crystalline low dimensional materials like Si, ZnO, Mg–Zn–O Alloy, SiO_2-Cr, ZnSe etc. [12] has been fabricated using this method.

Chemical beam epitaxy (CBE)

CBE forms an important class of deposition techniques for semiconductor layer systems, especially III-V semiconductor systems. The epitaxial growth process is performed in an ultra high vacuum system under low pressure (gas pressure less than 10^{-4} Torr) conditions. The reactants are in the form of molecular beams of reactive gases, typically as the hydride or a metalorganic. Here, the

transport of gas occurs by viscous flow and chemicals reach the surface by diffusion and only surface kinetics are determining the chemical reactions leading to growth of the epilayer. CBE offers many advantages over MBE like easier muliwafer scaleup, better for production environment, absence of oval defects, lower drifts in effusion conditions etc. Various low dimensional material such as gallium nitride (GaN) nanowires have been prepared [13] using this method.

Arc discharge

Arc discharge method involves the generation of an electric arc between two graphite electrodes one of them is usually filled with catalyst metal powder (iron, nickel, cobalt, yttrium, boron, gadolinium etc.) in a He-atmosphere (sometimes in argon atmosphere). This process is used for the synthesis of carbon nanotube [14], carbon nanotube decorated with Pd nanoparticles [15], Au [16], WO_3 [17] etc. It is a common technique for the production of single walled carbon nanotubes (SWCNTs) where carbon is vaporised between the two electrodes. Small diameter, single-walled nanotubes can be synthesized using a DC arc welder to maintain the optimal settings between two horizontal electrodes in helium or argon atmosphere. Nanotubes of dichalcogenides such as MoS_2, $MoSe_2$, WS_2 etc. are also obtained by this technique.

Plasma synthesis

Plasma synthesis method has been successfully used in the synthesis and preparation of advanced materials such as ceramics, nanometric metallic powders, biomaterials and superconductors. The typical size of the nanoparticles produced by this method ranges from 20 to 100 nm depending on the quenching conditions employed.

Electro-deposition

Template-assisted electro-deposition is an important technique for the synthesis of metallic nanomaterials with controlled shape and size by this method, employing either an active or restrictive template as a cathode in an electrochemical cell. The surface of the cathode can be used as a template to synthesize various desired nanostructures or morphologies for specific applications.

High energy ball milling

It is one of the simplest ways for synthesis nano/micro particles of some metals and alloys in the powder form. There are various types of mills viz. planetary, vibratory, rod, tumbler etc. Usually one or more containers are used at a time to make fine particles. Hardened steel or tungsten carbide balls are put in containers along with powder of materials of interest. The containers are rotated at high speed around their own axis at temperature ranging from 100 to 1100ºC. By controlling the speed of rotation, it is possible to grind the material into low dimensional materials, whose size can be quite uniform. Some of the materials like Cr, Co, W, Ni-Ti, Al-Fe, Ag-Fe etc. are made nano/micro crystaline using ball mill [18].

Ion beam techniques

There are a number of examples in which high energy (few keV to hundreds of keV) or low energy (<200ev) ions are used to obtain low dimensional materials. Ion beam techniques can be used to synthesize low dimensional materials like Ni, Au, TiO_2, Fe-Pt alloy etc. [19].

2.2. Bottom up approach

Bottom-up approach means from bottom (smaller) to top (larger). This approach refers to the building-up of material from the bottom- atom by atom, molecule by molecule or cluster by cluster

(Fig.2.2). This approach can be grouped into two categories: thermodynamic equilibrium approach and kinetic approach. The thermodynamic approach consists of (a) super saturation of the solution, (b) nucleation and (c) particle growth. In kinetic approach, formation of nano/micro particles occurs in limited amount of precursors. This approach consists of chemical methods which are based on solution-phase colloidal chemistry. Using chemical methods various nano/micro particles with uniform size and shapes have been synthesized over the last few decades. Advantages associated with this approach are the produced nano/micro particles have fewer defects, more homogeneous chemical composition and better short and long range ordering etc.

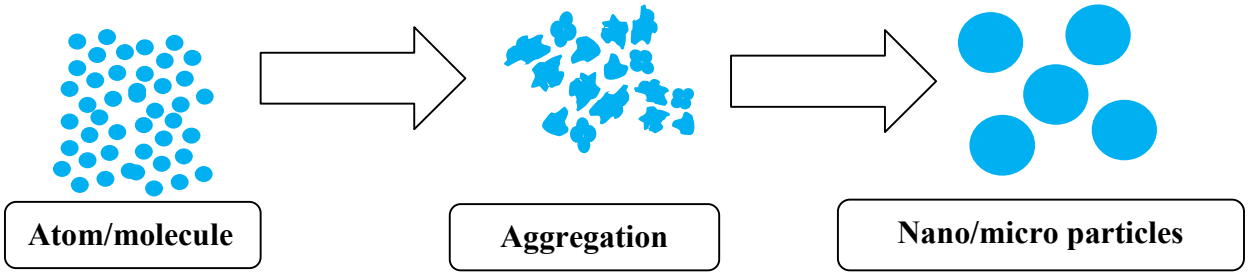

Figure 2.2: Schematic representation of 'Bottom-up' approach.

2.2.1. Mechanism of bottom up approach

The growth of low dimensional materials involves the process of precipitation of a solid phase from the solution phase. The solubility of a solute is constant for a given solvent at a particular temperature; as a result addition of any excess solute will result in precipitation and formation of nano/micro particles. Thus to form nano/micro particles nucleation is the first requirement and for that the solution must be super-saturated either by directly dissolving the solute at higher temperature and then cooling it to low temperature or by adding excess solute to make it super saturated. The precipitation processes then basically consists of a nucleation step followed by particle growth step [20]. Generally there are three kinds of nucleation processes: homogeneous nucleation,

heterogeneous nucleation and secondary nucleation. Homogeneous nucleation occurs in the absence of a solid interface by combining solute molecules to produce nuclei. A supersaturated solution possesses high Gibbs free energy (ΔG). This free energy (ΔG) is the sum of free energy due to the formation of a new volume and free energy due to new surface created. For spherical particles,

$$\Delta G = \frac{4}{V}\pi r^3 K_B T \ln(S) + 4\pi r^2 \gamma$$

Where V is the molecular volume of the precipitated species, r is the radius of the nuclei, K_B is the Boltzmann constant, S is the saturation ratio and γ is the surface free energy per unit surface area. When S > 1, ΔG has a positive maxima at a critical size (r^*). This maximum free energy is the activation energy for nucleation (Fig. 2.3). Nuclei larger than the critical size will further decrease their free energy and form stable nuclei which grow to form particles. The critical nuclei size can be obtained as follows-

$$\frac{d\Delta G}{dr} = 0 \qquad\qquad r^* = \frac{2V\gamma}{3K_B T \ln(S)}$$

After the initial nucleation, both the super-saturation of the growth species and the change in Gibbs free energy decreases. When the concentration reaches below the super-saturation, nucleation stops and the particles continue to grow by molecular addition until the equilibrium concentration of the precipitated species is reached. Uniform size distribution is achieved through a short nucleation processes that generates all the particles obtained at the end of reaction. Due to the large free energy for smaller particles than the larger ones, the smaller particles grow more rapidly than the larger one. On the other hand, when the reactants are consumed due to particle growth, Ostwald ripening will occur where larger particles grow and smaller ones get smaller and finally dissolved. Actually

Ostwald ripening occurs when saturation ratio (S) decreases and corresponding critical size (r^*) increases.

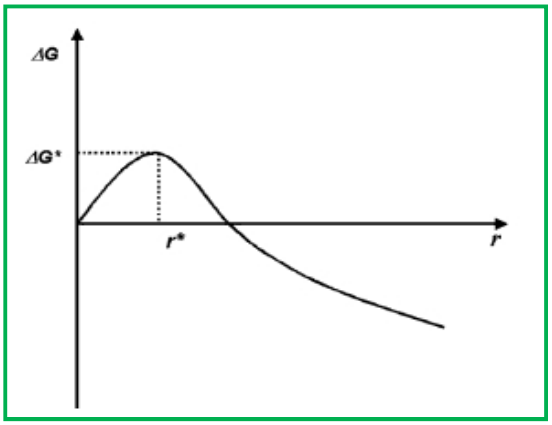

Figure 2.3: Plot showing the change in overall free energy (ΔG) as a function of particle size (r).

If the reaction stops speedily at this stage the particles have a broad size distribution. In addition to that, another type of growth process occurs, where soluble species are deposited on the solid surface, particles can grow by aggregation with other particles, which is known as secondary growth process. The rate of particle growth is much faster in secondary growth process than the growth occurs by homogeneous and heterogeneous process.

2.2.2. Stabilization of low dimensional materials

By the time of nucleation of any colloid, it faces many possible facts such as re-dissolution, ripening, coagulation or stabilization. The chief practical challenge is to prevent coagulation as that reduces the efficiency of the particles, for example, during catalysis the coagulation of colloidal particles used as catalyst leads to a significant loss of activity. The stabilization of low dimensional materials is a crucial aspect during their synthesis [21]. The van der Waals forces attract two particles

each other at short inter-particle distance. Consequently, in the absence of repulsive forces opposed to the van der Waals forces, the colloidal particles aggregate. Therefore, the use of a stabilizing agent is necessary to induce a repulsive force opposed to the van der Waals force to provide stability to nano/micro particles in solution. There are four kinds of stabilization procedures: (i) electrostatic stabilization, (ii) steric stabilization, (iii) electro-steric stabilization and (iv) stabilization by a ligand or solvent.

Electrostatic stabilization

The basic principle of electrostatic stabilization lies on manipulation of the balance between attractive and repulsive forces between the nano/microparticles. This plays an important role in dilute systems where the impact of charge can be quite effective. Ionic compounds such as halides, carboxylates or polyoxoanions, dissolved in aqueous solution can render the electrostatic stabilization. The adsorption of these compounds and their related counter ions on the particle surface generate an electrical double-layer around the particles (Fig. 2.4).

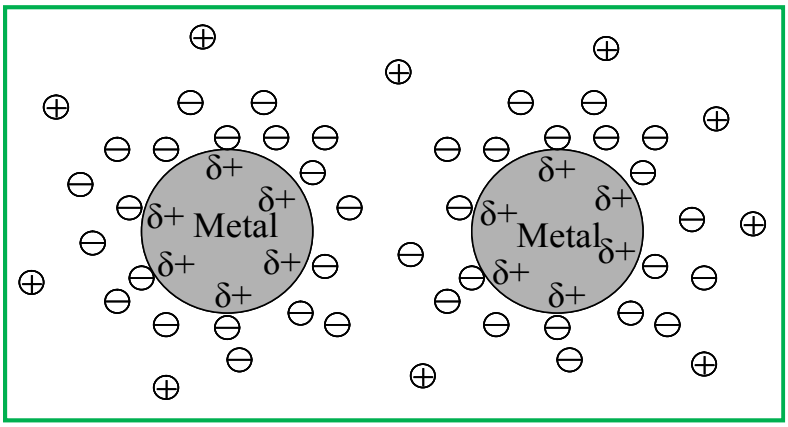

Figure 2.4: Schematic representation of electrostatic stabilization of colloids.

This leads in a Columbic repulsion between the particles [22]. If the electric potential associated with the double layer is high enough, then the electrostatic repulsion will prevent particle aggregation. Electrostatic stabilization is a kinetically controlled stabilization method.

Steric stabilization

Steric stabilization method is another method by which metal nano/microparticles can be prevented from aggregation (Fig. 2.5). It offers an additional advantage in the synthesis of nano/micro particles, particularly when narrow size distribution is required.

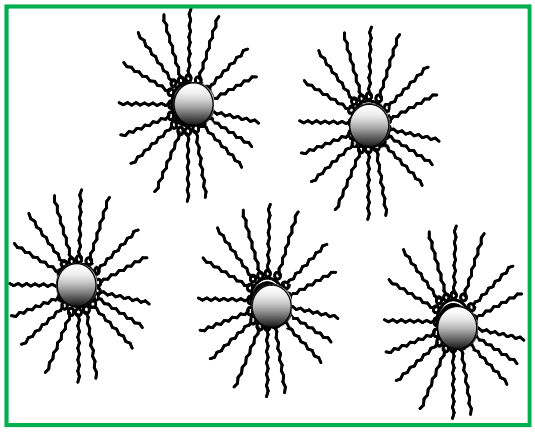

Figure 2.5: Schematic representation of steric stabilization of low dimensional materials.

The adsorption of the molecules such as polymer layer, long chain amines and thiols [23] on the surfaces of the particles provide a diffusion barrier to the growth species, resulting in a diffusion-limited growth in the subsequent growth of nuclei. Diffusion-limited growth reduces the size distribution of the initial nuclei which leads to the formation of mono-dispersed nano/micro particles. In presence of non-ionic group the hydrophobic interactions would bind the tail group to the nano/micro particles extending the polar head groups into solution. The polar head groups are hydrated and thereby provide a steric barrier preventing particle aggregation. Due to the advantage of

the dual functionalities of polymeric layer on the surface of the particles, steric stabilization is widely used in the synthesis of low dimensional materials.

Electrosteric stabilization

Sometimes both the electrostatic and steric stabilization are combined to obtain stable metallic nanoparticles in solution [24]. Generally, ionic surfactants provide this kind of stabilization. These surfactants bear a polar head group which can generate an electric double layer and a lypophilic side chain capable of providing steric repulsion (Fig. 2.6).

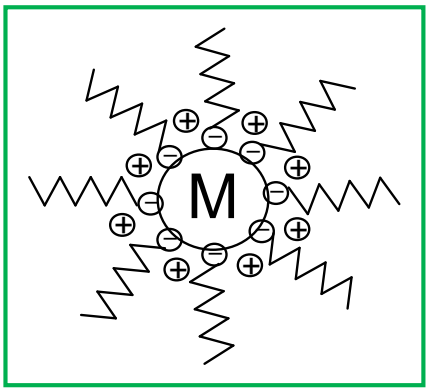

Figure 2.6: Schematic representation of electrosteric stabilization of low dimensional materials.

The electrosteric stabilization can also be generated from polyoxoanions such as the couple ammonium (Bu_4N^+)/polyoxoanion ($P_2W_{15}Nb_3O_{62}^{9-}$). The significant steric repulsion exerted by bulky Bu_4N^+ cations associated with the highly charged polyoxoanion counter anions provide an effective electrosterical stability toward agglomeration of the produced nano/micro clusters in solution.

Stabilization by ligand or solvent

Templated synthesis of low dimensional materials utilizes a prefabricated structure to collect multiple, discrete nano-objects into a larger, well-defined, ordered architecture. Ligands or polymers, especially solvent-soluble polymers, with some affinity for metals are often used as stabilizers of metal nanoparticles [25]. These functional polymeric materials include polyvinyl alcohols, cellulose, poly-(hydroxymethyl)acrylate, polychloromethylstyrene, polyacrolein, polyglutaraldehyde, polymethyl silica and so on. Sulphur-containing ligands [26], such as, xanthates and disulfides, resorcinarenetetrathiols and di- and trithiols have also been used to stabilize nanoscale materials. Other ligands e.g., carboxylate, amine, iodine, phosphine, phosphine oxide, isocyanide, acetone have also been used for this purpose [27].

2.2.3. Synthetic methods of low dimensional material by Bottom up approach

Various synthetic methods are used for the synthesis of low dimensional materials in the form of quantum dots, spheres, rods, tubes, wires, plates, thin films etc. Synthetic methods of low dimensional materials can be classified in two categories viz. chemical methods and biological methods. The method to be used depends upon the material of interest, dimensionality of the material viz. 0D, 1D or 2D material, size and quality etc.

2.2.3.1. Chemical methods

There are various chemical methods or “Bottom up” techniques for the preparation of low dimensional materials. Chemical methods have some advantages over the physical methods e.g. (a) simple techniques, (b) inexpensive, (c) less instrumentation required, (c) fine tuning of particle size

and shapes are possible, (d) require low temperature (<300ºC) (e) less time consuming etc. Different types of chemical methods are described below.

Photochemical method

Photochemical reduction of metal ions in solution is an important pathway of noble metal nanoparticle generation. In this method light of different wavelengths are irradiated either directly to a metal precursor, or with photosensitizers as intermediate species. In the most cases UV light is irradiated to produce radicals from a photosensitizeror from an appropriate solvent. Mainly ketyl radicals are produced which have been established as powerful reducing agents involved in metal ion reduction process [28]. Size of the synthesized nanoparticles can be controlled by controlling the concentration of metal ion precursor, frequency of induced light and exposure time. A. Callegari et al have demonstrated that the size and shape of silver nanoparticles can be controlled by choosing the wavelength(s) of light used to drive the photochemical growth [29]. A photochemical reduction of Au^{3+} with 254 nm UV light irradiation for about 30h in an aqueous solution of cetyl trimethyl ammonium bromide (CTAB) and tetradodecyl ammonium bromide (TDAB) lead the formation of gold nanorods [30]. Using photochemical reduction method Ag nanostructures such as nanorods and nanowires can be synthesized in the presence of citrate-capped Pt seeds at room temperature [31]. Besides noble metal nanoparticles, various other nanoparticles can also be prepared using this method such as Bismuth sulfide (Bi_2S_3) nanofibers have been successfully prepared by a photochemical method from an aqueous solution of bismuth nitrate ($Bi(NO_3)_3$) and thioacetamide (TAA) in the presence of complexing agents of nitrile triacetic acid (NTA) at room temperature [32]. Well-dispersed M@TiO2 (M = Ag, Pd, Au, Pt) nanocomposite particles with a diameter of 200–400 nm have been synthesized on a large scale by a clean photochemical route [33].

Solvothermal or hydrothermal method

In solvothermal method a metal precursor and a solvent is heated at a temperature well above the boiling point of the solvent by the increase in autogenous pressure resulting from heating. When the solvent is water the process is known as hydrothermal process. The temperature and pressure above the critical point of any solvent is said to be supercritical. Supercritical fluids exhibit characteristics of both a liquid and a gas. Supercritical fluids exhibit high viscosity and easily dissolve chemical compounds that would exhibit very low solubility under ambient condition. Silver nanostructures have been synthesized through simple solvothermal method by reducing silver nitrate (AgNO3) with ethylene glycol (EG) and using poly(vinylpyrrolidone) (PVP) as an adsorption agent [34]. Zhiqiang Yang et al have prepared silver nanowires by one-pot hydrothermal reduction process using only silver nitrate and sodium citrate; without any external seed or templte [35]. Single crystal ZnTe nanorods with diameters of 30-100 nm and lengths of 500-1200 nm were synthesized using Zn and Te metal powders as reactants and hydrazine hydrate as solvent by a solvothermal process [36].

Sonochemical approach

Low dimensional materials with tunable size and morphologies can be prepared through sonochemical method. When an ultrasonic irradiation (20 kHz to10 MHz) is applied to a solution acoustic cavitations are formed and these ultrasonic cavitations are concerned with the formation, growth and implosive collapse of bubbles. Transient localized hot spots with a variety of physical and chemical effects like extremely high temperature, pressure and cooling rate are created by these bubbles which could provide a unique environment for chemical reactions under extreme condition. Chemical bonds are snapped under such extreme condition and metallic nano/micro particles are created from the decomposition of volatile precursors within these rapidly collapsing bubbles. Crystalline CuS nanoplates with average sizes of about 20–40 nm have been successfully synthesized

without any surfactant by a sonochemical approach under ambient conditions [37]. ZnSe nanoparticles have been prepared by the sonochemical irradiation of an aqueous solution of selenourea and zinc acetate under argon environment [38]. TiO_2 nanoparticles were prepared through a simple sonochemical method with initial treatment in alkaline medium [39]. By applying a very intense ultrasound to aqueous $AgNO_3$ solution Ag nanoparticles have been synthesized [40].

Electrochemical method

Various metal and semiconductor nanoparticles have been prepared via electrochemical oxidation/reduction within a simple two-electrode type cell. Gold nanorods have been synthesized via this method by using a gold metal plate as anode and a platinum plate as cathode immersing in an electrolytic solution consisting of a cationic surfactant cetyl trimethyl ammonium bromide (CTAB) and a rod inducing co-surfactant tetra octyl ammonium bromide (TOAB) [41]. Many other nanostructures such as Ag nanoparticles [42], TiO_2 nanoparticles [43] etc. have also been prepared by this method.

Microwave irradiation method

One of the important methods for the synthesis of low dimensional materials is microwave irradiation method. Microwave radiation heats up a material through its dielectric loss, which converts the radiation energy into thermal energy. Microwave irradiation leads to a faster heating rate than the conventional heating through conduction and convection. During microwave heating interaction occurs between the electric field of microwave radiation and dipole moment of molecules. Hence the polar solvents like water and ionic liquids are the best solvents in microwave synthesis. Polar solvent and reactant molecules are heated instantaneously under microwave exposure within very short time resulting uniform nucleation and homogeneousness in the formation of nanoparticles. Uniform Ag nanoparticles are synthesized by microwave irradiation of a starch and silver nitrate

solution [44]. Size-controlled stable Au nanoparticles (NPs) are synthesized in large quantities in the presence of poly(*N*-vinyl-2-pyrrolidone) (PVP) under microwave heating for just 60 s in aqueous solutions [45]. Synthesis of metal oxide nanostructures including transitional metal oxide, metal ferrite, rare earth metal oxide like Fe_2O_3, ZnO, TiO_2 and CeO_2, were carried out by microwave-assisted route through the thermal decomposition of their respective metal precursors. [46]. Fluorescent carbon nanoparticles have been synthesized by microwave pyrolysis [47] of citric acid in presence of ethylene diamine.

Sol-gel method

The sol-gel process, as the name implies, involves the evolution of inorganic networks through the formation of a concentrated colloidal suspension of metallic oxide or hydroxide (sol) and gelation of the sol by dehydrating through evaporation or solvent extraction to form a semi-liquid continuous network (gel). Sols are a subclass of colloids in which solid particles are dispersed in a liquid whereas gels are the continuous networks of particles with pores filled with a liquid. This method is well adapted for oxide nanoparticles and composite nanopowder synthesis. The main advantages of this method for the preparation of nanomaterials are low temperature of processing, versatility and flexible rheology allowing easy shaping and embedding of particles. They offer unique opportunity for access to organic-inorganic materials. The most commonly used precursors of oxides are alkoxides, due to their commercial availability and high liability M-OR bond during processing. There are reports on the synthesis of low dimensional materials through sol-gel method such as nickel ferrite ($NiFe_2O_4$) nanoparticles [48], SnO_2 nanoparticles [49], Ag-TiO_2 nanoparticles [50] etc.

Chemical reduction

Chemical reduction is the commonest method for synthesis of metal nanoparticles as it involves very simple preparation technique and requires simple and inexpensive equipment. In this

method metal salts, dissolved in an appropriate solvent in presence of surfactants or surface passivators, are reduced using a suitable reductant to prepare metal nanoparticles. There are a large number of reports of nanostructure synthesis in the literature using various reductants such as sodium borohydride [51,52], hydroxyl amine [53], ascorbic acid [54,55], citric acid [56], DMF [57], ethyl alcohol [58,59], aldehydes [60], PVP [61], sugars [62], ethylene glycol [63-65], tin acetate [66], pectin [67] etc. In solution phase chemical reduction method encapsulating agent is used to control the shape of the synthesized nanoparticles in addition to the stabilization. For example, CTAB can induce the formation of nanorods like Ag nanorods [68], Au nanorods [69].

Seed-mediated growth

Synthesis of anisotropic low dimensional materials via seed-mediated growth method is one of the most favoured ways towards the large-scale production of nano/micro particles. Synthesis of anisotropic metal nanoparticles through seed-mediated growth method involves two steps. In the first step metal seed sol is produced by reducing metal salt solution with a strong reducing agent such as $NaBH_4$ in presence of a stabilizing agent. In the second step a growth solution containing meat salt, a stabilizing agent and a mild reducing agent such as ascorbic acid, is prepared. To this growth solution a small amount of seed sol is added to generate anisotropically grown metal nanoparticles. There are reports of synthesis of metal nanoparticles via seed-mediated growth approach in the literature such as multishaped gold nanoparticles (like spherical nanoparticles, bipyramids, nanorods, nanowires, T- and star-shaped nanoparticles, and triangular nanoplates) [70], silver nanorods [71] etc.

2.2.3.2. Biosynthesis Methods

Although the physical and chemical methods discussed earlier, can successfully produce well-defined low dimensional materials, these are usually expensive and involve the use of toxic chemicals. The chemical synthesis method may contribute to the presence of some toxic chemical

species being adsorbed on the surface of nanoparticles which may lead to adverse effects in medical applications. These nanoparticles may even have direct contact with the human body in which their associated toxicity become critical. Thus, one of the elementary goals of nanotechnology is to devise eco-friendly production methods that can produce nanoparticles without toxicity or with low toxicity. To achieve this goal, researchers have paid their attention towards biological methods for the synthesis of metal nanoparticles. Biosynthesis employing the enzymes, carbohydrates, proteins, lipids, DNA etc. of living organisms such as bacteria, fungi, algae, plants and plant products etc. become important for metallic nanoparticle synthesis.

Biosynthesis using bacteria

Microorganisms such as bacteria have developed a mechanism to detoxify the adjacent cell environment by reducing the toxic metal species into metal nanoparticles [72]. Many metal nanoparticles have been synthesized using various bacteria. Ag nanoparticles have been synthesized using different bacteria such as *Bacillus cereus* [73], *Bacillus flexus* [74], *Bacillus licheniformis* [75], *Bacillus thuringiensis* [76], *Brevibacterium casei* [75], *Corynebacterium* [77], *Escherichia coli* [78], *Klebsiella pneumonia* [79], *Lactobacillus farciminis* [80], *Lactobacillus fermentum* [80], *Lactobacillus plantarum* [80], *Pseudomonas stutzeri* [81], *Staphylococcus aureus* [82], *Stenotrophomonas maltophilia* [83], *Ureibacillus thermosphaericus* [84]. Au nanoparticles have been synthesized using various bacteria like *Actinobacter spp.* [85], *Bacillus licheniformis* [86], *Bacillus subtilis* [87], *Escherichia coli* [88], *Lactobacillus* [89], *Pseudomonas aeruginosa* [90], *Rhodobacter capsulatus* [91], *Rhodopseudomonas capsulate* [92], *Stenotrophomonas maltophilia* [93]. Pd nanoparticles having 50 nm size have been synthesized using *Desulfovibrio desulfuricans* [94].

Biosynthesis using fungi

A number of different taxonomic group of fungi have been investigated for the synthesis of metal nanoparticles and it has been found that fungi are very good candidates for generation of nano/micro particles as they secretes extracellular enzymes, that are responsible in reduction as well as stabilization of low dimensional materials. In addition to good monodispersity, nanoparticles with well-defined dimensions can be obtained by using fungi. This was first proven by Mukherjee *et al.* [95], where bioreduction of aqueous $AuCl_4$ was carried out using the fungus *Verticillium* species that produce gold nanoparticles with well-defined dimension and good monodispersity. Extracellular silver metal nanoparticles in the range of 20–50 nm have been produced by several *Fusarium oxysporum* strains [96]. Riddin *et al.* [97] have reported the biosynthesis of platinum nanoparticles having diameter in the range of 100-180 nm using the fungus *Fusarium oxysporum*. The fungi *Aspergillus flavus, Aspergillus funigatus* and *Phanerochaete chrysoparium* as well as white rot fungus *Coriolus versicolar* [98] produce stable silver nanoparticles from silver nitrate in aqueous medium.

Biosynthesis using algae

Green algae are enriched with electro-active pigments Chlorophyll A and B, along with carotenoids to capture energy from sunlight and store in food. Nowadays, various algae are being used in eco-friendly biosynthesis of metallic nanoparticles. J. Xie et al. [99] reported the synthesis of gold nanoplates using the extract of unicellular green alga *Chlorella vulgaris* . Intracellular synthesis of gold nanoparticles was accomplished at 25ºC and pH 7 using Fe (III)-reducing bacterium *Shewanella algae* (ATCC 51181). In this microbial reductive synthesis insoluble gold were deposited from $AuCl_4$ ions and the biogenic gold nanoparticles of 10-20 nm were laid in the periplasm [100]. G. Singaravelu et al. [101] proposed a synthesis procedure for rapid extracellular biosynthesis of gold nanoparticles using a marine alga *Sargassum wightii*.

Biosynthesis using Bio-molecules

The ability of different sugars as reducing agents for the synthesis of metallic nanoparticles was demonstrated by Panigrahi *et al.* [102]. Silver nanoparticle synthesis has also been reported using pure enzymes like lysozyme [103]. Wangoo *et al.* [104] demonstrated the preparation of Au nanoparticles in water directly by complexion with glutamic acid, where the amino acid acted as both the reducing and the stabilizing agent in a single one-step process. It was found that bovine serum albumin (BSA) could synthesize Au nanoplates in high yield, under acidic conditions at physiological temperature (37°C), by using its innate reducing and shape directing capabilities [105].

Biosynthesis using plant

Synthesis of low dimensional materials using plant biomass and plant extracts is a comparatively simple and cost-effective method than microorganism-mediated synthesis. This is especially useful if low-cost agricultural waste is used for this purpose, which is in compliance with the concept of "waste to wealth". Green plants or died plant parts contain immense amount of monosaccharide like glucose, fructose etc., polysaccharide like starch or cellulose etc., enzymes, proteins, vitamins, flavonoids, terpenoids, alkaloids etc. which are involved as either reducing or capping agents during the formation of nanoparticles, and their concentrations are vital in the shape directing process [106]. In an extracellular synthesis, Geranium (*Pelargonium graveolens*) leaf extract was used for the rapid reduction of silver ions resulting in the generation of silver nanoparticles in the size range 16-40 nm with an average size ~ 27 nm [107]. A leaf extract of *Cassia auriculata* has been used to synthesize spherical and triangular gold nanoparticles (15~25 nm) within 10 min at room temperature [108]. Pd nanoparticles have been synthesized using the leaf extract of *Cinnamomum camphora* [109], *Gardenia jasminoides Ellis* [110]. Cu nanoparticles have been synthesized by using the plant extract of *Magnolia kobus* [111].

2.2.3.3. Synthesis of organic low dimensional materials

Besides inorganic low dimensional materials organic nano/microparticles have also been investigated extensively during the last decade. Various methods have been developed to synthesize organic low dimensional material such as physical vapour deposition, reprecipitation, microemulsion, ultra-sonication, self-assembly in the liquid phase, self-assembly with solvent evaporation etc.

Physical vapour deposition (PVD) method

PVD is an effective and feasible method for the synthesis of low dimensional materials such as organic nano/micro materials, polymeric thin films and inorganic-polymer nanocomposites. However, the monodispersity of the synthesized materials is hard to control when small organic molecules are picked out as deposition sources. Synthesis of supported single-crystalline organic nanowires by PVD has been reported in the literature [112].

Reprecipitation method

Reprecipitation method is the most facile and commonly used method for the synthesis of organic low dimensional materials. In a typical synthesis, micro amount of a concentrated stock solution of an organic compound dissolved in a good solvent e.g. THF, acetonitrile, cyclohexane etc. is rapidly mixed, into macroamount of poor solvent e.g. water [113]. It is supposed that the rapid mixing of the stock solution and the poor solvent changes the micro-environment of the target compound molecules. The molecules are exposed to the poor solvent surroundings in a very short time, inducing the nucleation and growth of the molecules in nanoparticles. Various organic low dimensional materials such as nanoparticles [114, 115], nanosheets [116], sub-microtubes [117] etc. have been prepared by reprecipitation method.

Microemulsion method

Synthesis of low dimensional materials by microemulsion method is an area of considerable interest of researchers as it enables control of particle properties such as size, geometry, morphology, homogeneity and surface area [118]. Various microemulsion systems have been exploited to synthesize organic nanoparticles of cholesterol, rhodiarome, rhovanil, retinol [119]. The microemulsions used are AOT/heptanes/water, triton/decanol/water and CTAB/hexanol/water. The preparation of these organic nanoparticles involves the direct precipitation of the active compound in the aqueous cores of the microemulsion due to its insolubility in water. Organic nanoparticles of pharmaceutical interest like amoxicillin nanostructures have also been synthesized by this method [120].

Ultra-sonication method

Application of ultrasound has also attracted considerable interest for the development of organic nano/microparticles. Suslick et al pioneered sonochemical synthesis of protein microspheres. They showed that simple sonication of a protein solution like serum albumin produces microcapsules filled with air or a nonaqueous liquid [121,122]. These biocompatible and stable microspheres are of particular interest in various biomedical applications including use as contrast agents for magnetic resonance imaging (MRI), sonography, and optical coherence tomography (OCT) as well as oxygen or drug delivery carriers.

Self-assembly in liquid phase

Molecular self-assembly in liquid phase is a strategy used for nanofabrication involving designing of molecules and supramolecular entities. The self-assembly of organic molecules leading to the formation of nanostructures requires driving forces from the molecules themselves like hydrogen bond, π-π stacking, van der Waals interaction etc. [123]. Sometimes trigger from the

surroundings like the interactions between the organic molecules and the solvents is required for the self-assembly. Morphology-controllable synthesis of various pyrene nanostructures from nanoparticles to short nanorods and nanowires (long nanorods) was achieved by a simple self-assembly method [124].

Self-assembly with solvent evaporation

Most of the organic materials dissolved in certain solvents will aggregate and self-assemble when the solvents are evaporated. However, the size, shape and uniformity of the assembled products are not easy to control, especially in the nanometer scale, although it is possible to achieve well-defined macroscopic single crystals. Recently, Yao et al have introduced sonication to the solvent evaporation process and prepared 2,4,5-triphenylimidazole (TPI) 1D nanomaterials with tunable morphologies [125].

References

[1] Y. Xia, P. Yang, Y. Sun, Y. Wu, B. Mayers, B. Gates, Y. Yin, F. Kim, H. Yan, *Adv. Mater.* 15, **2003**, 353

[2] M. Ohring, *The Materials Science of Thin Films,* Academic Press, San Diego, CA, **1992**

[3] K. Nakaso, B. Han, K.H. Ahn, M. Choi, and K. Okuyama, *J. Aerosol Sci.*, 84, **2003**, 869

[4] Z. Chen, W. Ren, L. Gao, B. Liu, S. Pei, H.M. Cheng, *Nature Mater.*10, **2011**, 424

[5] R. Leon, D. Margolese, G. Stucky, P.M. Petroff, *Phys. Rev. B,* 52, **1995**, R2285

[6] P.A. Pandey, G.R. Bell, J.P. Rourke, A.M. Sanchez, M. D. Elkin, B.J. Hickey, N.R. Wilson, *Small*, 7, **2011**, 3202

[7] V. Amendola, S. Polizzi, M. Meneghetti, *Langmuir,* 23, **2007**, 6766

[8] M. Ganjali, P. Vahdatkhah, S.M.B. Marasshi, *Procedia Mat. Science* , 11, **2015**, 359

[9] D. Jang, D. Kim, *Appl. Phys. A* ,79, **2004**, 1985

[10] M.A. Herman, H. Sitter, *Molecular Beam Epitaxy-Fundamentals and Current Status,* Springer-Verlag, Berlin, **1989**.

[11] Y.W. Heo, V. Varadarajan, M. Kaufman, K. Kim, D.P. Norton, F. Ren, P.H. Fleming, *Appl. Phys.Lett.* 81, **2002**, 3046

[12] B. Fuhrmann, H.S. Leipner, H.R. Hoche, *Nano Lett.* 5, **2005**, 2524.

[13] R.A. Munden, M.A. Reed, *ACS Symposium Series*, 1183, **2014**, 13

[14] P. Hou, C. Liu, Y. Tong, S. Xu, M. Liu, H. Cheng, *J. Mater. Res.* 16, **2001**, 2526.

[15] D. Bera, S. C. Kuiry, M. McCutchen, S. Seal, H. Heinrich, G. C. Slane, *J. Appl.Phys.* 96, **2004** , 5152.

[16] J.K. Lung, J. C. Huang, D. C. Tien, C. Y. Liao, K. H. Tseng, T. T. Tsung, W. S. Kao, T.H. Tsai, C. S. Jwo, H. M. Lin, L. Stobinski, *Journal of Alloys and Compounds*, 655, **2007**, 434

[17] A. Ashkarran, A. Irajizad, M. M. Ahadian, S. A. M. Ardakani, *Nanotechnology*, 19, **2008**, 19570.

[18] N. Salah, S.S. Habib, Z.H. Khan, A. Memic, A. Azam, E. Alarfaj, N. Zahed, S. Al-Hamedi, *Int. J. Nanomedicine,* 6, **2011**, 863

[19] H. Kumar, S. Ghosh, D.K. Avasthi, D. Kabiraj, A. Mücklich,S. Zhou, H. Schmidt, J.P. Stoquert, *NanoscaleRes. Lett.* 6, **2011**,155.

[20] B.R. Pamplin, *Crystal Growth*, Pergamon Press, New York, **1975**

[21] C.S. Hirtzel, R. Rajagopalan, *Colloidal Phenomena: Advanced Topics*, New Jersey, **1985**

[22] D. Aiken, R. G. Finke, *J. Mol. Catal. A: Chem.* 145, **1999**, 1

[23] M. Brust, M. Walker, D. Bethel, D.J. Schiffrin, R. Whyman, *J. Chem. Soc., Chem. Commun.* 7, **1994**, 801.

[24] Y. Lin, R. G. Finke, *J. Am. Chem. Soc.* 116, **1994**, 8335

[25] X. M. Li, M.R. de Jong, K. Inoue, S. Shinkai, J. Huskens, D.N. Reinhoudt, *J. Mater. Chem.* 11, **2001**, 1919.

[26] R. Balasubramanian, B. Kim, S.L. Tripp, X. Wang, M. Lieberman, A. Wei, *Langmuir,* 18, **2002**, 3676

[27] H.B. Na, I.S. Lee, H. Seo, Y. Park, J.H. Lee, S.W. Kim, T. Hyeon, *Chem. Commun.*, **2007**, 5167.

[28] A. Henglein, D. Meisel, *Langmuir*, 14, **1998**, 7392

[29] A. Callegari, D. Tonti, M. Chergui, *Nano Letters,* 3, **2003**, 1565

[30] F. Kim, J.H. Song, P. Yang, *J. Am. Chem. Soc.* 124, **2002**, 14316

[31] H.H. Park, X. Zhang, Y.-J. Choi, H.H. Park, R.H. Hill, *J. Nanomaterials,* **2011**, Article ID 265287, 7 pages

[32] W.B. Zhao, J.J. Zhu, Y. Zhao, H.Y. Chen, *Mater. Science Eng. B,* 110, **2004**, 307

[33] S.F. Chen, J.P. Li, K. Qian, W.P. Xu, Y. Lu, W. X. Huang, S.H. Yu, *Nano Res.* 3, **2010**, 244

[34] D. Chen, X. Qiao, X. Qiu, J. Chen, R. Jiang, *J Mater Sci: Mater Electron,* 22, **2011**, 6

[35] Z. Yang, H. Qian, H. Chen, J. N. Anker, *Journal of Colloid and Interface Science*, 352, **2010**, 285

[36] Y. Li, Y. Ding, and Z. Wang, *Adv. Matter.,* 11, **1999**, 847

[37] Y. Mizukoshi, R. Oshima, Y. Maeda, Y. Nagata, *Langmuir*, 15, **1999**, 2733.

[38] J. Zhu, Y. Koltypin, A. Gedanken, *Chem. Mater.* 12, **2000**, 73

[39] H. Arami, M. Mazloumi, R. Khalifehzadeh, S.K. Sadrnezhaad,*Materials Letters*, 61, **2007**, 4559

[40] V.-S. Mănoiu, A. Aloman, U.P.B. *Sci. Bull., Series B*, 72, **2010**, 179

[41] Y.-Y. Yu, S.-S. Chang, C.-L. Lee, C. R. C. Wang, *J. Phys. Chem. B*, 101, **1997**, 6661

[42] B. Yin, H. Ma, S. Wang, S. Chen, *J. Phys. Chem. B*, 107, **2003**, 8898

[43] I.Bezares, A.del Campo, P.Herrasti, A. Muňoz-Bonilla, *Phys. Chem. Chem. Phys*, 17, 2015, 29319

[44] K.J. Sreeram, M. Nidhin, B.U. Nair, *Bull. Mater. Sci.,* 31, **2008**, 937

[45] S. Kundu, K. Wang, H. Liang, *J. Phys. Chem. C,* 113, **2009**, 5157

[46] N.P. Herring, A.B. Panda, K. AbouZeid, S.H. Almahoudi, C.R. Olson, A. Patel, M.S. El-Shall, *Microwave synthesis of metal oxide nanoparticles (Metal Oxide Nanomaterials for Chemical Sensors),* Springer-Verlag, New York, **2012**

[47] X. Y. Zhai, P. Zhang, C. J. Liu, T. Bai, W. C. Li, L .M. Dai, W. G. Liu, *Chem. Commun.* 48, **2012**, 7955

[48] D.-H. Chen, X.-R. He, *Mat. Res. Bull.* 36, **2001**, 1369

[49] F. Gu, S.F. Wang, M.K. Lü, G.J. Zhou, D. Xu, D.R. Yuan, *J.Phys.Chem.B*, 108, **2004**, 8119

[50] S. Ramesh, J. Nanoscience, 2013, **2013**, Article ID 929321, 8 pages

[51] R.P. Bagwe, K.C. Khilar, *Langmuir, 16,* **2000,** 905

[52] C.-H. Kuo, T.-F. Chiang, L.-J. Chen, M.H. Huang, *Langmuir, 20,* **2004,** 7820

[53] N. Leopold, B. Lendl, *J. Phys. Chem. B,* 107, **2003**, 5723

[54] Y. Wang, P.H.C. Camargo, S.E. Skrabalak, H. Gu, Y. Xia, *Langmuir*, 24, **2008**, 12042

[55] D. M. Ledwith, A.M. Whelan, J.M. Kelly, *J. Mater. Chem.,* 17, **2007**, 2459

[56] Z.S. Pillai, P.V. Kamat, *J. Phys. Chem. B,* 108, **2004**, 945

[57] I. Pastoriza-Santos, L.M. Liz-Marzán, *Langmuir*, 15, **1999**, 948

[58] R. Das, S.S. Nath, D. Chakdar, G. Gope, R. Bhattacharjee, *Journal of Experimental Nanoscience,* 5, **2010**, 357

[59] L.M. Liz-Marzán, I. Lado-Touriño, *Langmuir,* 12, **1996,** 3585

[60] M. Darroudi, M. B. Ahmad, A. H. Abdullah, N. A. Ibrahim, K. Shameli, *Int. J. Mol. Sci.* 11, **2010**, 3898

[61] Y. Xiong, I. Washio, J. Chen, H. Cai, Z.-Y. Li, Y. Xia, *Langmuir*, 22, **2006**, 8563

[62] S. Panigrahi, S. Kundu, S.K. Ghosh, S. Nath, T. Pal, *J. Nanoparticle Res.* 6, **2004**, 411.

[63] D. Chen, X. Qiao, X. Qiu, J. Chen, R. Jiang, *J Mater Sci: Mater Electron,* 22, **2011**, 6

[64] X.C. Jiang, S.X. Xiong, C.Y. Chen, W.M. Chen, A.B. Yu, *J. Nanopart Res.* 13, **2011**, 5087

[65] L. Gou, M. Chipara, J.M. Zaleski, *Chem. Mater.,* 19, **2007,** 1755

[66] R. Shankar, L. Groven, A. Amert, K.W. Whites, J.J. Kellar, *J. Mater. Chem.,* 21, **2011**, 10871

[67] J. M. Kong, C. V. Wong, Z. Q. Gao, X. T. Chen, *Synthesis and Reactivity in Inorganic, Metal-Organic, and Nano-Metal Chemistry,* 38, **2008**, 186

[68] N.R. Jana, L. Gearheart, C. J. Murphy, *Chem. Commun.*, **2001**, 617

[69] S. Eustis, M. El-Sayed, *J. Phys. Chem. B,* 109, **2005**, 16350

[70] H.M. Chen, R.-S. Liu, D. P. Tsai, *Crystal Growth & Design,* 9, **2009**, 2079

[71] Y. Yang, L. Xiong, J. Shi, M. Nogami, *Nanotechnology,* 17, **2006**, 2670

[72] K. Deplanche, L.E. Macaskie, *Biotechnology and Bioengineering,* 99, **2008**, 1055,

[73] M.M.G. Babu, R. Gunasekaran, *Colloids and Surfaces B: Biointerfaces,*74, **2009**, 191

[74] S. Priyadarshini, V. Gopinath, N.M. Priyadharsshini, D.M. Ali, P. Velusamy, *Colloids and Surfaces B: Biointerfaces,* 102, **2013**, 232,

[75] K. Kalishwaralal, V. Deepak, S. Ramkumarpandian, H. Nellaiah, G.Sangiliyandi, *Materials Letters,* 62, **2008**, 4411

[76] D. Jain, S. Kachhwaha, R. Jain, G. Srivastava, S.L. Kothari, *Indian Journal of Experimental Biology,* 48, **2010**, 1152

[77] H.R. Zhang, Q.B. Li, Y.H. Lu, D.H. Sun, X.P. Lin, X. Deng, N. He, and S.Z. Zheng, *Journal of Chemical Technology & Biotechnology,* 80, **2005**, 285

[78] K. Natarajan, S. Selvaraj, V.R. Murty, *Digest Journal of Nanomaterials and Biostructures,* 5, **2010**, 135

[79] A.R. Shahverdi, S. Minaeian, H.R. Shahverdi, H. Jamalifar, A.A. Nohi, Process *Biochemistry*, 42, **2007**, 919

[80] L. Sintubin, W. DeWindt, J. Dick, J. Mast, D. van der Ha, W. Verstraete, N. Boon, *Applied Microbiology and Biotechnology,* 84, **2009**, 741

[81] T. Klaus, R. Joerger, E. Olsson, C.G. Granqvist, *Proceedings of the National Academy of Sciences of U.S. A.,* 96, **1999**, 13611

[82] A. Nanda, M. Saravanan, *Nanomedicine: Nanotechnology, Biology and Medicine*, 5, **2009**, 452

[83] M. Oves, M.S. Khan, A. Zaidi, A.S. Ahmed, F. Ahmed, E. Ahmad, A. Sherwani, M. Owais, A. Azam, PLoS One, 8, 2013, 1,

[84] M.M. Juibari, S. Abbasalizadeh, G.S. Jouzani, and M. Noruzi, *Materials Letters,* 65, **2011**, 1014,

[85] A. Bharde, A. Kulkarni, M. Rao, A. Prabhune, M. Sastry, *Journal for Nanoscience and Nanotechnology,* 7, **2007**, 4369

[86] K. Kalishwaralal, V. Deepak, S.R.K. Pandian, S. Gurunathan, *Bioresource Technology,* 100, **2009**, 5356

[87] G. Southam, T.J. Beveridge, *Geochimica et Cosmochimica Acta,* 60, **1996**, 4369

[88] L. Du, H. Jiang, X. Liu, E. Wang, *Electrochemistry Communications,* 9, **2007**, 1165

[89] M.I. Husseiny, M.A. El-Aziz, Y. Badr, M.A. Mahmoud, *Spectrochimica Acta Part A: Molecular and Biomolecular Spectroscopy,* 67, **2007**, 1003

[90] B. Nair, T. Pradeep, *Crystal Growth & Design*, 2, **2002**, 293

[91] Y. Feng, X. Lin, Y. Wang, Y. Wang, J. Hua, *Materials Letters,* 62, **2008**, 4299

[92] S. He, Z. Guo, Y. Zhang, S. Zhang, J. Wang, N. Gu, *Materials Letters*, 61, **2007**, 3984

[93] Y. Nangia, N. Wangoo, N. Goyal, G. Shekhawat, C.R. Suri, *Microbial Cell Factories,*8, **2009**, 1

[94] P. Yong, N.A. Rowson, J.P. Farr, I.R. Harris, L.E. Macaskie, *Biotechnology and Bioengineering,* 80, **2002**, 369

[95] P. Mukherjee, A. Ahmad, D. Mandal, S. Senapati, S.R. Sainkar, M.I. Khan, R. Parishcha, P.V. Ajaykumar, M. Alam, R. Kumar, M. Sastry, *Nano Letters*, 1, **2001**, 515

[96] A. Ahmad, P. Mukherjee, P. Senapati, D. Mandal, M.I. Khan, R. Kumar, M. Sastry, *Colloids and Surfaces B: Biointerfaces*, 28, **2003**, 313

[97] T.L. Riddin, M. Gericke, C.G. Whiteley, *Nanotechnology*, 17, 2006, 1

[98] K.C. Bahamas, S.F. Disouza, *Colloids and Surfaces B: Biointerfaces*, 47, **2006**, 160

[99] J. Xie, J. Y. Lee, D.I.C. Wang, Y.P. Ting, *Small* 3,**2007**, 672

[100] Y.K. Sakai, K. Ohno, N. Saitoh, T. Nomura, S. Nagamine, *Bio Micro and Nanosystems Conference,* **2006**. BMN '06; On Page(s): 29 – 29

[101] G. Singaravelu, J.S. Arockiamary, V. G. Kumar, K. Govindaraju, *Colloids and Surfaces B* 57, **2007**, 97

[102] S. Panigrahi, S. Kundu, S. Ghosh, S. Nath, T. Pal, *Journal of Nanoparticle Research*, 6, **2004**, 411

[103] D.M. Eby, N.M. Schaeublin, K.E. Farrington, S.M. Hussain, G.R.Johnson, *ACS Nano*, 3, **2009**, 984

[104] N. Wangoo, K.K. Bhasin, S.K. Mehta, C.R. Suri, *Journal of Colloid and Interface Science,*323, **2008**, 254

[105] J.P. Xie, J.Y. Lee, D.I.C. Wang, *Journal of Physical Chemistry C*, 111, **2007**, 10226

[106] Y. Zhou, W. Lin, J. Huang, W. Wang, Y. Gao, L. Lin, Q. Li, M. Du*, Nanoscale Research Letters*, 5, **2010**, 1351

[107] S.S. Shankar, A. Ahmad, M. Sastry, *Biotechnol. Prog*. 19, **2003**, 1627

[108] V.G. Kumar, S.D. Gokavarapu, A. Rajeswari, T.S. Dhasa, V. Karthick, Z. Kapadia, T. Shrestha, I.A. Barathy, A. Roy, S. Sinhab, *Colloids and Surfaces B: Biointerfaces*, 87, **2011**, 159

[109] X. Yang, Q. Li, H. Wang, J. Huang, L. Lin, W. Wang, D. Sun, Y. Su, J.B. Opiyo, L. Hong, Y. Wang, N. He, L. Jia, *Journal of Nanoparticle Research*, 12, **2010**, 1589

[110] L. Jia, Q. Zhang, Q. Li, H. Song, *Nanotechnology*, 20, **2009**, 385601

[111] H.J. Lee, J.Y. Song, B.S. Kim, *Journal of Chemical Technology and Biotechnology*, 88, **2013**, 1971

[112] A. Borras, M. Aguirre, O. Groening, C. Lopez-Cartes, P. Groening, *Chem. Mater.,* 20, **2008**, 7371

[113] B.Yang, J. Xiao, J.I. Wong, J. Guo, Y. Wu, L. Ong, L.L. Lao, F. Boey, H. Zhang, H.Y. Yang, Q. Zhang, *J. Phys. Chem. C,* 115, **2011**, 7924

[114] R. O. Al-Kaysi, A.M. Müller, T.-S. Ahn, S. Lee, C.J. Bardeen, *Langmuir,* 21, **2005,** 7990

[115] H.-B. Fu, J.-N. Yao, *J. Am. Chem. Soc.* 123, **2001**, 1434

[116] Y. Lei, Q. Liao, H. Fu, J. Yao, *J. Phys. Chem. C,* 113, **2009**, 10038

[117] Y. S. Zhao, W. Yang, D. Xiao, X. Sheng, X. Yang, Z. Shuai, Y. Luo, J. Yao, *Chem. Mater.* 17, **2005,** 6430

[118] A. Hu, Z. Yao, X. Yu, *J. Appl. Polym. Sci.,* 113, **2009**, 2202

[119] C. Destree, F. Debuigne, S. George, B. Champagne, M. Guillaume, J. Ghijsen, J.B. Nagy, *Colloid. Polym. Sci.,* 286, **2008**, 1463

[120] T. Xike, F. Jinbo, C. Zhenbang, L. Yang, A. Dongyue, *Nanomed.: Nanotech. Biol. Med.,* 1, **2005**, 323

[121] K. S. Suslick, M. W. Grinstaff, *J. Am. Chem. Soc.*, 112, **1990**, 7807

[122] K. S. Suslick, M. W. Grinstaff, K. J. Kolbeck, M. Wong, *Ultrason. Sonochem.* 1, **1994**, S65.

[123] M. Jaseer, E. Prasad, *J. Photochem. Photobiol. A,* 214, **2010**, 248.

[124] X. Zhang, X. Zhang, W. Shi, X. Meng, C. Lee, S. Lee, *J. Phys. Chem. B,* 109, **2005,** 18777

[125] Y.S. Zhao, W. Yang, J. Yao, *Phys. Chem. Chem. Phys.* 8, **2006**, 3300

Chapter III

Characterization techniques

Characterization techniques

A better fundamental understanding and various potential applications of the low dimensional materials demands characterizations of these materials. Characterization techniques such as UV-Visible spectroscopy, Transmission Electron Microscope (TEM), Selected Area Electron Diffraction (SAED), Scanning Electron Microscopy (SEM), X-ray diffraction (XRD) and Fourier transform infrared spectroscopy (FTIR) were used in the experimental work and described in the following section.

3.1. UV-Vis spectroscopy

UV-Vis spectroscopy refers to the absorption or reflectance spectroscopy in the ultraviolet-visible region where atoms and molecules undergo electronic transition. In this spectroscopy absorption measures the electronic transitions from the ground state to the excited state. This spectroscopy is one of the most common and fundamental techniques to get useful information regarding the size, shape and degree of aggregation of low dimensional materials [1]. Metal nanoparticles exhibit a strong absorption band in the UV-Visible region, which can be assigned to the surface plasmon band of the metal nanoparticles. The origin of this light absorption by metallic nanoparticles is the coherent oscillation of the conduction electrons stimulated by the interacting electromagnetic field. The electric field of an incoming light induces a polarization of the free electrons relative to the cationic lattice. A net charge difference occurs at the nanoparticles' boundaries, which in turn acts as a restoring force. In this way, a dipolar oscillation of electrons, called dipole plasmon, is generated with a certain frequency. When the frequency of the dipole plasmon is exactly the same as the incident light, a resonance condition is established, leading to constructive interference and the strongest signal for the plasmon which is referred to as *surface plasmon resonance* (SPR). The frequency and intensity of the surface

plasmon band depends upon the size and shape of the metal nanoparticles as well as the dielectric constant of the metal itself and its surrounding medium.

A schematic diagram of a double beam UV-visible spectrophotometer is shown in figure 3.1.

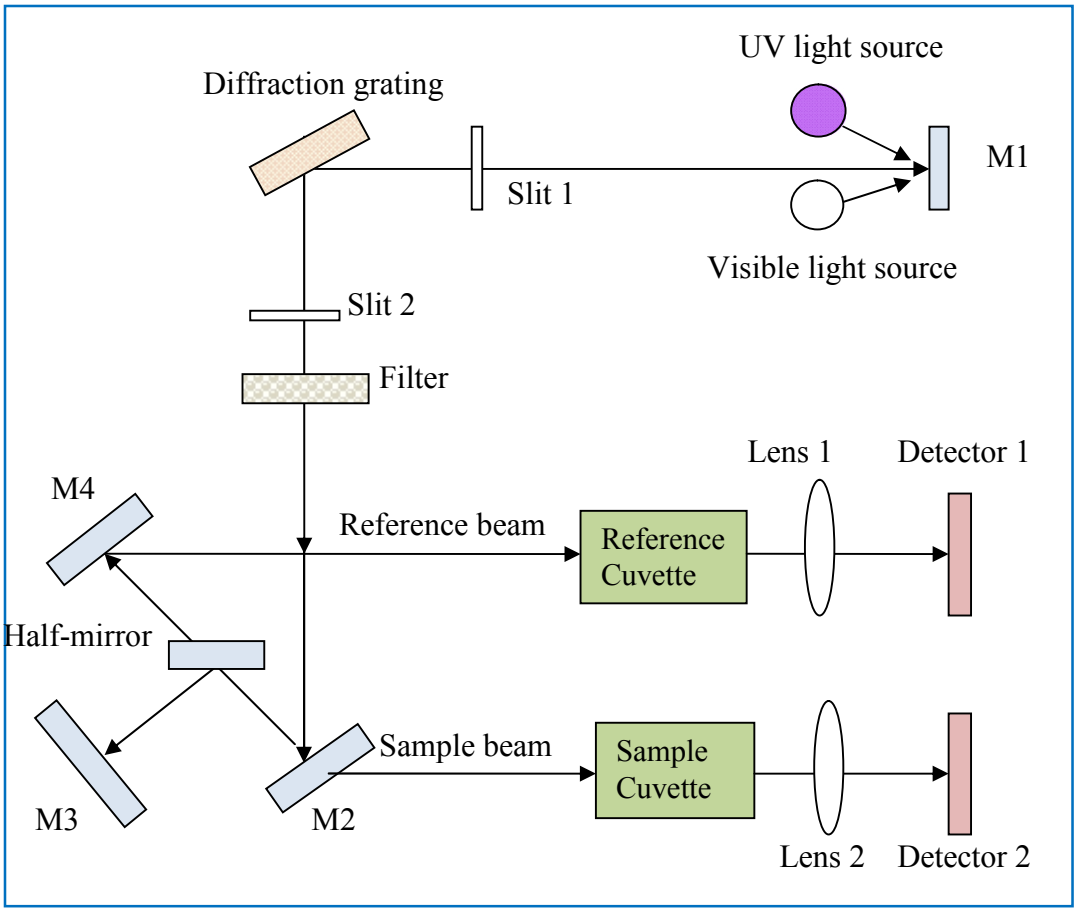

Figure 3.1: *Schematic diagram of a double beam UV-visible spectrophotometer (M1, M2, M3 and M4 are mirrors).*

The principle and experimental set up is very simple. In this spectrophotometer, the entire UV-Vis spectrum is taken from 190 to 900 nm range. Sample is well dispersed in a suitable solvent and the pure solvent is used as a reference. The sample and the reference are taken in quartz cuvettes, a small transparent container, as these are transparent throughout the UV, visible and near infrared regions. The reference beam in the spectrophotometer travels from the light source to the detector without interacting with the sample. The sample beam interacts with the sample exposing it to the

UV-Vis light of continuously changing wavelength. When the incident wavelength corresponds to the energy level which promotes an electron to a higher molecular orbital, energy is absorbed. The detector records the ratio between reference and sample beam intensities (I_0/I). Absorption of the solvent cancels out to give spectrum of the pure sample. The absorption is different at different wavelengths and is characteristic of the sample. The wavelength of the maximum absorbance is designated as 'λ_{max}'.

Different materials may feature different absorption peak and absorbance. The absorbance may be calculated from the Lambert-Beer law according to which '*the absorbance of a solution is directly proportional to the concentration of the absorbing species in the solution and the path length*'. Therefore, UV-vis spectroscopy can be used to determine the concentration of the absorbing species in a solution by taking the absorbance at a fixed path length. Practically, UV-vis spectrophotometer measures the intensity of light transmitted through a sample (I), and compares it to the intensity of light before it passes through the sample (I_0). The ratio I/I_0 is known as the transmittance, and is usually expressed as a percentage (% T). Then the absorbance, A, can be written as:

$$A= \varepsilon cl = \log_{10}(I_0/I)= \log_{10}(100/T)$$

where 'l' and 'c' are the path length and concentration of the sample respectively. For each sample and wavelength of light, 'ε' is a constant known as the molar extinction coefficient or molar absorbtivity. This constant is a fundamental molecular property of a given solvent.

UV–Vis spectroscopic study of the low dimensional materials presented in this thesis was done using SHIMADZU UV-1601 and SHIMADZU UV-1800 spectrophotometer. The photographs of a SHIMADZU UV-1601 and a SHIMADZU UV-1800 Spectrophotometer are shown below (Fig. 3.2).

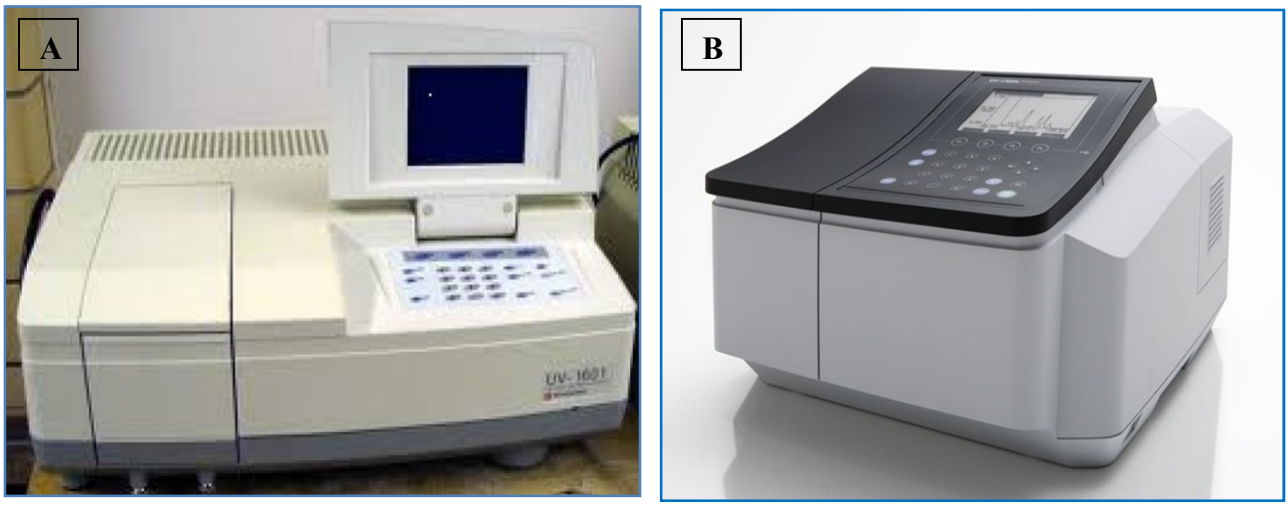

Figure 3.2: (A) SHIMADZU UV-1601 and (B) SHIMADZU UV-1800 Spectrophotometer.

3.2. Fluorescence spectroscopy

Fluorescence spectroscopy is fundamentally concerned with electronic and vibrational states of a species. In fluorescence spectroscopy, by absorbing a photon the species is first excited from its ground electronic state to one of its several vibrational states in the excited electronic state. Collisions with the other neighboring molecules drive the excited molecule to lose vibrational energy until it reaches the lowest vibrational energy level of the excited electronic state. Fluorescence occurs when the species emits photons as it returns to its initial ground electronic state from the lowest vibrational energy level of the excited electronic state, in less than 10^{-9} sec. Since some energy of the species is lost through heat or vibration in non-radiative way so that the emitted energy is less than the excitation energy; i.e., the emission wavelength is always longer than the excitation wavelength. The above fluorescence process is elegantly described by the Jablonski diagram as given below.

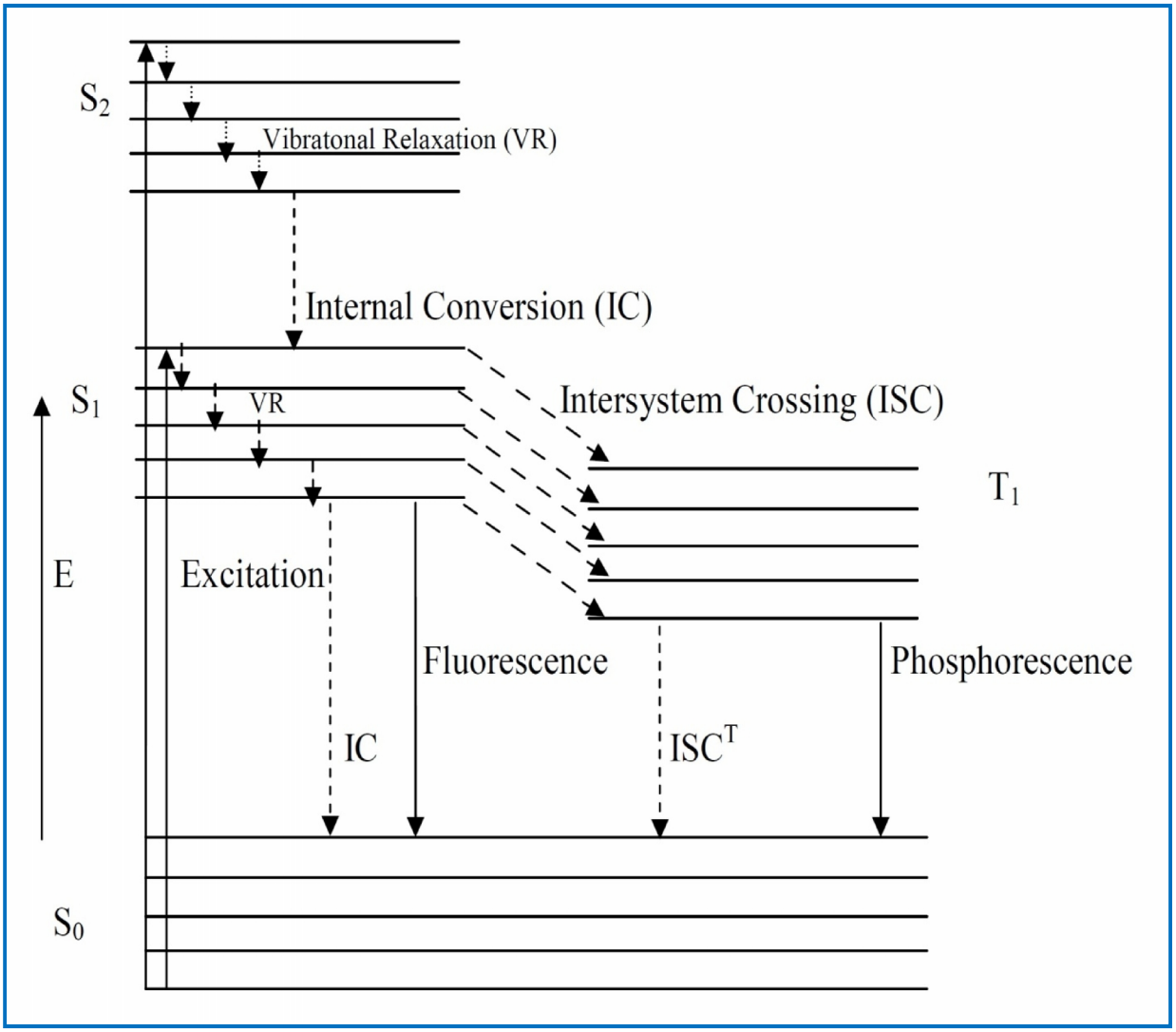

Figure 3.3: *The Jablonski diagram of fluorophore excitation, radiative decay and nonradiative decay pathways. [E = energy scale; S_0 = ground singlet electronic state; S_1 & S_2 = higher energy excited singlet electronic states; T_1 = lowest energy triplet state; ISC^T = Reverse ISC].*

The difference between the excitation and emission wavelengths is known as the Stokes shift. The Stoke shift depicts the observation that fluorescence radiation is longer in wavelength than the excitation radiation. The fluorescence absorption and emission spectra speculate the vibrational level structures in the ground state and the excited electronic states, respectively. According to the Frank-Condon principle the vibrational levels are not significantly changed during electronic transitions.

The resemblance in the vibrational level structures in the ground and excited electronic states often results in the absorption and emission spectra having reverberated characteristics. Schematic diagram of photoluminescence set up is shown in the following figure.

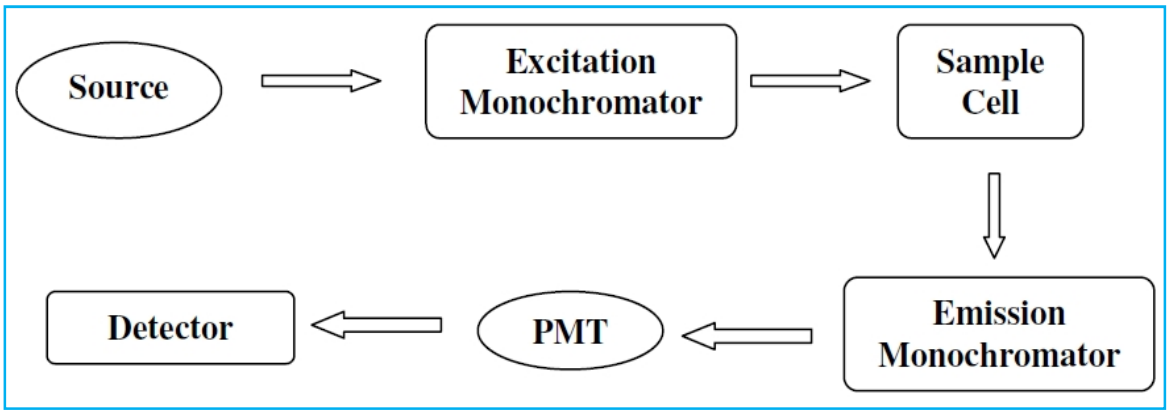

Figure 3.4: *Schematic diagram of photoluminescence set up*

Xenon arc lamps are used as the most common light sources for fluorimeter because these lamps provide a relatively uniform intensity over a broad spectral range from the ultraviolet to the near infrared region. Photons strike on the excitation monochromator which selectively transmits light in a narrow range centred about the specified excitation wavelength. The transmitted light is passed through adjustable slits to control the magnitude and resolution. The selected wavelengths pass into the sample causing fluorescent emission by fluorophores within the sample. Emitted light gets into the emission monochromator, which is positioned at 90º angle with the excitation light path to reject background signal and minimize noise resulting from stray light. The emitted light is transmitted in a narrow range of wavelengths centred about the specified emission wavelength and gets out through adjustable slits. Next, the emitted light enters into the photomultiplier tube (PMT). Amplification of the signal and creation of a voltage proportional to the measured emitted intensity occurs. There are two types of detectors viz. single-channelled or multi-channelled. The single-channelled detector can only detect the intensity of one wavelength at a time, while the multichannel detects the intensity at all wavelengths simultaneously. The

excitation spectrum records fluorescent intensity as a function of excitation wavelength at a constant emission wavelength whereas the emission spectrum describes the fluorescent intensity measured as a function of emission wavelength at a constant excitation wavelength. Fluorescence intensity measurement allows the determination of the presence of fluorophores and their concentration. Fluorescence spectra of all the samples were obtained using a HITACHI F-7000 Fluorescence Spectrophotometer (Fig. 3.5). The photograph of the instrument is shown below:

Figure 3.5: HITACHI F-7000 Fluorescence Spectrophotometer

3.3. Transmission electron microscopy (TEM)

TEM is a microscopic technique whereby a beam of electrons is transmitted through an ultra thin specimen and interacts as it passes through the sample. An image is formed from the electrons transmitted through the specimen, magnified and focused by an objective lens and appears onto an imaging device, such as a fluorescent screen or on a layer of film, or to be detected by a sensor such as a camera (CCD). Size and shape of the low dimensional materials with very high magnification ranging from 50 to 10^6 can be obtained using TEM. In TEM, the sample is illuminated by an electronic radiation and the electrons transmitted through the sample

are detected. The electrons are accelerated to ~ 100 KeV projected onto a thin specimen (less than 200 nm) by means of the condenser lens system.

The major instrumentation parts of TEM include the following.

a) **Illumination system:** It collects the electrons from the gun and transfers them as either a broad beam or a focused beam to the specimen. In a ray-diagram, the components above the specimen belong to the illumination system.

b) **The objective lens and stage:** This combination is called as the heart of TEM.

c) **The TEM imaging system:** It includes the intermediate lens and projector lens.

A schematic ray-diagram is given below (Fig. 3.6) showing the various parts of a transmission electron microscope (TEM).

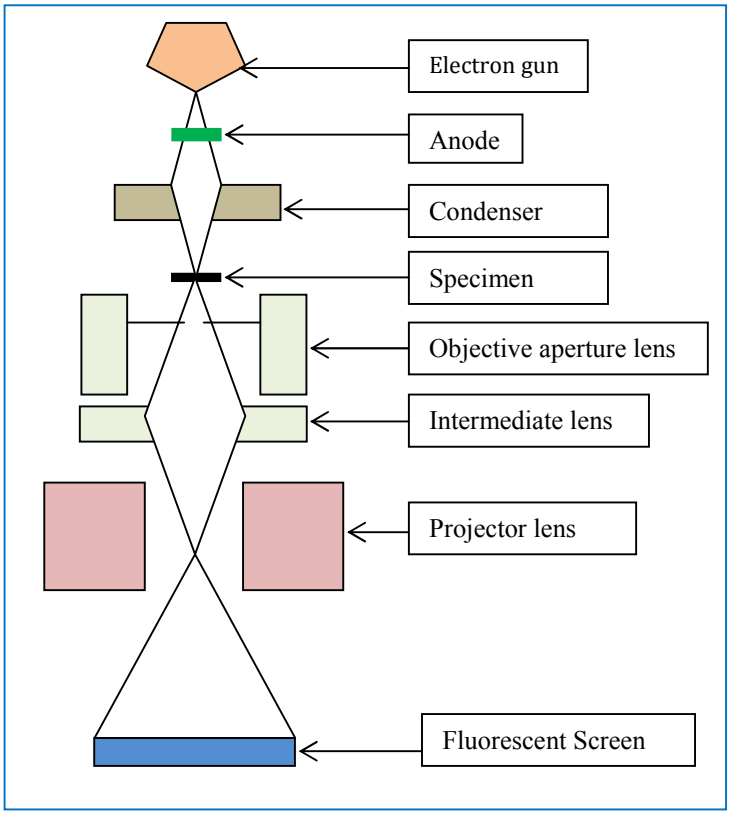

Figure 3.6: A schematic diagram of the transmission electron microscope (TEM)

In an electron microscope, electrons are usually generated by thermal emission from a tungsten filament. Then the electrons are accelerated by an electric potential (~100 KeV to 1 MeV) and focused by electrostatic and electromagnetic lenses on the sample. When electrons impact on any specimen, they may back scattered, generate secondary electrons, or transmit them. The entire arrangement, including the specimen has to be placed in high vacuum i.e. in very low pressure, typically on the order of 10^{-4} to 10^{-8} kPa to avoid scattering and absorption of electrons by air and to allow uninterrupted passage of electrons. The intensity of the diffraction depends on the orientation of the atomic planes in a crystal relative to the electron beam. At certain angles the electron beam is diffracted strongly from the axis of the incoming beam whereas at other angles the beam is predominantly transmitted. A high contrast image can be formed by barring electrons deflected away from the optical axis of the microscope by placing the aperture to allow only unscattered electrons which produces a variation in the electron density that reveals information on the crystal structure. Modern TEM machines are designed in such a way that allow the external insertion of the sample with minimal disruption to the vacuum inside and tilting the specimen to a range of angles in order to obtain specific diffraction conditions. Preparation of TEM sample is done by placing a drop of aqueous suspension of low dimensional materials on the carbon coated copper grids which are 3 mm diameter brass ring, with a thickness of 100 μm. The high resolution transmission electron microscope (HRTEM) studies are also useful to investigate crystallographic structure, the faceting, crystallinity and ordering of a sample. Theoretically, the maximum resolution with a light microscope has been limited by the wavelength of the photons that are being used to probe the sample, λ and the numerical aperture of the system [2]. The high magnification or resolution of all TEM is a result of the small effective electron wavelengths, λ**,** which **is** given by the de Broglie relationship:

$$\lambda = \frac{h}{\sqrt{(2mqV)}}$$

where m and q are the electron mass and charge, h is Planck's constant, and V is the potential difference through which electrons are accelerated. If the operating voltage of a TEM instrument is higher, its lateral spatial resolution will be greater. High-voltage TEM instruments (with e.g. 400KV) have point-to-point resolutions better than 0.2 nm. High-voltage TEM instruments have the additional advantage of greater electron penetration because high-energy electrons interact less strongly with matter than lower energy electrons. So it is possible to work with thicker samples on a high voltage TEM.

Our synthesized nano/micro particles presented in this thesis have been studied in TECNAI-FE12 and JEOL-JEM-2100 high-resolution transmission electron microscope. The photographs of the TECNAI-FE12 and JEOL-JEM-2100 transmission electron microscope are shown below (Fig.3.7):

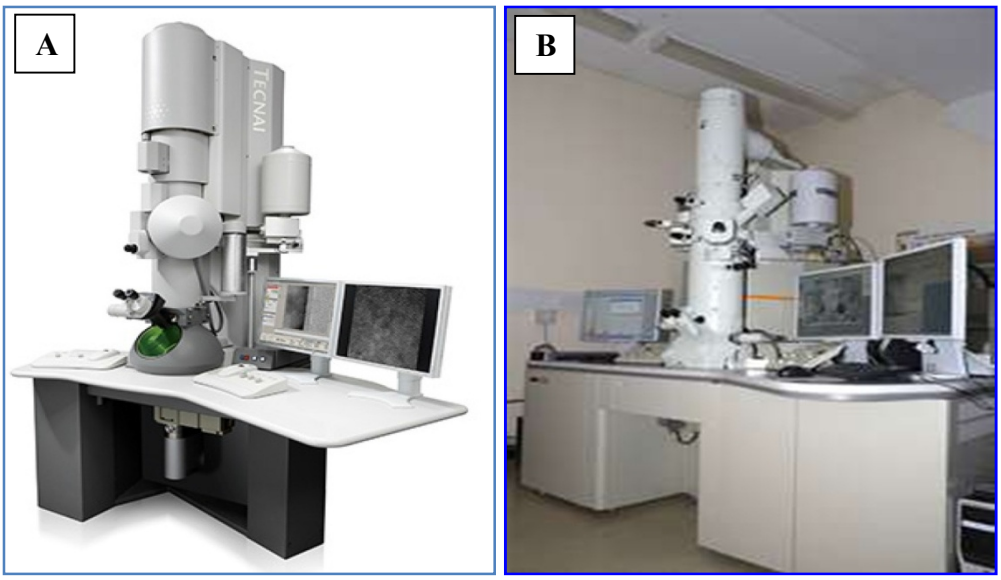

Figure 3.7: (A) TECNAI FE-12 and (B) JEOL-JEM-2100 high-resolution transmission electron microscope.

3.3.1. Selected Area Electron Diffraction (SAED)

Selected area electron diffraction is a TEM technique in which diffraction patterns are obtained resulting from the electron beam scattered by the sample lattice. We can index the diffraction spots in the pattern as the electrons are scattered elastically by the lattice obeying the Bragg's law. Every spot in the SAED pattern corresponds to the lattice planes of a certain miller indices in single crystal. As a result, it offers a unique potentiality to determine the crystal structure of individual low dimensional materials such as nanocrystals of different parts in the sample. From the SAED pattern the material scientists can obtain various structural information of the sample like unit cell parameter, crystalline symmetry, phase analysis and space group etc. Almost all the TEM machines with a parallel electron beam source are capable of SAED test. In SAED the condenser lenses are defocused to generate parallel illumination at the specimen and selected area aperture is used to limit the diffracting volume.

3.4. Scanning Electron Microscopy (SEM)

Scanning electron microscope is a type of electron microscope which produces the images of a sample by scanning it with a focused beam of electrons. In a typical SEM**,** a stream of electrons having energy ranging from 0.2 KeV to 40 KeV is focused by means of one or two condenser lenses into a beam, with a very fine spot size of ~ 0.4 to 5 nm diameter. The electron beam is generated by thermionical emission from an electron gun fitted with a tungsten filament or lanthanum hexaboride cathode. The beam passes through pairs of scanning coils or pairs of deflector plates in the electron column, typically in the final lens, which deflect the beam in the *x* and *y* axes so that it scans in a raster fashion over a rectangular area of the sample surface. When the beam of electrons strikes the surface of the specimen and interacts with the atoms of the specimen, signals in the form of secondary electrons (SE) due to inelastic scattering, back scattered electrons (BSE) due to elastic scattering and characteristic X-rays resulting from the

electronic transition of excited atoms are generated which can provide information regarding the sample's surface topography, composition etc. Imaging of the sample surface is done by detecting the SE which is the most commonly used technique for the topography of the surface. In this technique the low energy electrons ejected from the K cell of the atoms by the inelastic scattering of the incident electron beam are collected by a detector, which is basically a scintillator-photomultiplier system. The electrons are accelerated to a high energy by high bias voltage which finally impact the scintillator to produce photons, which are further magnified by the photomultiplier and collected as a 2D intensity distribution. Electronic devices are used to detect and amplify the signals and display them as an image on a cathode ray tube in which the raster scanning is synchronized with that of the microscope. The image displayed is therefore a distribution map of the intensity of the signal being emitted from the scanned area of the specimen. The brightness of the signal depends on the number of secondary electrons reaching the detector. If the beam gets into the sample perpendicular to the surface, then the activated region is uniform about the axis of the beam and a certain number of electrons will scatter from the sample. As the angle of incidence increases more secondary electrons will be emitted and hence inclined surfaces and edges tend to be brighter than flat surfaces. A schematic diagram of the instrumentation of a scanning electron microscope is shown below in figure 3.8.

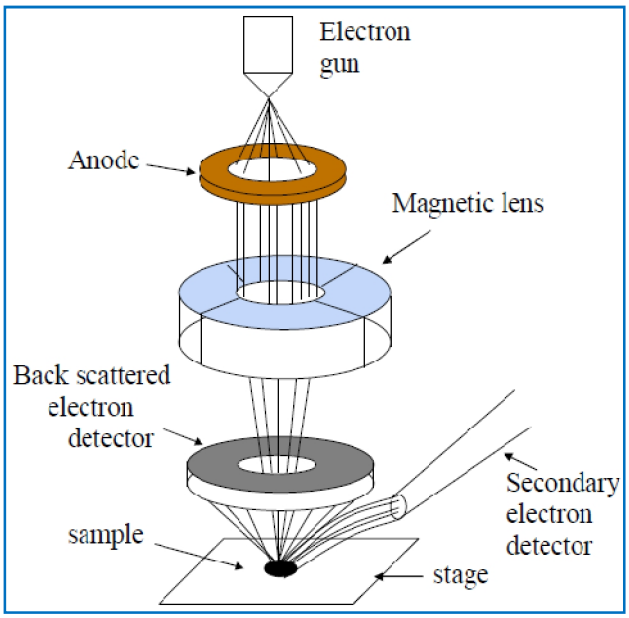

Figure 3.8: Schematic diagram of a Scanning Electron Microscope.

SEM requires that the specimen should be conductive for the electron beam to scan the surface and that the electrons have a path to ground for conventional imaging. Non-conductive solid specimen is generally coated with an ultrathin layer of conductive material (usually gold) by low vacuum sputter coating or high vacuum evaporation. This is done to prevent the accumulation of static electric charge on the specimen during electron irradiation. A circular Cu slab was used as the sample holder. Samples were mounted on the holder by conducting copper/carbon tape. The magnification of the image can be as high as from ~ 10 to 5×10^5. The SEM can reveal very high-resolution images of a sample surface, providing details about 1-5 nm in size in its primary or standard detection mode i.e. secondary electron imaging, since the SE are emitted from very close to the specimen surface. Characteristic X-rays are the second most common imaging mode as these X-rays can be used to identify the elemental composition of the sample by a technique known as energy dispersive X-ray (EDX). Back scattered electrons (BSE) coming from the sample can also be used to form an image which is often used in analytical SEM along with the spectra made from the characteristic X-rays as clues for the elemental composition of the sample

because the intensity of the BSE signal is strongly related to the atomic number (Z) of the specimen. Size and shape of the synthesized microparticles, presented in this thesis have been characterized by an Evo 18, Carl-ZEISS scanning electron microscope. The photograph of the instrument is shown below in figure 3.9.

Figure 3.9: EVO 18, Carl-ZEISS Scanning Electron Microscope.

3.5. X-ray diffraction (XRD)

X-ray diffraction (XRD) study is a rapid analytical technique for the characterization of crystalline low dimensional materials. X-rays are used to produce the diffraction pattern as their wavelength λ is typically the same order of magnitude (1–100 angstroms) as the spacing *d* between the planes in a crystal. Various crystals posses many sets of planes passed through their atoms. Each set of planes has a specific inter planer spacing and will produce a characteristic angle for X-ray diffraction. For a given set of lattice planes with an inter-planar spacing of 'd', the condition for occurring a diffraction can be simply written by Bragg's equation:

$$n\lambda = 2d \sin \theta$$

where, 'λ' is the wavelength of the X-rays, 'θ' is the scattering angle and 'n' is an integer.

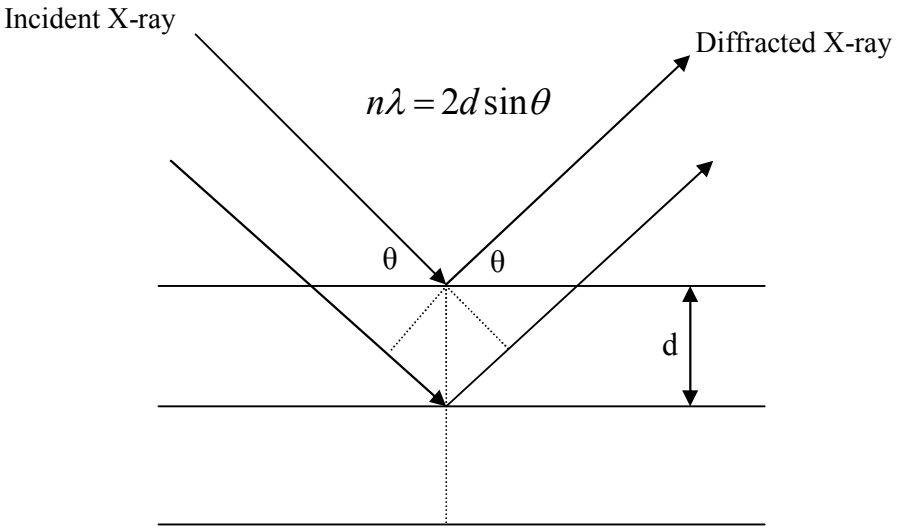

Figure 3.10: Bragg's Law diagram.

A set of 'd-spaces' obtained from a single material will represent the set of planes that can be passed through the atoms and can be used for comparison with sets of d-spaces obtained from standard compounds. In 1913, the famous English physicists Sir W. H. Bragg and his son Sir W. L. Bragg derived the above equation. They were awarded the Noble prize in physics in 1915 for their work in determining crystal structures.

Crystal structure including unit cell dimensions and geometry, orientation of single crystals, preferred orientation of polycrystalline material, measurement of sample purity etc. can be studied using XRD. X-ray diffraction is based on the constructive interference of monochromatic X-rays and a crystalline sample. These X-rays are generated in a cathode ray tube by heating a filament to produce electrons, accelerating the electrons towards a target material (Cu, Fe, Mo, Cr etc.) by applying a voltage, and bombarding the target with the electrons. The X-rays generated are filtered to produce monochromatic radiation, paralleled to concentrate, and directed towards the sample. The specific wavelengths of the X-rays are characteristic of the target material. Copper is the most common target material for single-crystal diffraction, with CuKα radiation = 1.5418Å. When a crystal is bombarded with X-rays of a specified wavelength

and at certain incident angles, intense reflected X-rays are produced when constructive interference occurs between the wavelengths of the scattered X-rays. Such constructive interference occurs when the geometry of the incident X-rays impinging the sample satisfies the Bragg Equation, and a peak in diffractogram appears. A detector records and processes this X-ray signal and converts the signal to a count rate which is then output to a device such as a printer or computer monitor. By scanning the sample through a range of 2θ angles, all possible diffraction directions of the lattice should be accomplished due to the random orientation of the powdered material. Conversion of the diffraction peaks to d-spacings allows identification of the crystalline material because each crystalline material has a set of unique d-spacings. Typically, this is done by comparison with d-spacings with standard reference patterns. The crystallinity and particle size of the nanoparticles are often experimentally determined by X-ray diffraction [3]. X-ray diffraction (XRD) data of the samples in the thesis are obtained using 'Rigaku Miniflex-II' and "X'Pert PRO PANalytical-PW 3040/60" X-ray diffractometer. The photograph of the 'Rigaku Miniflex-II' diffractometer is shown below (Fig. 3.11):

Figure 3.11: Rigaku Miniflex-II' X-ray diffractometer

3.6. Fourier transform infrared spectroscopy (FTIR)

The crucial part of a low dimensional material influencing its properties is its surface. The surface represents the interface between a particle and its environment and it determines how the two communicate and and influence each-other. Therefore, there is a motivation to characterize the surface structure and chemistry of the low dimensional materials. Fourier transform infrared (FTIR) spectroscopy is used to identify the functional groups on the surface [4] to study the physisorption of molecules at the surface [5], to evoke information about specific surface area, surface charge density and concentration of a nanomaterial [6]. All the FT-IR measurements are done using Perkin Elmer (Spectrum 2) spectrophotometer (Fig. 3.12). The photograph of the instrument is shown below.

Figure 3.12: Perkin Elmer (Spectrum 2) infrared spectrophotometer

A molecule which is exposed to infrared rays absorbs infrared radiation at frequencies which are characteristic to the molecule. During FTIR analysis, a spot on the specimen is subjected to a modulated IR beam. The specimen's absorbance (or transmittance) of the infrared rays at different frequencies is interpreted into an IR absorption plot consisting of reverse peaks. A basic IR spectrum is essentially a graph of infrared light absorbance (or

transmittance) on the vertical axis vs. frequency or wave numbers on the horizontal axis. The resulting FTIR spectra is analyzed and checked with known features of identified materials in the FTIR library.

For sample preparation powder samples are mixed with alkali halides and pressed in the sample holder. Alkali halides such as NaCl, KBr or CsI are often used due to their good infrared radiation transmission capability. A small amount of the powder sample (~ 0.1-2% of the KBr amount) is mixed with a spatula full of KBr powder. The mixture is ground for 3-5 minutes to reduce the particle size to less than 5 mm in diameter (until crystallites can no longer be seen and it becomes somewhat "pasty" and sticks to the mortar) because the large particles scatter the infrared beam and cause a slope baseline of spectrum.

For liquid samples several drops of the sample are taken onto an aperture plate and sandwiching it under another aperture plate, such that no gas bubbles are trapped. This type of cell is called a 'demountable cell' because the holder, aperture plates and spacers can be disassembled and then re-assembled to perform measurements. The commonly used aperture plate materials are alkali halides such as NaCl, KBr or CsI due to their good IR transparency. However, these materials are deliquescent and soluble in water. As a result, such aperture plates cannot be used with solutions containing water. KRS-5(thallium bromide/iodide) aperture plates are comparatively tolerant to water. Arsenic selenide (As_2Se_3) and zinc selenide (ZnSe) apertures are insoluble in water and hence can be used for aqueous solution.

References:

[1] C. Burda, X. Chen, R. Narayanan, M.A. El-Sayed, *Chem. Rev.* 105, **2005**, 1025.

[2] B. Fultz, J. Howe, *Transmission Electron Microscopy and Diffractometry of Materials,* Springer, **2007**, ISBN:3-540-73885-1

[3] D. Zanchet, B. D. Hall, D. Ugarte, *J. Phys. Chem. B*, 104, **2000**, 11013.

[4] B. Zhang, B. Yan*, Anal. Bioanal. Chem.* 396, **2010**, 973

[5] I.A. Mudunkotuwa, A. Al Minshid, V.H. Grassian, *Analyst*, 139, **2014**, 870

[6] L.D. Tickanen, M.I. Tejedor-Tejedor, M.A. Anderson, Langmuir, 13, **1997**, 4829

Chapter IV

Synthesis of silver nanostructures of varying morphologies through seed mediated growth approach

*A part of this chapter has been published in the article, **Sadhan Samanta**, Santanu Pyne, Priyanka Sarkar, Gobinda P. Sahoo, Harekrishna Bar, Dipak Kr. Bhui, Ajay Misra, **Journal of Molecular Liquids 153 (2010) 170–173**

Synthesis of silver nanostructures of varying morphologies through seed mediated growth approach

4.1. Introduction:

Among the noble metal nanoparticles silver is perhaps the most widely studied because of its possible applications in areas such as photonics [1-3], microelectronics [4], photo catalysis [5-7] and lithography [8,9]. Again silver nanoparticles show a very strong surface plasmon resonance (SPR) band in the visible region of light with an extinction coefficient up to four times than that of gold nanoparticles [10]. The efficiency of the interaction of nanosized silver particles with light is attributed to the large density of conducting electrons and the unique frequency dependence of the real and imaginary parts of the dielectric function [11].

To utilize and optimize the chemical and physical properties of nanosized metal particles, a large spectrum of research has been focused to control the size and shape, which is crucial in tuning their physical, chemical and optical properties. Various methods, including physical and chemical means, such as chemical reduction [12-14], electrochemical reduction [15], photochemical reduction [16], green synthesis [17, 18], heat evaporation [19], laser ablation [20], chemical vapor deposition [21], thermal decomposition in organic solvents [22], molecular beam epitaxy [23] are being used for the synthesis of metal nanoparticles. For physical methods high temperature, vacuum and expensive equipments are required but chemical methods are convenient, simple and inexpensive. Silver nanoparticles with different shapes have been synthesized. These include zero dimensional spherical or tetrahedral quantum dots [24], one dimensional silver nanorods and wires [25] and two dimensional nanoplates [26], nanoprisms [27]

and nanodisks [28]. Among these particles two dimensional nanoparticles are attractive due to their significant ability to control optical properties.

In this chapter, we are going to discuss a new solution phase seed mediated growth approach for the synthesis of silver nanoparticles of various morphologies. Since the shape of seed particles plays a vital role in controlling the morphology of nanoparticles during the growth process, we have decided to use sodium dodecyl sulphate (SDS) as soft template to obtain different twined structured particles. As synthesized silver sol obtained through seed mediated growth process is pink in colour and shows two sharp intense SPR band; the red one (537 nm) is due to longitudinal SPR and the blue one (423 nm) due to transverse SPR transition. TEM study shows a mixture of morphologies of the particles with a predominant triangular plate like structure. We believe that the above approach is a very simple one where a fine tune of one or more reaction parameters can help to synthesize silver nanoparticles of a particular morphology. Researches in this direction are in progress in our laboratory.

4.2. Experimental:

4.2.1. Chemicals:

Chemicals used in all the experiments were analytic reagent (AR) grade. Silver nitrate ($AgNO_3$, >99.8%) was purchased from RFCL Ltd. (India). Sodium borohydride ($NaBH_4$, >99%) was purchased from S.D.Fine Chem.Ltd. Trisodium Citrate ($C_6H_5Na_3O_7.2H_2O$, >99%), Sodium dodecyl sulphate ($C_{12}H_{25}NaO_4S$, >90%), Ascorbic acid ($C_6H_8O_6$, >99%) and Sodium hydroxide (NaOH, >97%) were obtained from E.Merck (India) Ltd. All solutions were prepared using triply distilled de-ionized water.

4.2.2 Preparation of Silver Seed:

A typical procedure for the synthesis of silver seed hydrosol was as follows. 0.5 ml 10^{-2}(M) $AgNO_3$ solution and 2ml 2.5×10^{-3}(M) trisodium citrate solution were added to 17.5 ml distilled water, taken in a two necked round bottom flask and the solution was kept under ice cold condition for 15 minutes. Then 0.3 ml 10^{-2} (M) ice cold aqueous $NaBH_4$ solution was added all at once with vigorous stirring and the stirring was continued for 45 sec. Solution became golden yellow in colour, indicating the formation of silver hydrosol. Resulting silver hydrosol was heated to 75-80°C for 10 min. to decompose excess $NaBH_4$ present in solution. Silver hydrosol thus prepared was aged for 2 hrs. at room temperature before using as seed.

4.2.3. Preparation of silver nanostructures of varying morphologies.

Growth solution containing aqueous solution of 0.5 ml 10^{-2}(M) $AgNO_3$, 10ml 0.1 (M) SDS and 0.2 ml 0.1 (M) ascorbic acid was prepared in a 25 ml conical flask. 0.5 ml silver seed solution was added to this growth solution and stirred for few seconds for well mixing. Next, 0.05 ml 1(M) NaOH solution was added to it with constant stirring and the solution turned pink in colour within few seconds indicating the formation of anisotropically grown silver nanostructures.

4.2.4. Instrumentations and measurements:

On-line monitoring of synthesized silver hydrosol has been done by UV-Vis spectroscopic study using a 'SHIMADZU UV-1601' spectrophotometer. Morphology and size of particles were investigated using Philips 'TECNAI-FE12' Transmission Electron Microscope (120 keV). Crystallinity of metallic nanoparticles was examined using 'Rigaku Miniflex-II' X-ray diffractometer.

4.3. Results and discussion:

4.3.1: TEM Study:

Fig.4.1A shows the TEM image of silver nanoseed and it illustrates that majority of the particles are spherical in shape. Percentage particle's size distribution is shown as a histogram plot in fig.4.1B. Histogram plot suggests that majority of the seed particles have diameter in the range between 8-16 nm.

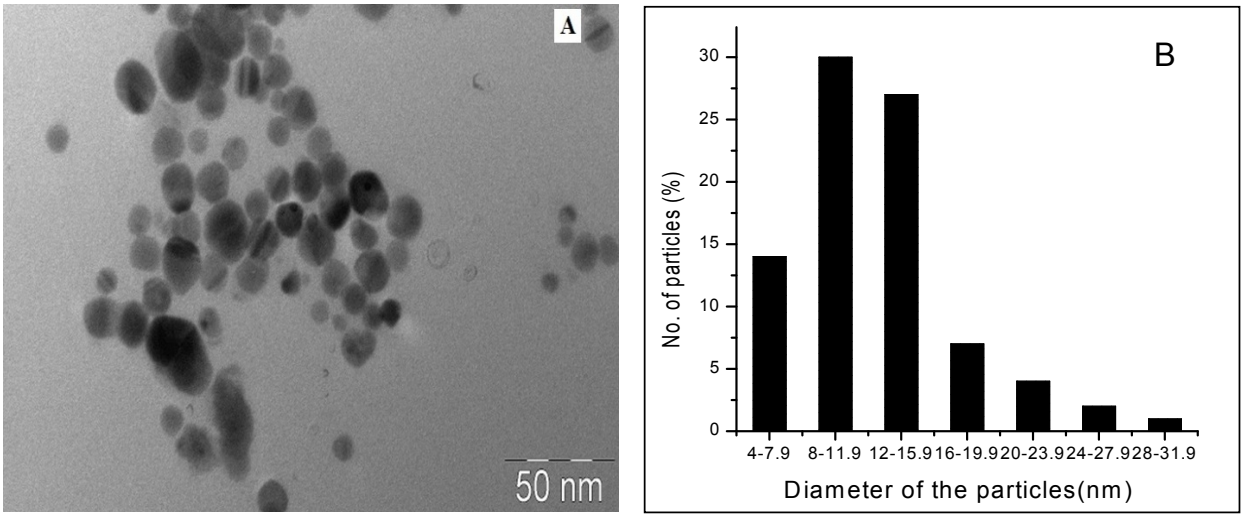

Fig.4.1: (A) TEM image and (B) histogram showing particle distribution of silver seed particles.

TEM micrograph of pink coloured silver sol obtained through seed mediated growth approach is shown in fig.4.2A. It shows the presence of silver nanostructures of different morphologies like triangular, pentagonal, hexagonal plates and rods like particles.

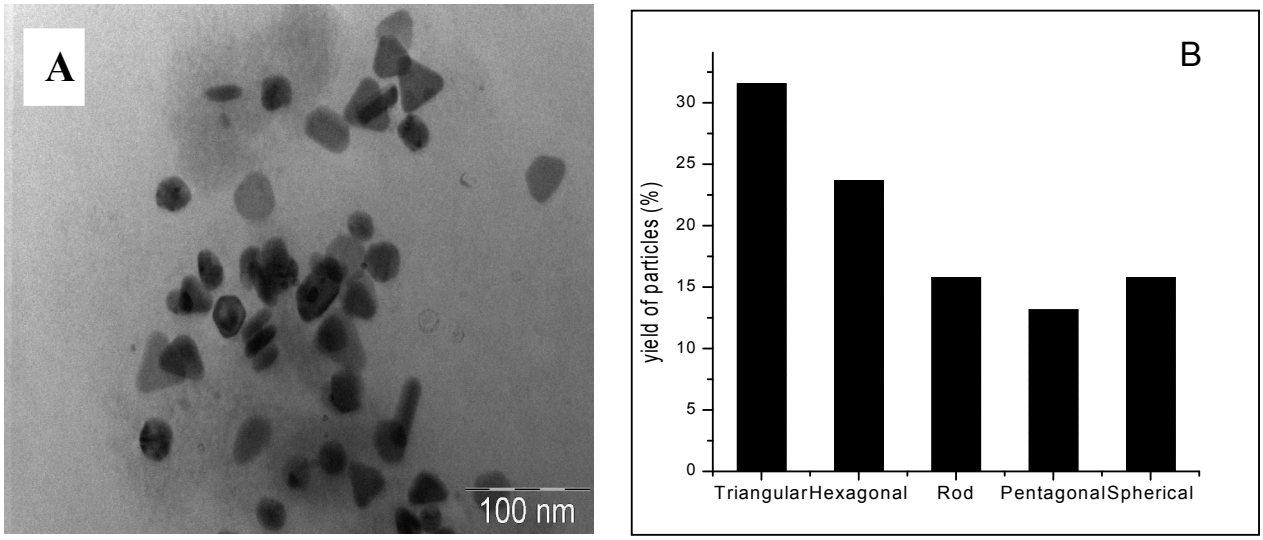

Fig.4.2: (A) TEM image and (B) histogram showing particle distribution of silver particles synthesized through seed mediated growth process.

A histogram plot showing the percentage distribution of different shaped silver nanostructures is given in fig.4.2B. It is clear from the histogram plot that the triangular shaped particles are predominant in growth solution.

4.3.2: UV-Vis spectroscopic study:

In general, on line synthesis of silver nano hydrosol is characterized by the UV-Vis spectroscopic study. It has been observed that silver nanoparticles interact with visible light more effectively than any known inorganic or organic chromophore, resulting in the existence of surface plasmon resonance (SPR). The position of surface plasmon resonance band in UV-Vis spectra is sensitive to particle's shape, size, its interaction with the medium, local refractive index and the extent of charge transfer between medium and the particles.

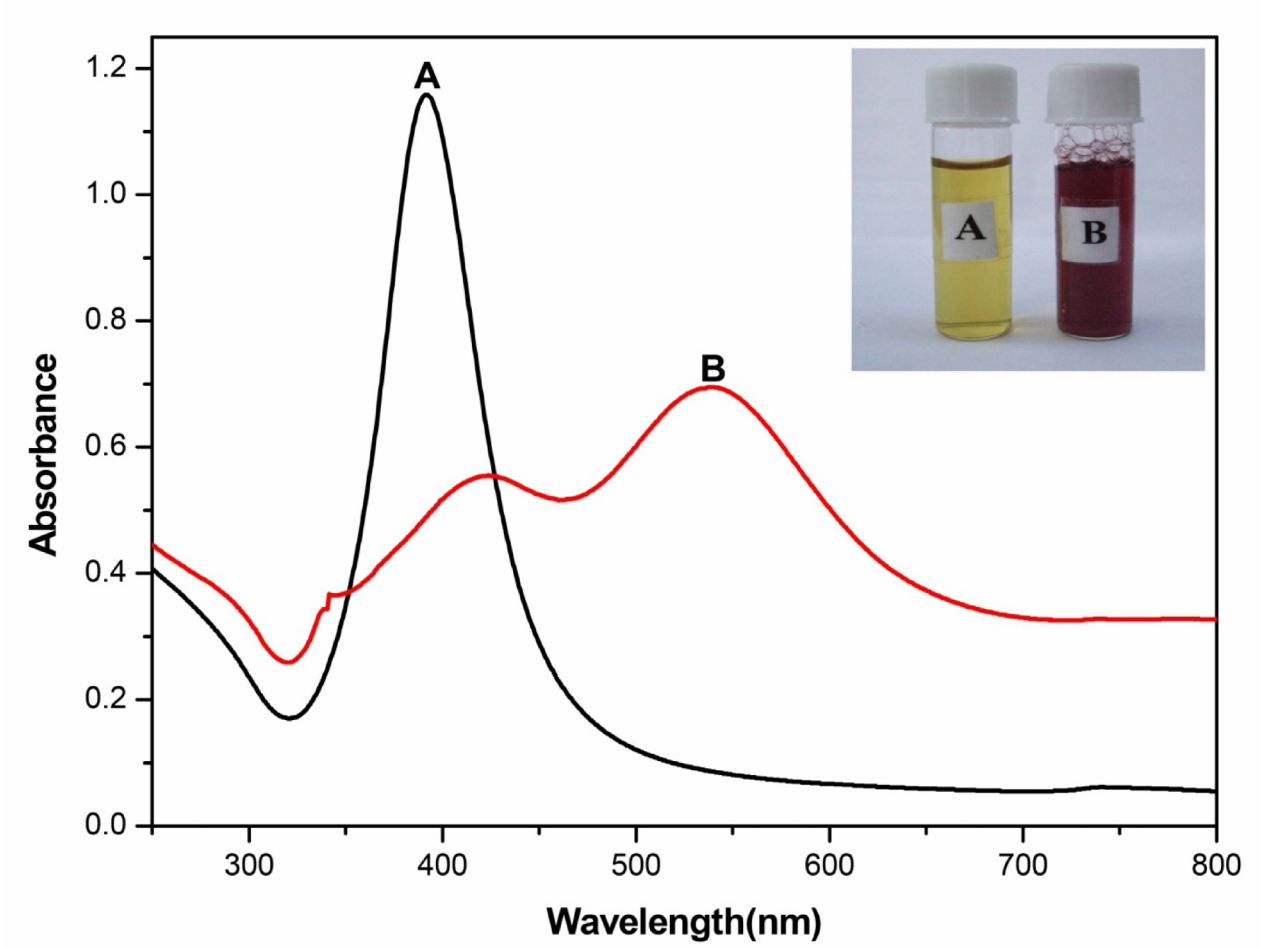

Fig.4.3: UV-Vis extinction spectra of (A) silver seed sol and (B) silver sol synthesized through seed mediated growth process. (Inset shows the colour of silver hydrosols.)

Fig.4.3 shows the UV-Vis extinction spectra of silver seed solution and the silver sol obtained through seed mediated growth process. The yellow coloured (inset of fig.4.3) citrate stabilized silver seed hydrosol displays a sharp band at λ_{max} ~ 390 nm. This observed absorption peak at ~390 nm is generally attributed to the surface plasmon resonance (SPR) of spherical silver nanoparticles. UV-Vis extinction spectra of pink coloured (inset of fig.4.3) SDS stabilized silver sol obtained through the seeding growth approach shows three distinct plasmon absorption bands located at ~340 nm, ~423 nm and ~537 nm. For nonspherical metallic NPs, the surface plasmons are unevenly distributed around them, manifesting in a shape dependence of the SPR absorption

spectra [29]. The plasmon resonance of metallic nanorods, for example, splits into two peaks: (i) a strongly red-shifted long axis or longitudinal mode (L) polarization parallel to the long axis) and (ii) a slightly blue-shifted transverse mode (T) polarization perpendicular to the long axis). As the aspect ratio of a nonspherical metal particle increases, the separation between the two plasmon bands becomes more pronounced. Triangular metallic NPs exhibit multipole plasmon resonances along with the SPR band due to longitudinal and transverse modes [30, 31]. The band located at ~340 nm is attributed to the out-of-plane quadrupole resonance [32]. The bands at 423 nm and 537 nm are due to out-of -plane (transverse) dipole resonance and in-plane (longitudinal) dipole resonance respectively. Various research groups have already reported similar type of SPR bands for triangular nanoplates [32, 33]. TEM image of the growth solution (fig.4.2A) shows that majority of the particles are triangular in shape. In general, the broad longitudinal band at ~537 nm can be attributed to the presence non-spherical particles in the sample. The band at ~423 nm is attributed in part to the presence of the spherical particles.

4.3.3: Role of sodium hydroxide in growth solution:

UV-Vis spectra of silver hydrosol synthesized in presence and absence of sodium hydroxide in the growth solution are shown in fig.4.4. Both the spectra show the transverse and longitudinal SPR bands and thus indicating the formation of anisotropically grown silver nanoparticles.

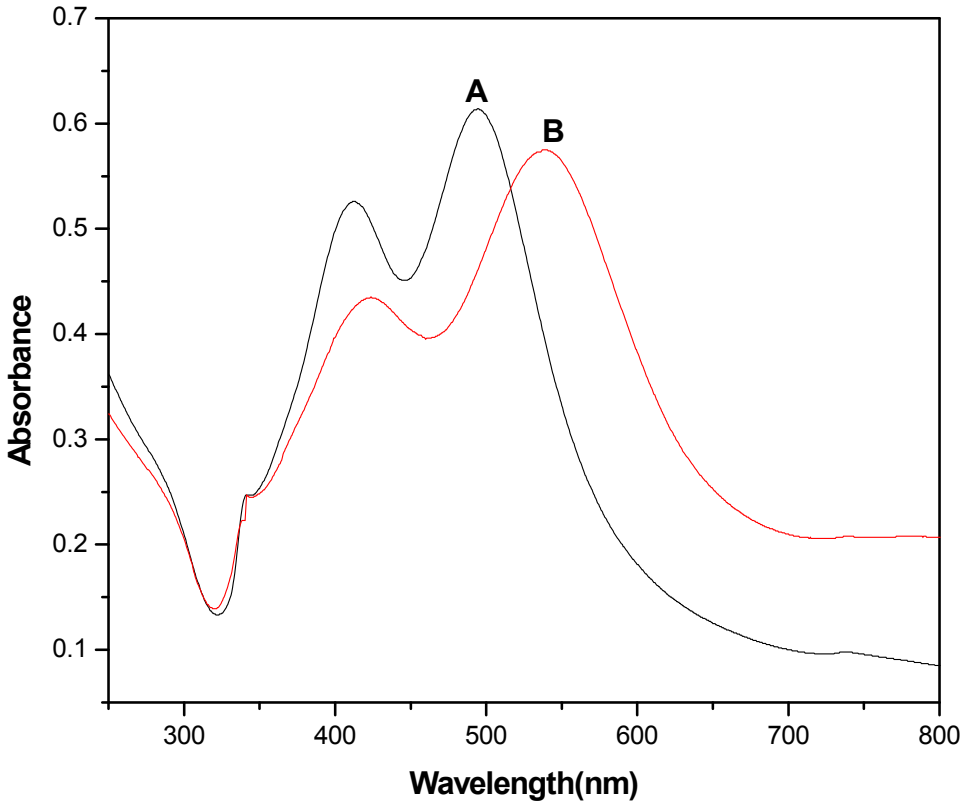

Fig.4.4: UV-Vis extinction spectra of silver hydrosol synthesized through seed mediated growth processes (A) in absence and (B) in presence of NaOH

Fig.4.4 also illustrates that both the bands shifted to the red, particularly the longitudinal SPR band shifted more (40 nm) to the red and broaden when NaOH was added during the growth process. There are reports on increased reducing power of ascorbic acid (the values of pKa_1 and pKa_2 are 4.10 and 11.79 respectively) at higher p^H [34]. In presence of NaOH, more and more silver ions are reduced at a faster rate and deposited on the silver nanocrystal surfaces, which are relatively less protected by SDS. This results the formation of anisotropically grown bigger silver nanostructures.

4.3.4: XRD analysis:

Fig.4.5(A & B) shows the XRD patterns of vacuum dried silver nanoseed and the particles obtained through growth process respectively.

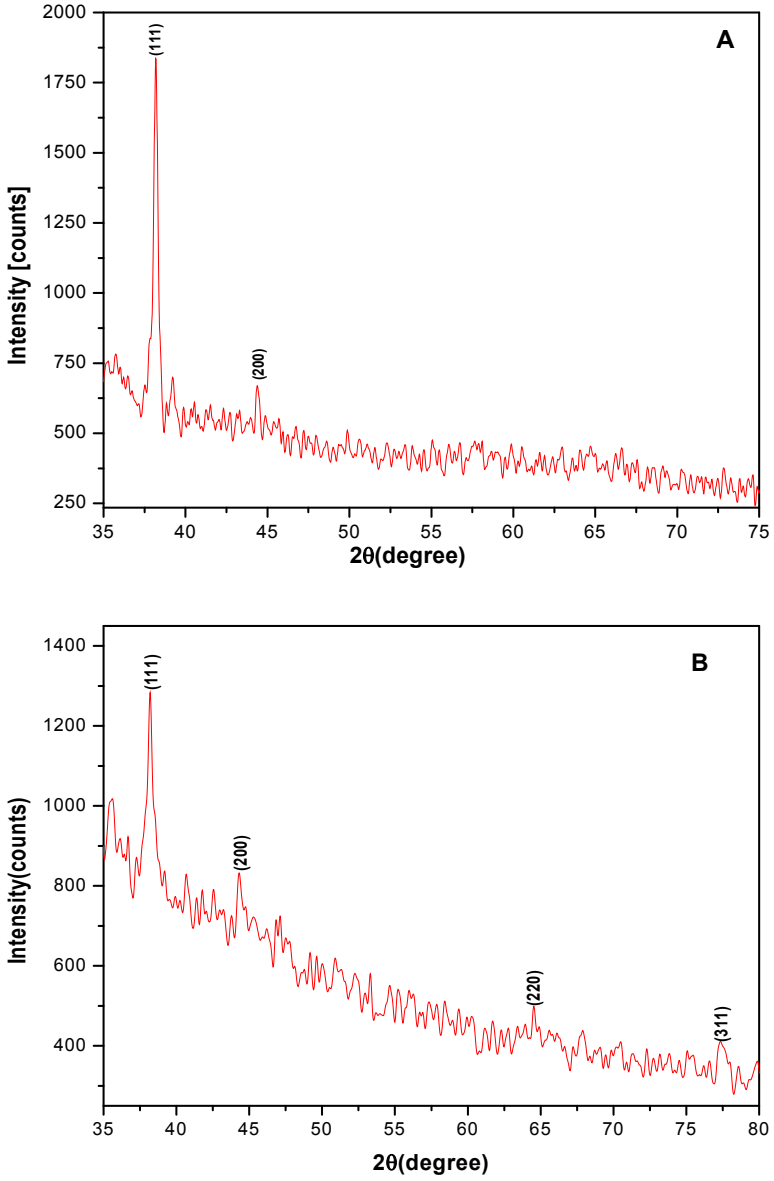

Fig.4.5: XRD diffractogram of (A) silver nanoseed and (B) silver nanoparticles synthesized through seed mediated growth process.

A number of Bragg reflections with 2θ values of 38.25° and 44.40° are observed for seed particles and 38.31°, 44.43°, 64.60° and 77.30° for growth particles. These diffraction angles correspond to the presence of (111) and (200) lattice planes of face centered cubic (fcc) lattice of silver in seed and (111), (200), (220) and (311) lattice planes in growth [35]. This XRD pattern confirms crystalline nature of the synthesized nanoparticles. As shown in figure 4.5 (A&B), the overwhelmingly intense diffraction peaks located at 2θ = 38.25° and 38.31° for seed and growth respectively, which are from the (111) lattice plane of face centered cubic (fcc) silver, indicates that the silver nanoparticles are made of pure silver and abundant in (111) facets, and their (111) planes tended to be preferentially oriented parallel to the surface of the supporting substrate [36].

4.4. Conclusions:

We have developed a seeding growth approach for the synthesis of silver nanostructures of different morphologies i.e. triangular, hexagonal and pentagonal plates and rod shaped particles. Important features of a useful synthetic procedure are that the particles should be stable and secondarily it is desirable for processes such as biofunctionalization i.e. preparation should be carried out in aqueous environment. The present synthetic method has made considerable progresses in overcoming these issues. We believe that this present method of synthesis is simple and straightforward and a fine tune of one or more parameter can be useful to synthesize silver nanoparticles of a particular morphology.

References:

[1] Y. Wang, N. Toshima, *J. Phy. Chem. B* 101, **1997**, 5301

[2] J.C. Lin, C.Y. Wang, *Mater. Chem. Phys.* 45, **1996**, 136

[3] I.R. Gould, J.R. Lenhard, A.A. Muenter, S.A. Godleski, S. Farid, *J. Am. Chem. Soc.* 122, **2000**, 11934

[4] W.A. de Heer, *Rev. Mod. Phys.* 65, **1993**, 611

[5] M.G. Bawendi, M.L. Steigerwald, L.E. Brus, *Annu. Rev. Phys. Chem.* 41, **1990**, 477

[6] Y. Kayanuma, *Phys. Rev. B,* 38, **1988**, 9797

[7] S. Wang, Q. Gong, Y. Zhu, J.Liang, *Appl. Surface. Sci.,* 255, **2009**, 8063

[8] Y. Xia, J.A. Rogers, K.E. Paul, G.M. Whitesides, *Chem. Rev.* 99, **1999**, 1823

[9] A.N. Shipway, M. Lahav, I. Willner, *Adv. Mater.* 12, **2000**, 993

[10] S. Link, Z.L. Wang, M.A. El-Sayed, *J. Phys. Chem. B*, 103, **1999**, 3529

[11] P. Taneja, P. Ayyub, R. Chandra, *Phys. Rev. B*, 65, **2002**, 245412 (6 pages)

[12] B.L. Cushing, V.L.Kolesnichenko, C.J. O'Connor, *Chem.Rev*.104, **2004**, 3893

[13] D.K. Bhui, P. Sarkar, H. Bar, G.P. Sahoo, S.P. De, A. Misra, *J Mol. Liqs.* 145, **2009**, 33

[14] P. Sarkar, D.K. Bhui, H. Bar, G.P. Sahoo, S.P. De, A. Misra, *J. Lumin.* 129, **2009**, 704

[15] Y.C. Liu, L.H. Lin, *Electrochem. Commun*. 6, **2004**, 1163

[16] K. Mallick, M.J. Witcomb, M.S. Scurrell, *Mater. Chem. Phys.* 90, **2005**, 221

[17] H. Bar, D.K. Bhui, G.P. Sahoo, P. Sarkar, S.P. De, A. Misra, *Colloids Surf.A*, 339, **2009**, 134

[18] H. Bar, D.K. Bhui, G.P. Sahoo, P. Sarkar, S. Pyne, A. Misra, *Colloids Surf.A,* 348, **2009**, 212

[19] A.B. Smetana, K.J. Klabunde, C.M. Sorensen, *J. Colloid Interface Sci.,* 284, **2005**, 521

[20] J. Hu, B. Zhao, W. Xu, Y. Fan, B. Li, Y. Ozaki, *Langmuir,* 18, **2002**, 6839

[21] N. Satoh, K. Kimura, Bull. Chem. Soc. *Japan,* 62, **1989**, 1758

[22] K. Esumi, T. Tano, K. Torigoe, K. Meguro, *Chem. Mater.,* 2, **1990**, 564

[23] A. Colli, S. Hofmann, A.C. Ferrari, C. Ducati, F. Martelli, S. Cabrini, A. Franciosi J. Robertson, *Appl. Phys. Letters,* 86, **2005**, 153103 (3 pages)

[24] Z.L. Wang, S.A. Harfenist, I. Vezmar, R.L. Whetten, J. Bentley, N.D. Evans, K.N. Alexander, *Adv. Mater.,* 10, **1998**, 808

[25] Y. Sun, B. Gates, B. Mayers, Y. Xia, *Nano Lett.,* 2, **2002**, 165

[26] C.L. Haynes, R.P. Van Duyne, *J. Phys. Chem. B,* 105, **2001**, 5599

[27] Y. Yin, P Alivisatos, *Nature,* 437, **2005**, 664

[28] Y. Sun, Y. Xia, *Adv. Mater.,* 15, **2003**, 695

[29] Y. G. Sun, Y.N. Xia, *Proc. SPIE,* 5221, **2003**, 164

[30] J. Kottmann, O. Martin, D. Smith, S. Schultz, *Opt. Express,* 6, **2000**, 213

[31] E. Hao, R. C. Bailey, G. C. Schatz, J. T. Hupp, S. Li, *Nano Lett.,* 4, **2004**, 327

[32] R. Jin, Y.C. Cao, E. Hao, G.S. Metraux, G.C. Schatz, C.A. Mirkin, *Nature,* 425, **2003**, 487

[33] R.C. Jin, Y.W. Cao, C.A. Mirkin, K.L. Kelly, G.C. Schatz, J.G. Zheng, *Science,* 294, **2001**, 1901

[34] C.C. Huang, Z. Yang, H.T Chang, *Langmuir,* 20, **2004**, 6089

[35] Joint committee on powder diffraction standard data files (JCPDS 04-0783).

[36] V. Germain, J. Li, D. Ingert, Z.L. Wang, M.P. Pileni, *J. Phys. Chem. B,* 107, **2003**, 8717

Chapter V

Synthesis of silver nanodiscs and triangular nanoplates in PVP matrix: Photophysical study and simulation of UV-Vis extinction spectra using DDA method

*A part of this chapter has been published in the article, **Sadhan Samanta**, Priyanka Sarkar, Santanu Pyne, Gobinda Prasad Sahoo, Ajay Misra, **Journal of Molecular Liquids 165 (2012) 21–26**

Synthesis of silver nanodiscs and triangular nanoplates in PVP matrix: Photophysical study and simulation of UV-Vis extinction spectra using DDA method

5.1. Introduction:

Among the metallic nanostructures, silver is the most attractive because of its high conductivity and intense colorimetric effect in nanoscale size. By processing silver into well defined dimensions, its performance in most of the applications could be significantly enhanced. Silver nanoparticles with different shapes like zero dimensional spherical or tetrahedral quantum dots [1], one dimensional silver nanorods and nanowires [2-4], and two dimensional nanoplates [5], nanoprisms [6], and nanodiscs [3,7] have been synthesized by various group of researchers. These nanostructures display a strong UV-Vis extinction band which is not present in the spectrum of the bulk metal. Their peak wavelength and localized surface plasmon resonance significantly depend on their morphology, size, interparticle spacing, intrinsic dielectric properties and local environment including solvents, substrates and adsorbates [8]. Any changes of these parameters could lead to the optical drift in absorption spectrum and thus influence the optical applications in practice. To utilize and optimize the chemical and physical properties of metal nanoparticles, a large spectrum of research [7, 9-13] has been focused to control the size and shape, which is important in tuning their physical, chemical and optical properties.

Synthesis of anisotropic metal nanoparticles motivates the development and innovation of theoretical methods for describing the unique properties of these nanoparticles. The study of

colours of metal nanoparticles can be traced back to 19th century when Michael Faraday studied the colour of gold colloid in stained glass windows [14]. Mie presented an analytical solution to Maxwell's equations which describe an isolated spherical particle in 1908 [15]. Although many extensions of Mie theory have been made for covering different aspects including magnetic and coated spheres [16, 17], this analytical method has a fundamental limitation that the exact solutions are restricted only to highly symmetric particles such as spheres and spheroids. Recently, a number of theoretical approaches have been developed, based on more advanced scattering theories for anisotropic metal nanoparticles. These include the generalized multipole technique (GMT) [18], the T-matrix method [19], the discrete dipole approximation (DDA) [20] and the finite different time domain (FDTD) method [21]. The first two methods can be classified as surface-based methods where only the particle's surface is discretized and solved numerically. The latter methods are referred to as volume-based methods where the entire volume is discretized. Among these methods, DDA has been demonstrated to be one of the most powerful and flexible electrodynamics methods for computing the optical spectra of particles with an arbitrary geometry. DDA involves replacing each particle by an assembly of finite cubical elements, each of which is small enough that only dipole interactions with an applied electromagnetic field and with induced fields in other elements need to be considered. This reduces the solution of Maxwell's equation to an algebraic problem involving many coupled dipoles. The DDA method has been widely used to describe the shape dependence of plasmon resonance spectra, including studies of triangular prism [22], discs[3, 23], cubes [24], truncated tetrahedral [25], shell-shaped particles [26], small clusters of particles [27] and many others [2, 28]. Recently, Schatz group [29] has carried out extensive studies showing that DDA is suited for optical calculations of the extinction spectrum and the local electric field distribution in metal particles with different geometries and environments. Again, Lee and El-Sayed [30] have

investigated the systematic dependence of nanorod absorption and scattering on their aspect ratio, size and medium refractive index using DDA based simulation method.

This chapter focuses on the synthesis of silver nanostructures of different morphologies via seeding growth approach, using MC and PVP polymer as soft template and different amount of seed have been used in the growth solution. It is shown that amount of added seed in the growth solution plays important role in controlling the morphology of the nanoparticles. We also present the theoretical calculations for extinction efficiency of nanospheres and nanodiscs by employing the discrete dipole approximation (DDA) methodology.

5.2. Materials and Methods:

5.2.1. Chemicals:

All chemicals used in the experiment were analytic reagent (AR) grade. Silver nitrate ($AgNO_3$, >99.8%) was purchased from RFCL Ltd. (India). Sodium borohydride ($NaBH_4$,>99%) was purchased from S.D. Fine Chem.Ltd. Ascorbic acid ($C_6H_8O_6$,>99%) and Methyl cellulose (degree of methylation ~2 and viscosity 4000 cPs for 2% w/v; at 20°C) were purchased from E.Merck Ltd. (India). Polyvinyl pyrrolidone (PVP, M_w=40,000) was received from Loba Chem.Ltd. (India). Triple distilled deionized water was used throughout the experiments. All the glassware were cleaned by freshly prepared aqua regia and washed with triple distilled deionized water prior to the experiments.

5.2.2. Preparation of methyl cellulose (MC) solution:

85 mg methyl cellulose was taken in a 100 mL dry R.B. flask. It was heated to 85-90^0 C with triple distilled water for ~1 hour. The turbid white solution was kept in deep freeze for an hour and clear MC solution was obtained.

5.2.3. Preparation of silver seed nanoparticles:

0.5 ml 0.01 M aqueous $AgNO_3$ and 15 ml 0.085 % (w/v) MC solution were added to 4.5 mL distilled water taken in a two necked round bottom flask. The mixture was cooled in ice bath for few minutes. Then 0.05 mL 0.01 M ice cooled $NaBH_4$ solution was added all at once with vigorous stirring. Colour of the whole solution turned yellow within few second. Solution was kept at room temperature for about 2 hrs to decompose excess borohydride and used as seed in the subsequent growth processes.

5.2.4. Preparation of silver nanodiscs and triangular nanoplates:

A number of growth solutions containing 800 mg PVP, 10 ml distilled water and 0.5 ml 0.01 M $AgNO_3$ solution, were prepared. To each of these growth solutions, diffrent amounts of aged (2hrs) seed sol (0.5 ml and 0.2 mL respectively) was added after the addition of 0.06 ml 0.1 M ascorbic acid. The mixtures were stirred for few second for homogeneous mixing. Pink (sol-b) and blue (sol-c) colour silver sols are obtained within few minutes. This indicates the formation of anisotropically grown silver nanoparticles.

5.2.5. Instrumentations and measurements:

Characterization of nanoparticles was done by UV-Vis spectroscopy and transmission electron microscopy (TEM). On-line monitoring of the synthesized silver hydrosol has been carried out using a 'SHIMADZU UV-1601' spectrophotometer. Morphology and size of particles were investigated by transmission electron microscopic (TEM) study using JEOL-JEM-2100 high-resolution transmission electron microscope.

5.2.6. Discrete Dipole Approximation (DDA):

DDA is a numerical method in which the object studied is represented as a cubic lattice of N-polarizable point dipoles localized at r_j, j=1,2,……,N, each one characterized by a polarizability α_j. There is no restriction on the localization of cubic lattice sites so that DDA represents a particle of arbitrary shape and composition. Polarization of each dipole, P_j, is then described under the electric field at the respective position by

$$\mathbf{P}_j = \alpha_j \mathbf{E}_{loc}(\mathbf{r}_j) \quad \text{……..(1)}$$

Where E_{loc} is the electric field at r_j that is the sum of the incident field $E_{inc,j}$ and the field radiated by all other N-1 induced dipoles $E_{other,j}$. The incident field $E_{inc,j}$ is given by

$$\mathbf{E}_{inc,j} = \mathbf{E}_0 \exp(i\mathbf{k}\cdot\mathbf{r}_j - i\omega t) \quad \text{……..(2)}$$

Where, r_j is the position vector, t is the time, ω and k are the angular frequency and the wave vector respectively. The local field at each dipole is then represented by

$$\mathbf{E}_{loc,j} = \mathbf{E}_{inc,j} + \mathbf{E}_{other,j} = \mathbf{E}_0 \exp(i\mathbf{k}\cdot\mathbf{r}_j - i\omega t) - \sum_{j\neq k} \mathbf{A}_{jk}\cdot\mathbf{P}_k \quad \text{……..(3)}$$

where P_j is the dipole moment of the j^{th} element and $-A_{jk}P_k$ is the electric field at including retardation effects. Each element A_{jk} is a 3N×3N matrix which represents the interaction between all dipoles as given below:

$$\mathbf{A}_{jk}\cdot\mathbf{P}_k = \frac{\exp(ikr_{jk})}{r_{jk}^3} \times \left\{ k^2 \mathbf{r}_{jk} \times (\mathbf{r}_{jk} \times \mathbf{P}_k) \times \frac{1 - ikr_{jk}}{r_{jk}^2} \times \left[r_{jk}^2 \mathbf{P}_k - 3\mathbf{r}_{jk}(\mathbf{r}_{jk}\cdot\mathbf{P}_k) \right] \right\}, (j \neq k) \quad \text{….(4)}$$

Where $r_{jk}=r_j-r_k$ and $k=||k||$. Defining $Ajj= \alpha_j^{-1}$, reduces the scattering problem to finding the polarization P_k that satisfy a system of N inhomogeneous linear complex vector equations.

$$\sum_{k=1}^{N} \mathbf{A}_{jk}\mathbf{P}_k = \mathbf{E}_{loc,j} \quad \text{……..(5)}$$

Once, equation (5) has been solved for the unknown polarizations P_j, the extinction C_{ext}, absorption C_{abs} and scattering C_{sca} cross sections may be evaluated from the optical theorem, thus giving

$$C_{ext} = \frac{4\pi k}{|\mathbf{E}_0|^2} \sum_{j=1}^{N} \mathrm{Im}(\mathbf{E}^*_{loc,j} \cdot \mathbf{P}_j) \quad \text{.....(6)}$$

$$C_{abs} = \frac{4\pi k}{|\mathbf{E}_0|^2} \sum_{j=1}^{N} \left\{ \mathrm{Im}\left[\mathbf{P}_j \cdot \left(\alpha_j^{-1}\right)^* \mathbf{P}_j^*\right] - \frac{2}{3} k^3 |\mathbf{P}_j|^2 \right\} \quad \text{.....(7)}$$

where, the superscript asterisk denotes the complex conjugate. The scattering cross-section $C_{sca} = C_{ext} - C_{abs}$ may also be directly evaluated once the polarization P_j is known. We defined the absorption efficiencies as $Q_{abs} = C_{abs}/A$ where $A = \pi a_{eff}^2$, and a_{eff} is known as "effective radius" and defined through the concept of an effective volume equal to $4\pi a_{eff}^3/3$ i.e the radius of a sphere having a volume equal to that of the particle. A given scattering problem is then characterized by the dimensionless "size parameter"

$x \equiv k a_{eff} = 2\pi a_{eff}/\lambda$

The target particle in the surrounding dielectric medium is considered by using a dielectric function of the target ε relative to that of the medium ε_m, which is reflected in the DDA calculation in the form of dipole polarizability. The dielectric function of silver is generated from the bulk experimental data of Johnson and Christy [31] and the medium is assumed to have a refractive index n_m of 1.34, close to that of the water. DDA can be applied to any scattering problem of particles with arbitrary shape if we can generate the dipole array to represent the continuum target. The chief requirement for the applicability of DDA is that the interpole separation '*d*' be small compared to any structural dimensions of the target and the wavelength of light λ, or, in other words, that a sufficient number of dipoles be employed to represent the target. This criterion is quantitatively expressed as $|m|kd < 1$, where m is the complex refractive index of the target material, and $k \equiv 2\pi/\lambda$, where λ is the wavelength in vacuum. For the noble metals like Ag and Au

with a large value of extinction coefficient, better accuracy of the DDA calculation can only be achieved by using a larger number of dipoles and it can be achieved by reducing the *d* value. DDA is not suitable for a very large values of the size parameter '*x*', or vary large value of refractive index, '*m*'.

The complex linear equation (5) for the induced polarization is solved by using the DDSCAT7.0 program written by Drain and Flatau [32]. Dipole polarizabilities are assigned by the lattice dispersion relation (LDR) developed by Drain and Goodman [33], which includes a radiative reaction correction term and suited, for finite dipole arrays. The code incorporates Fast Fourier Transform (FFT) methods. DDSCAT 7.0 includes capability to calculate scattering and absorption by targets that are periodic in one or two dimensions-array of nanostructures.

5.3. Results and Discussion:

5.3.1. UV-Vis spectroscopic study:

UV-Vis spectroscopy is one of the most important techniques to characterize the metal nanoparticles. The absorption behavior arises due to surface plasmon resonance (SPR), which originates from coherent oscillations of electrons in the conduction band of nanoparticles induced by the electromagnetic field. Silver nanoparticles show a very strong surface plasmon resonance (SPR) band in the visible region of light with an extinction co-efficient upto four times than that of gold nanoparticles [34]. The efficiency of interaction of nanosized silver particles with light is attributed to the large density of conducting electrons present and the unique frequency dependence of the real and imaginary parts of the dielectric function [35]. The UV-Vis spectrum of yellow coloured silver seed sol displays (fig.5.1) intense peak centered at 400 nm with a full width at half maximum (FWHM) of 48 nm, which is conventionally observed for spherical silver nanoparticles. UV-Vis spectra of sols synthesized through seed mediated growth method (sol-b

and c) exhibit three distinct bands (fig.5.1). Sample-b shows three bands at 336, 415 and 583 nm whereas sample-c shows three bands located at 336, 452, and 741 nm.

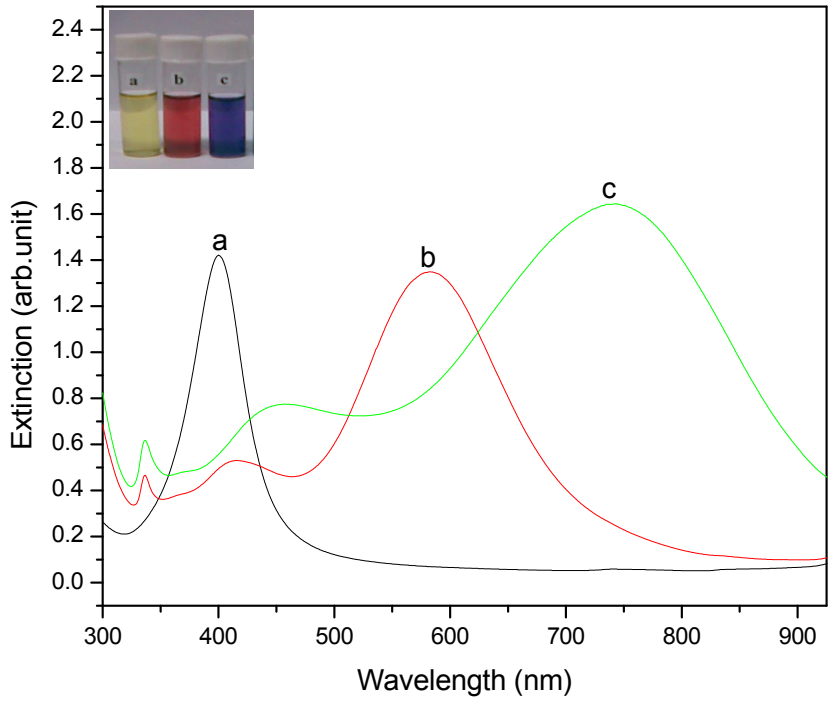

Fig.5.1: UV-Vis spectra of silver nano (a) seed; sol a, (b) growth; sol b, and (c) growth; sol c (inset shows the colour of hydrosols).

According to theoretical calculations by Schatz and co-workers [36], these three bands could be assigned to the out-of-plane quadruple resonance, out-of- plane dipole resonance (transverse) and in-plane dipole resonance (longitudinal) bands respectively. Presence of these three bands indicates the presence of anisotropically grown nanoparticles in the growth sol [37]. The bands at 415 and 452 nm are attributed in part to the presence of spherical particles in the samples b and c. Red shifting of in-plane dipole resonance (longitudinal) indicates increased size of nanoparticles in growth sol-c compared to that in sol-b which is confirmed by TEM study.

5.3.2. TEM and SAED study:

Fig.5.2a shows the transmission electron microscopy (TEM) image of silver nanoparticles of sol a (seed). It displays that these silver nanoparticles are essentially spherical in shape. Histogram of particles as shown in fig.5.2b suggests that more than 80 % of particles has diameter in the range 13-17 nm. Fig.5.2c shows the SAED image of the particles confirming crystalline nature of these particles.

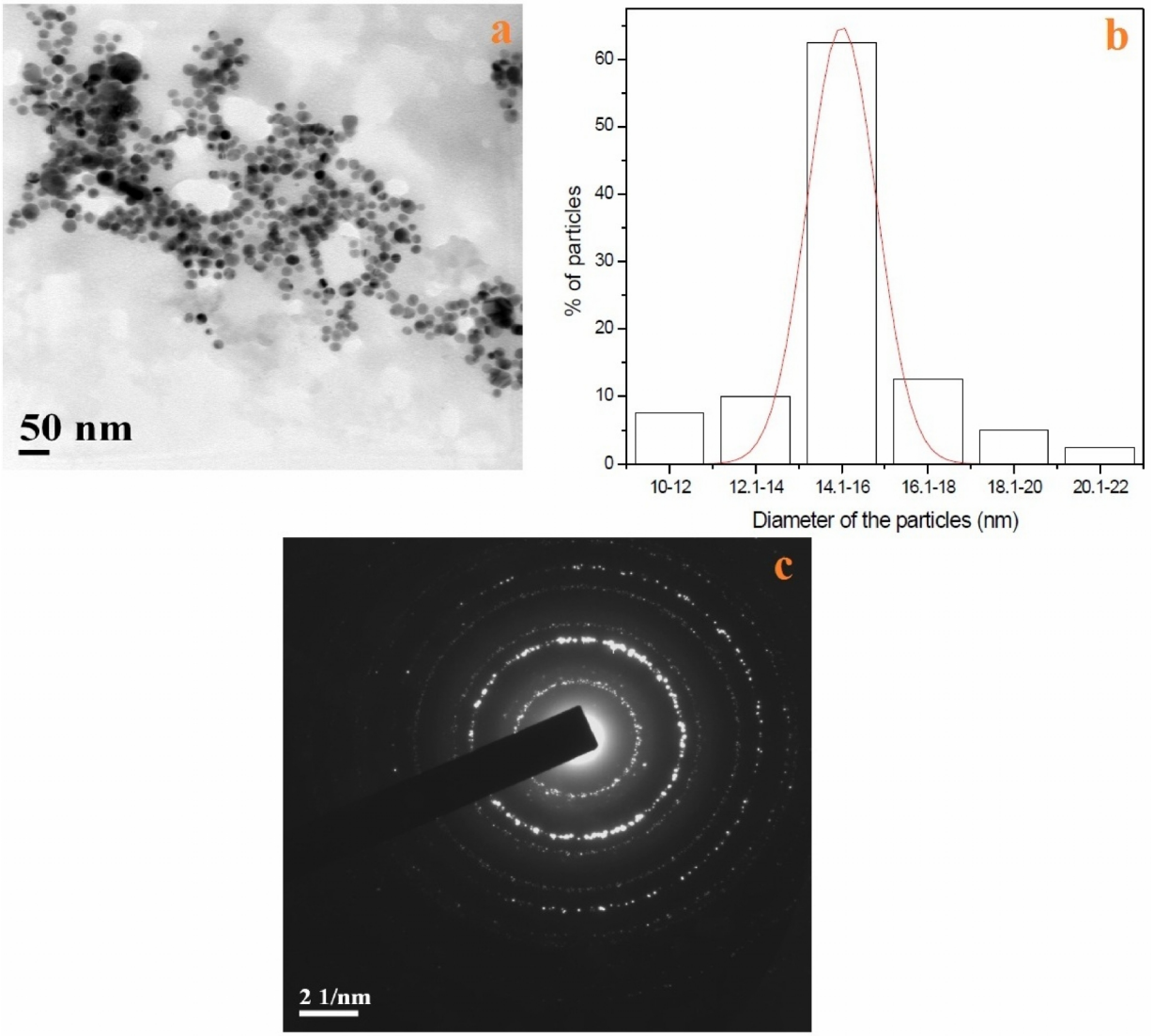

Fig.5.2: (a) TEM image (b) histogram showing particle distribution and (c) selected area electron diffraction (SAED) pattern, of silver nano seed.

TEM micrograph of sol b (fig.5.3a) illustrates that particles are mostly circular disc like and nearly 75% disc structure have diameter in the range 30-45 nm (fig.5.3b). Fig.5.3c shows the SAED image of the particles and it suggests the crystalline nature of the synthesized nanoparticles.

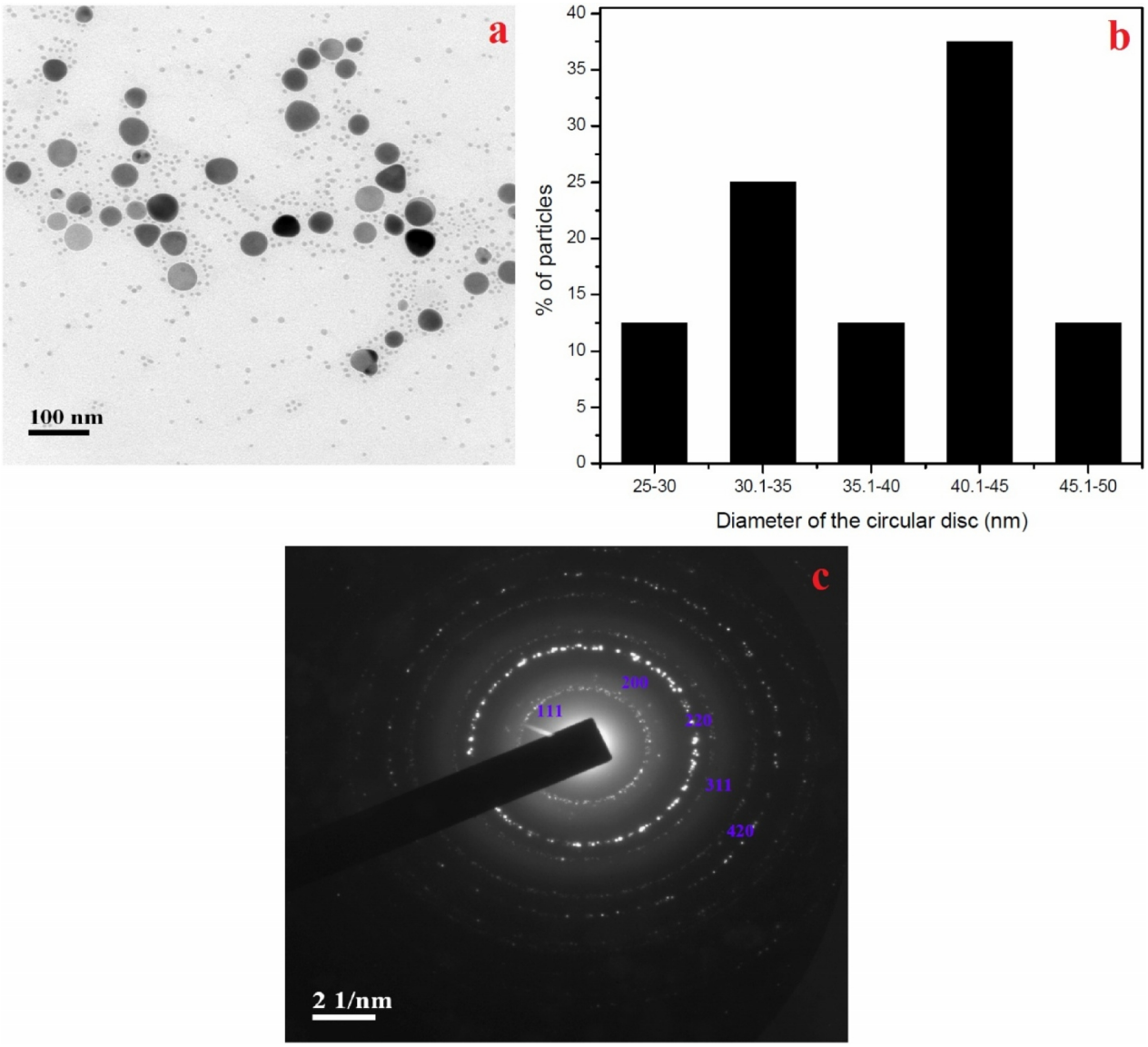

Fig. 5.3: (a) TEM image (b) histogram showing distribution of circular discs and (c) selected area electron diffraction (SAED) pattern, of growth sol b

On the other hand, TEM picture of silver sol c (fig.5.4a) where lower seed concentration are being used shows that nearly 70% particles are either triangular plate or truncated triangular plate like, ~20% are circular disc like (fig.5.4b).

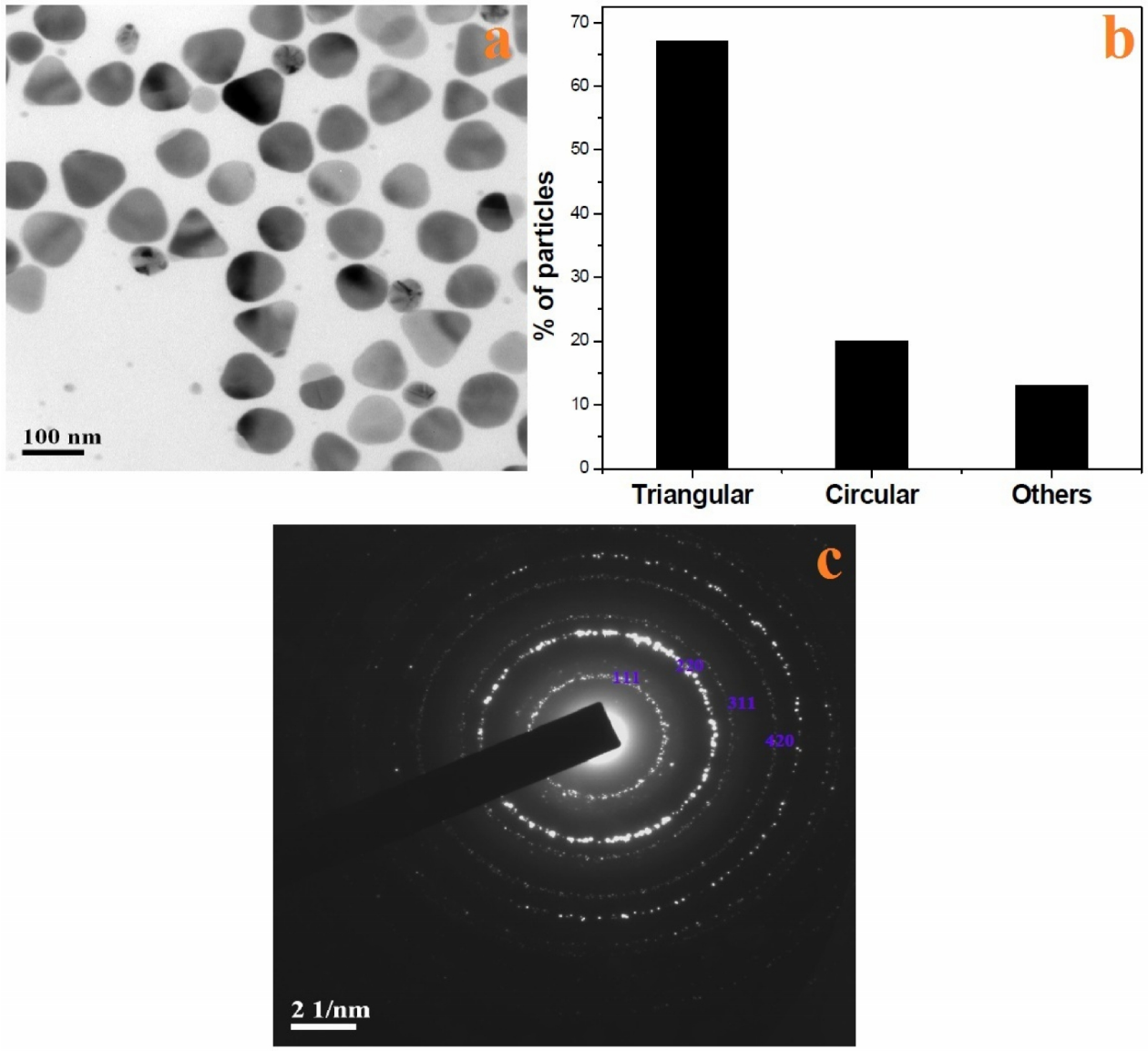

Fig. 5.4: (a) TEM image (b) histogram showing particle distribution and (c) selected area electron diffraction (SAED) pattern, of growth sol c

The increased size of nanoparticles in sol c compared to that in sol b can be explained by the fact that larger quantities of Ag^{+} ions per seed particle are available during the growth process

in sol c compare to sol b. The single crystalline structure of these nanoparticles was confirmed by their electron diffraction patterns. Fig.5.3c and 5.4c give the selected area electron diffraction (SAED) patterns that were obtained by aligning the electron beam perpendicular to the triangular facets of an individual nanoplate of sol b and sol c respectively. Three sets of spots could be identified from the diffraction pattern: the set with the strongest intensity could be indexed to the {220} planes of face centered cubic (fcc) silver with a corresponding lattice spacing of 1.44 Å (1.445Å in JCPDS File 04-0783). The outer set with the weakest intensity was caused by reflections from {422} planes. The inner set with a weaker intensity correspond to the formally forbidden 1/3{422} reflections (with a lattice spacing of 2.50Å). All these observations were consistent with previous studies on silver (or gold) nanocrystals bounded by atomic flat surfaces [38]. These spots are forbidden in a single crystal fcc metal, but can appear when two twin planes are parallel to one another. Particle distribution diagram of sol c shows that (fig.5.4b) majority of the particles are triangular in shape and it is clear from the TEM images that the triangular nanoparticles are truncated in shape. To get the information about the degree of truncation (T) and the edge length (d) of these particles, as shown in fig.5.5a, we assume that the particle is a right triangle and is included into a parent triangle with side length of a, and the truncated triangle is thus composed by an inner triangle with side length of b, three one third circles with equal radius and three rectangles. The degree of truncation is defined as T = b/a. Clearly, the shape of a particle will be of a perfect triangle if T = 1 and that will be a circle when T =0. By measuring the required parameters from TEM image, the average value of T obtained is 0.343 which suggests that the particles are very much truncated in nature. Fig.5.5b displays the distribution of degree of truncation (T) of the triangular particles in sample-c.

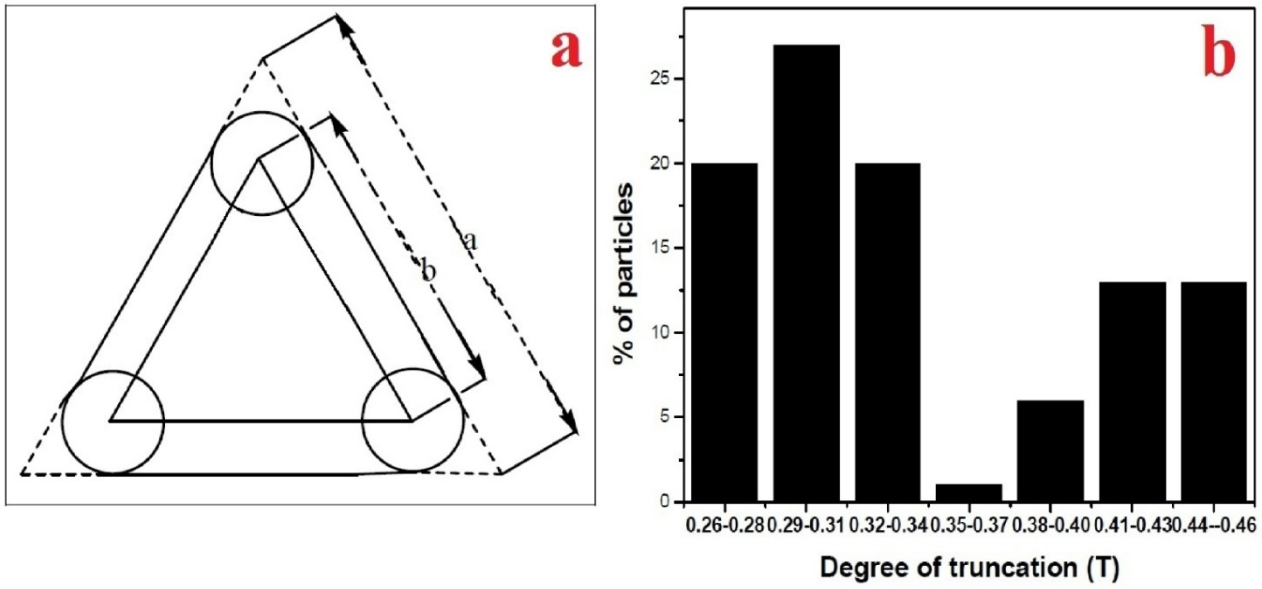

Fig. 5.5: (a) Schematic illustration of truncation and (b) histogram showing truncation distribution, in growth sol c

5.3.3. Simulation of UV-Vis extinction spectra using DDA method:

We carry out the analytical calculations for silver nanosphere using the modified Bohren and Hoffman code [39] based on Mie scattering theory and compared the results with the convergent solution of DDA. Fig.5.6 shows the extinction efficiency factors, $Q_{ext}(\lambda) = C_{ext}(\lambda)/(\pi a^2)$, of silver sphere, having radius of ~13 nm, both experimentally and also theoretically calculated by using the Mie scattering theory and also by the DDA method. In these calculations, the refractive index of the surrounding medium is approximated to have a value of 1.34 at all wavelengths, close to that of water. From fig.5.6, it is obvious that the DDA calculations are almost in good agreement with the results of the Mie scattering theory and also to that of the results obtained from experiments.

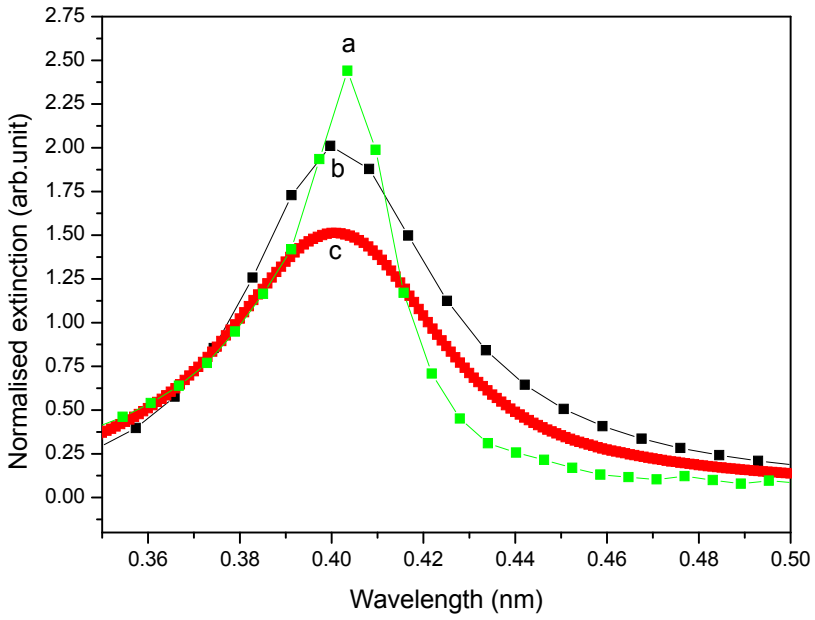

Fig. 5.6: Simulated spectra using (a) DDA (b) Mie's theory and (c) experimental UV-Vis spectrum of silver nano seed.

Theoretical calculation of extinction efficiency of circular silver nanodisks is performed using DDA methodology. For this calculation, we adapt the DDSCAT 7.0 code developed by Drain and Flatau [31] and the characterization of circular silver nanodisk has been done. Nanodisks absorb and scatter light more strongly because its circular symmetry gives it a larger effective dipole moment [40]. Several resonance modes can be taken into account in the absorption spectra of silver nanodisks: (i) dipolar in-plane resonance, the most studied resonance and located in general in the wavelength range between 600 and 1000 nm; (ii) dipolar out-of-plane resonance located around 400-600 nm; (iii) quadrupolar out-of-plane resonance located around 340 nm. The position as well as intensity of all these resonances varies as a function of the nanodisc geometry and size.

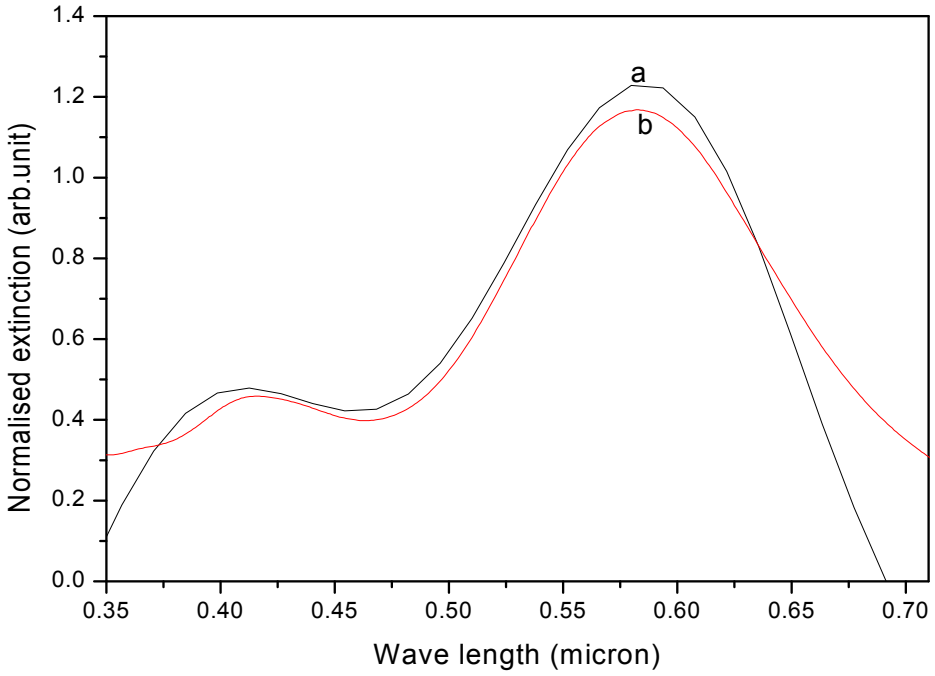

Fig. 5.7: (a) Simulated spectrum using DDA method and (b) experimental UV-Vis spectrum, of growth sol b

Effect of size on the optical scattering and absorption efficiencies and their relative contributions to the total extinction are systematically investigated for Ag nanodiscs. TEM micrograph shows the picture of silver nanodiscs having diameter ranging from 25-50 nm. Accordingly, we have simulated the extinction spectra of nanodisks by taking average diameter ~ 33 nm and the simulated spectrum is compared with the experimentally obtained spectrum which is shown in fig. 5.7. It is obvious, from this figure that the simulated spectrum is in good agreement with the experimental one.

5.4. Conclusions:

We have developed a new seeding growth approach to synthesize silver nanostructures having morphologies like circular disc and truncated triangular plates. It has been observed that

the colour of the synthesized sols and morphology of the particles can be tuned by varying the amount of seed concentration in the growth solution. Important feature of a useful synthetic procedure is that the particles should be stable and secondly it is desirable for processes such as biofunctionalization i.e. preparation should be carried out in aqueous environment without the use of toxic reagents. The present synthetic method has made considerable progress in overcoming these issues. These silver nanoparticles exhibit interesting optical properties. Investigation of optical absorption and scattering and their contributions to the total extinction was done using the discrete dipole approximation (DDA) method. Experimentally obtained UV-Vis extinction spectra for the spherical seed nanoparticles was compared with the resulting simulated plots obtained by using DDA based simulation and the well-known exact analytical solutions of Maxwell's equation derived from Mie theory for a sphere. Our present simulation of extinction spectra using DDA method suggests the potentiality of DDA methodology while calculating the extinction spectra of anisotropically grown silver particles.

References:

[1] A. Taleb, C. Petit, M.P. Pileni, *J. Phys. Chem B,* 102, **1998**, 2214

[2] P. Sarkar, D.K. Bhui, H. Bar, G.P. Sahoo, S. Samanta, S. Pyne, A. Misra, *Plasmonics,* 6, **2011**, 43

[3] P. Sarkar, D.K. Bhui, H. Bar, G.P. Sahoo, S. Samanta, S. Pyne, A. Misra, *Nanoscale. Res. Lett.* 5, **2010**, 1611

[4] Y. Sun, B. Gates, B. Mayers, Y. Xia, *Nano Lett.,* 2, **2002**, 165

[5] C.L. Haynes, R.P. Van Duyne, *J. Phys. Chem. B,* 105, **2001**, 5599

[6] G.S. Metraux, Y. Cao, R.C. Jin, C.A. Mirkin, *Nano Lett.* 3, **2003**, 519

[7] L. Jiang, S. Xu, J.M. Zhu, J. Zhang, J.J. Zhu, H. Chen, *Inorg. Chem.* 43, **2004**, 5877

[8] M.C. Daniel, D. Astruc, *Chemical Reviews*, 104, **2004**, 293

[9] I.A. Wani, S. Khatoon, A. Ganguly, J. Ahmed, A.K. Ganguli, T. Ahmad, *Mater.Res. Bull.* 45, **2010,** 1033

[10] B. Tang, J. An, X. Zheng, S. Xu, D. Li, J. Zhou, B. Zhao, W. Xu, *J. Phys. Chem. C,* 112**,** **2008**, 18361

[11] P. Schwinté, J.C. Voegel, C. Picart, Y. Haikel, P. Schaaf, B. Szalontai, *J. Phys.Chem.B,* 105, **2001**, 11906

[12] P. Sarkar, D.K. Bhui, H. Bar, G.P. Sahoo, S.P. De, A. Misra, *J. Lumin.*, 129, **2009**, 704

[13] H. Bar, D.K. Bhui, G.P. Sahoo, P. Sarkar, S.P. De, A. Misra, *Colloids Surf. A,* 339, **2009**, 134

[14] M. Faraday, *Philos.Trans,* The Royal Society of London, 147, **1857**, 145

[15] G. Mie, *Annals of Phys.* 25, **1908**, 377

[16] M. Kerker, D.S. Wang, C.L.Giles, Electromagnetic scattering by magnetic spheres, *J. Opt. Soc. Am.* 73, **1983**, 765-767

[17] Z.S. Wu, Y.P. Wang, *Radio. Sci.,* 26, **1991**, 1393

[18] A.C. Ludwig, *Comput. Phys. Commun.* 68, **1991**, 306

[19] M.I. Mishchenko, L.D. Travis, D.W. Mackowski, *J. Quant. Spectrosc. Radiat. Transfer.* 55, **1996**, 535

[20] B.T. Drain, P.J. Flatau, *J. Opt. Soc. Am. A,* 11, **1994**, 1491

[21] J.P. Kottman, O.J.F. Martin, D.R. Smith, S. Schultz, *Opt. Express,* 6, **2000**, 213

[22] L. J. Sherry, R. Jin, C.A. Mirkin, G.C. Schatz, R.P. Van Duyne, *Nano Lett.,* 6, **2006**, 2060

[23] L. Qin, S. Zou, C.Xue, A. Atkinson, G.C. Schatz, C.A. Mirkin, Designing, *Proc. Natl. Acad. Sci. U.S.A.* 103, **2006**, 13300

[24] L.J. Sherry, S.H. Chang, G.C. Schatz, R.P. Van Duyne, B.J. Wiley, Y. Xia, *Nano Lett.,* 5, **2005**, 2034

[25] A.J. Haes, J. Zhao, S. Zou, C.S. Own, L.D. Marks, G.C. Schatz, R.P. Van Duyne, *J. Phys. Chem. B,* 109, **2005**, 11158

[26] E. Hao, S. Li, R.C.Bailey, S. Zou, G.C. Schatz, J.T. Hupp, *J. Phys. Chem. B,* 108, **2004**, 1224

[27] E. Hao, G.C. Schatz, *J. Chem. Phys.*, 120, **2004**, 357

[28] L. Zhao, S.Zou, E. Hao, G.C. Schatz, *Theor. Appl. Comput. Chem.,* Amsterdam, The Netherlands, **2005**

[29] G.C. Schatz, *Theochem*. 573, **2001**, 73

[30] A. Brioude, M.P. Pileni, *J. Phys. Chem. B,* 109, **2005**, 23371

[31] P.B. Johnson, R.W. Christy, *Phys. Rev. B,* 6, **1972**, 4370

[32] B.T. Draine, P.J. Flatau, "User Guide for the Discrete Approximation Code DDSCAT 7.0", http://arxiv.org/abs/0809.0337v4. **2008**

[33] B.T. Draine, J. Goodman, *J. Astrophys.* 405, **1993**, 685

[34] S.Link, Z.L.Wang, M.A. El-Sayed, *J. Phys. Chem.B,* 103, **1999**, 3529

[35] P. Taneja, P. Ayyub, R. Chandra, *Phys. Rev. B*, 65, **2002**, 245412 (6 pages)

[36] R. Jin, Y. Cao, C.A. Mirkin, K.L.Kelly, G.C. Schatz, J.G. Zheng, *Science,* 294, **2001**, 1901

[37] Y. Sun, Y. Xia, *Adv. Mater.* 15, **2003**, 695

[38] V. Subbulakshmi, A.K. Ghosh, T.Das, P.K Roy, *Biochem. Biophys. Res. Commun.,* 250, **1998**, 15

[39] C.F. Bohren, D.R. Hoffman, *Absorption and scattering of light by small particles,* Wiley, New York, **1983**

[40] J. Aizpurua, G.W. Bryant, L.J. Richter, F.J. Garcia de Abajo, B.K. Kelly, T. Mallouk, *Phys. Rev. B,* 71, **2005**, 235420 (13 pages)

Chapter VI

Hydrothermal synthesis of hexagonal ZnO micro structures in HPMC polymer matrix and their catalytic activities

*A part of this chapter has been published in the article, Gobinda Prasad Sahoo, **Sadhan Samanta**, Dipak Kumar Bhui, Santanu Pyne, Ashim Maity, Ajay Misra, **Journal of Molecular Liquids 212 (2015) 665–670**

Hydrothermal synthesis of hexagonal ZnO micro structures in HPMC polymer matrix and their catalytic activities

6.1. Introduction

ZnO is one of the most promising materials for UV light emitting devices [1], field emission devices [2], high performance nanosensors [3] etc. Again ZnO is an intrinsic n-type semiconductor due to the presence of oxygen vacancies and/or zinc interstitials. Various ZnO particles with micro- and nano-structure have been attracted much attention in the recent years because of their applications in electronics and optoelectronics such as solar cells [4], gas sensor [5], UV lasers [6], transparent conductors [7] and hydrogen-storage devices [8]. Moreover, ZnO is also one of the promising materials for its catalytic properties [9], including antibacterial effect, self-cleaning and self-sterilizing materials, phototherapeutic agents [10] as well as degrading organic contaminants in the environment.

Different morphologies and sizes of ZnO materials, such as hexagonal ZnO microprism [11], nanobelts [12], tubes [13], hexagonal nanoplate [14], needle [15], flower-like [16], nanowire [17], nanorod [18] and nanosheet [19], etc. have been synthesized via various methods by various research groups. Researchers are trying to develop facile, template assisted, solution-based, morphology controlled approaches [20] to build novel self-generated architectures. The developments of a simple, effective, and economical approach for synthesizing ZnO nano materials with desired architectures remain a key research challenge.

Many synthetic methods were developed for synthesis of ZnO nano/micro materials e.g. chemical vapor decomposition (CVD), spray pyrolysis, spray deposition, gas-phase reaction,

freeze drying, biosynthesis etc [21-23]. Unfortunately, the rigorous conditions and complicated procedures of these methods severely restrict their large-scale application for industry. On the contrary, wet chemical routes have provided a promising option for their simple, fast, and less expensive nature, such as chemical deposition, sol–gel process, ultrasonication, microwave technique and hydrothermal synthesis [24, 25]. Among these, hydrothermal route is a promising method for synthesizing ideal ZnO materials with variable morphologies via a simple, fast, low cost, high yield and scalable process. Additionally, highly crystallized powders with narrow grain size-distribution and high purity without heat treatment at high temperature are the advantages of hydrothermal technique. In order to control the morphology of ZnO crystals, organic additives such as ethylene diamine tetraacetic acid (EDTA) [26], poly ethylene glycol (PEG) [27] and sodium dodecyl sulfate (SDS) [28], cetyl trimethyl ammonium bromide (CTAB) [29] are commonly introduced into the reaction system to manipulate the nucleation and growth process in hydrothermal and solvothermal reactions.

Recently catalytic applications of metal oxide nanoparticles, ZnO in particular, have received increasing attention and the examples include the Friedel-Craft reaction [30], degradation of different dyes, such as methyl orange (MO) [31], rhodamine B [32], o-acylation of alcohol and phenol [33], methanol synthesis [34], synthesis of β-acetamido ketones/esters via a multi-component reaction [35], synthesis of poly substituted pyrroles [36] etc. Of late, catalysis by nano/micro materials has become an area of interest, as these materials exhibit better catalytic activity compared to their bulk counterparts.

In the present chapter we have developed a simple one step solution phase hydrothermal route for synthesizing ZnO hexagonal micro rod, bar and both end open bar at 90°C temperature. SEM study shows the homogeneous morphology in all the cases of ZnO micro structure. The catalytic efficiency of all the ZnO microstructures was evaluated by studying the degradation of Methelyne blue (MB) under UV irradiation. All of these micro crystals showed good catalytic

properties and can easily be separated by centrifuging from the solution for recycling. The kinetic data indicate that both end open bar like ZnO hexagonal microparticles are catalytically more active than ZnO hexagonal micro rod and ZnO hexagonal bar.

6.2. Experimental Section

6.2.1. Reagents and Instruments

6.2.1.1. Reagents

Zinc acetate $Zn(OOCCH_3)_2$. $2H_2O$), Methelyne Blue (MB) and Hexamethylene Tetramine (HMTA) were purchased from Sigma-Aldrich Chemicals Co. HPMC (50 cps of 2% HPMC solution) was purchased from Merck India Ltd. All chemicals used in the experiment were analytic reagent (AR) grade and used as received. All solutions were prepared in triple distilled deionized water. Glassware were first rinsed with aqua regia and then washed thoroughly by triple distilled deionized water before use.

6.2.1.2. Instruments

Characterization and catalytic activities of ZnO hexagonal micro rod, bar and one end open bar were done by XRD, SEM, UV-Vis and Fluorescence spectroscopic study. UV-VIS spectroscopic measurements were carried out using a 'SHIMADZU' UV-1800 *spectrophotometer*. SEM study of the particles was done using an Evo 18, Carl-ZEISS Scanning Electron Microscope (SEM). Photoluminescence measurements were carried out using an Hitachi F7000 fluorescence spectrophotometer. The phase and purity of the ZnO hexagonal microcrystals were determined using a X'Pert PRO PAnalytical-PW 3040/60 X-ray diffractometer with Cu Kα radiation (λ = 1.5418 Å). Scans were collected on dry nanomaterials in the range of 20-80□.

6.2.2. Synthesis

6.2.2.1. Synthesis of hexagonal rod, bar and both end open bar like ZnO microstructures

$Zn(CH_3COO)_2 \cdot 2H_2O$ and hexamethylene tetramine (HMTA) were used for the synthesis of ZnO microcrystals. In a typical procedure, 32.92mg of $Zn(CH_3COO)_2 \cdot 2H_2O$ and 21.01mg HMTA were dissolved in 15 ml deionized water under constant stirring for 30 min. Subsequently, the mixture was transferred to a Teflon-lined stainless steel autoclave which was sealed and maintained at 90°C for 24h. After the reaction was over, it was allowed to cool slowly to room temperature. The resulting solid products were filtered and washed with deionized water for several times to remove the unreacted Zn^{2+}, CH_3COO^-, HMTA and other undesirable species for further experiments. Synthesized ZnO microcrystals were hexagonal rod like in shape (Sample-A).

On the other hand for the synthesis of hexagonal ZnO micro bar (Sample-B) and both end open bar (Sample-C) like ZnO hexagonal microcrystals we used 15ml aqueous solution of 0.1% HPMC and 0.5% HPMC respectively. All other steps i.e. heating, washing and removal of unreacted species were identical as previously.

6.2.2.2. Photocatalytic Tests

Methelyne Blue (MB) was employed as a representative dye indicator to evaluate the UV photocatalytic activity of Sample-A, Sample-B and Sample-C respectively. 1ml of each ZnO hydrosol was ultrasonically dispersed into the ethanolic solution of MB (10μM, 9mL) and the mixture was stirred with continuous exposure of UV light from a low pressure Hg tube (Philips TUV 6W, strongest emission at 254 nm). The decolourization of MB was monitored by UV-Vis absorption study.

6.3. Result and Discussion:

6.3.1. SEM study

ZnO microparticles are known to exhibit a large variety of morphologies which are responsible for its interesting physical properties. Therefore, shape controlled synthesis of ZnO structures has always been a critical issue. In our experiment, the morphology of the ZnO microstructures are tailored by changing the concentrations HPMC during the hydrothermal process. Figure 6.1-6.3 shows the representative SEM images of ZnO microstructures using different concentration of HPMC.

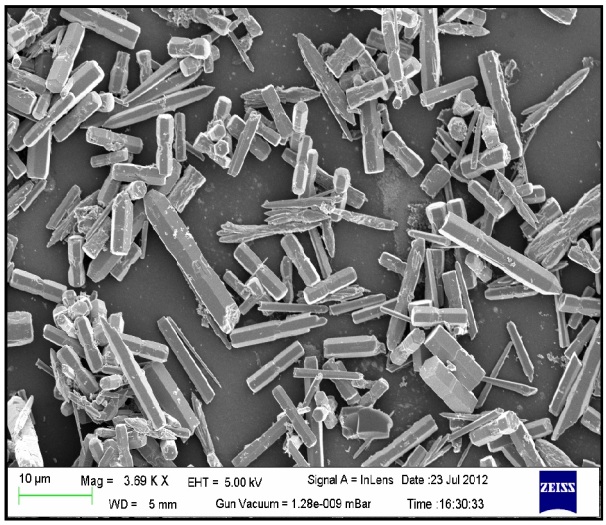

Figure 6.1: SEM image of hexagonal rod shaped ZnO microcrystals synthesized in the absence of HPMC (Sample-A).

Fig.6.1 illustrates the morphological and structural characterizations of hexagonal rod like ZnO microparticles (Sample-A). A number of images were taken by focusing different portion of grid and extensive pattern of hexagonal rod shaped ZnO microparticles are observed in all locations of the grid.

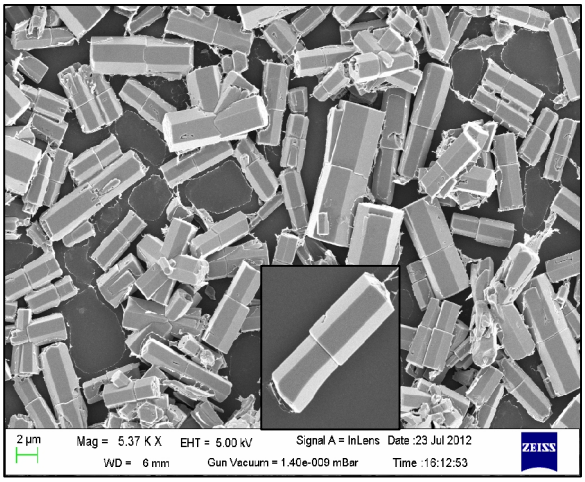

Figure 6.2: SEM image of hexagonal bar like ZnO microcrystals synthesized in the presence of 0.1% aqueous HPMC solution (Sample-B). In set shows high magnification SEM image.

Fig.6.2 shows SEM image of the hexagonal bar like morphology of the as synthesized ZnO microparticles in 0.1% HPMC polymer matrix (Sample-B) and Fig.6.3 shows SEM image of ZnO both end open bar synthesized in 0.5% HPMC matrix (Sample-C).

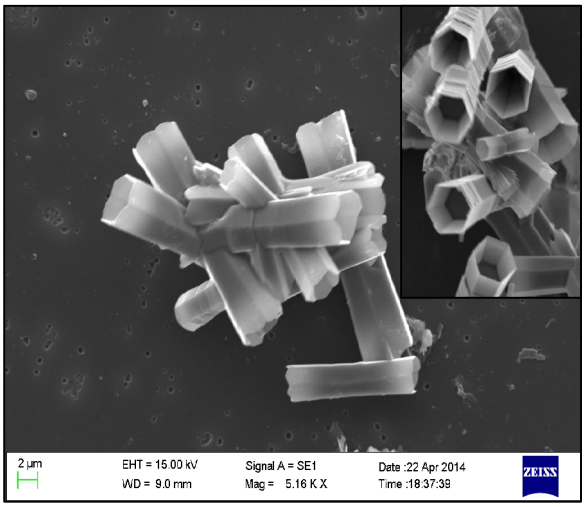

Figure 6.3: SEM image of hexagonal both end open bar like ZnO microcrystals synthesized in the presence of 0.5% aqueous HPMC solution (Sample-C). In set shows high magnification SEM image.

6.3.2. XRD study

The purity and crystallinity of the ZnO microstructures were examined by powder X-ray diffraction (XRD) study.

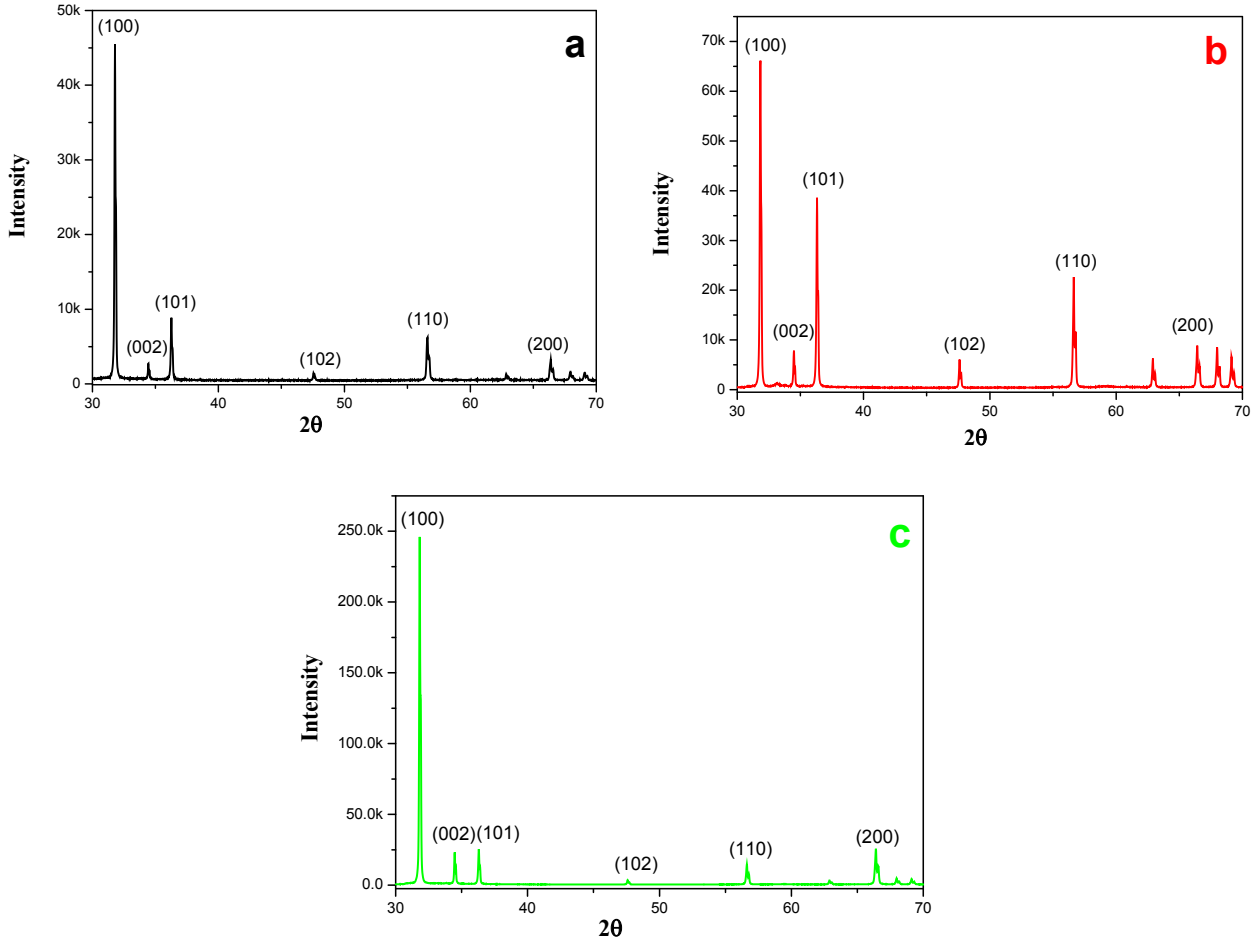

Figure 6.4: XRD patterns of ZnO microcrystals synthesized in the presence of (a) Sample-A; 0% HPMC, (b) Sample-B; 0.1% HPMC and (c) Sample-C; 0.5% HPMC.

Figure 6.4a displays a typical XRD pattern obtained from the as synthesized ZnO hexagonal micro rod (Sample-A). All the diffraction peaks can be well indexed to pure wurtzite structure of ZnO with lattice constants of a=3.249Å, c=5.206Å, which are consistent with the

values in the standard card (JCPD file No. 79-0206) and a number of Bragg reflections with 2θ values of 31.83˚, 34.46˚, 36.33˚, 47.68˚, 56.62˚ and 66.63˚. These peaks correspond to the diffractions from (100), (002), (101), (102), (110) and (200) planes. Figure 6.4b and 6.4c show the XRD pattern of hexagonal ZnO micro bar (Sample-B) and both end open bar (Sample-C). No characteristic peaks from impurities are detected within experimental error and the sharp and small widths of the diffraction peaks indicate that all of the ZnO microstructures have excellent crystallinity.

6.3.3 Role of Hexamethylene tetramine (HMTA)

$$HMTA + 6H_2O \rightarrow 4NH_3 + 6HCHO \quad \text{(1)}$$

$$NH_3 + H_2O \rightarrow NH_4^+ + HO^- \quad \text{(2)}$$

$$Zn^{2+} + 4\ HO^- \rightarrow [Zn(OH)_4]^{2-} \quad \text{(3)}$$

$$[Zn(OH)_4]^{2-} \rightarrow Zn(OH)_2 + 2HO^- \quad \text{(4)}$$

$$Zn(OH)_2 \rightarrow ZnO + H_2O \quad \text{(5)}$$

Herein, $Zn(CH_3COO)_2 \cdot 2H_2O$ provides the required Zn^{2+} ion and water molecules provides O^{2-} ion in alkali medium for building of ZnO micro structures. HMTA is a nonionic cyclic tertiary amine. It acts as a weak base and pH buffer [37] under the present experimental condition. HMTA is readily hydrolyzes in water and slowly produces HCHO and NH_3 at 90°C. This is the critical point of the present synthesis process. HMTA is hydrolyzed very quickly and produced a large amount of OH^- in a short period of time and the Zn^{2+} ions in solution is precipitate out quickly as $Zn(OH)_2$ owing to the high pH environment. This eventually would result the fast consumption of the nutrient ($[Zn(OH)_4]^{2-}$) and prohibit the oriented growth of ZnO microstructures. From reactions (3) and (4), NH_3—the product of the decomposed HMTA produces a basic environment that is necessary for the formation of $Zn(OH)_2$. In reaction (1), seven moles of reactants produce ten moles of products, so there is an increase in entropy during reaction. It further suggests that increasing of reaction temperature will push the equilibrium in the forward direction. The rate of

HMTA hydrolysis decreases with increasing p^H and vice versa. It can also be noticed that the above five reactions proceed extremely slowly at room temperature.

6.3.4. Emission Study

Room temperature photo luminance spectra of hexagonal ZnO architectures obtained in presence and absence of HPMC were measured upon excitation at 340 nm. PL spectrum of hexagonal ZnO micro rod contain one sharp and intense UV emission band centered at 386 nm and a broad blue emission in the range 420-470nm (fig.6.5a).

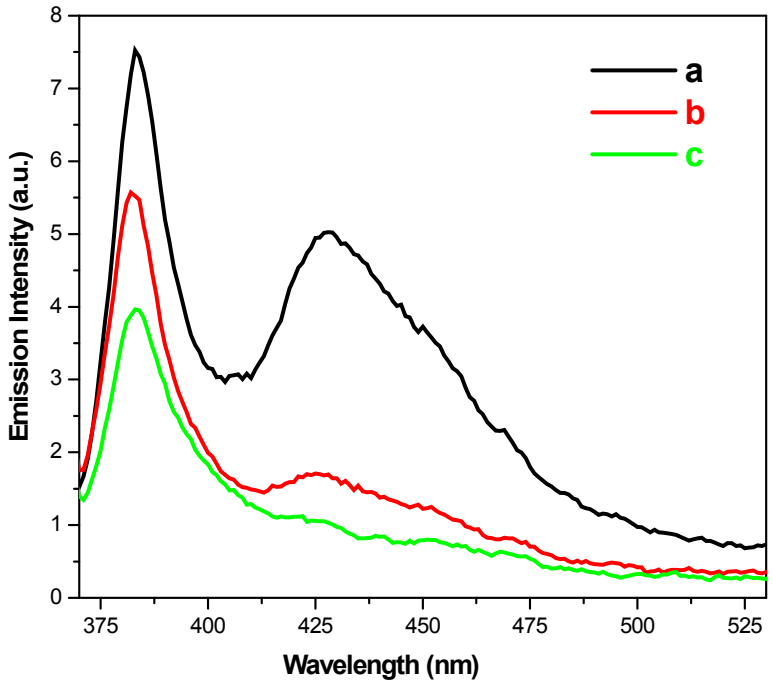

Figure 6.5: Photo luminance spectra of ZnO microparticles synthesized in presence of (a) Sample-A; 0% HPMC, (b) Sample-B; 0.1% HPMC and (c) Sample-C; 0.5% HPMC with various morphologies.

The UV emission is a characteristic of near-band-edge transition. There are some and not many reports in literature on the blue emission of ZnO nano/micro clusters [38]. However, the mechanism of this emission is not clear yet. Fu and co-workers [39] had calculated the energy levels of various defect centers, such as vacancies of oxygen and zinc, interstitial oxygen and zinc and antisite oxygen in bulk ZnO. The gap between conduction band and level of oxygen vacancies is 2.28 eV (about 540nm) and that from interstitial zinc level to valance band in 2.9 eV (about 425nm). The 540nm is well consistent with the normal green emission of ZnO. The blue emission in this study could be attributed to interstitial zinc in ZnO micro rods. Our observed blue emission from ZnO micro rod is asymmetric, i.e. though the peak is at 425nm, it is extended upto 480nm. This asymmetric broad blue emission can be explained nicely by the mechanism given by Zeng et. al. [40]. In their proposed model they suggested the presence of extended Zn_i state which is responsible for broad blue emission from ZnO.

On the other hand, our synthesized bar and both end open bar shaped ZnO microstructures in presence of HPMC show, very weak (Sample-B) and almost no blue emission (Sample-C) as shown in (Fig.6.5b & 6.5c). The ratio of UV to other (blue, green, yellow) emission intensity (I_{BL} : I_{UV}) provides a versatile measurement of the quality of ZnO material. The I_{BL} : I_{UV} ratio of our synthesized ZnO samples are 0.679 (Sample-A), 0.321 (Sample-B) and 0.269 (Sample-C). The higher intensity of blue emission for sample will be useful for light emitting and fluorescence labeling application. In general, high I_{BL} : I_{UV} ratios can be obtained by high temperature processing or a subsequent annealing by selecting different gas atmospheres. Up to now, it is still a challenge to get high quality ZnO products by the solution process. Therefore our present method of synthesis of well ordered ZnO microcrystals in presence of HPMC is one step forward in this direction.

6.3.5 UV light driven Photocatalysis and Photocatalytic Mechanism

Methylene blue (MB) is selected as a representative organic pollutant to evaluate the photocatalytic performance of hexagonal rod, bar and both end open bar like ZnO microcrystals. Change in optical density of MB (at 665nm) with time under UV illumination in presence of ZnO hexagonal rod, bar and both end open bar like ZnO microcrystals are shown in fig. 6.6(a-c).

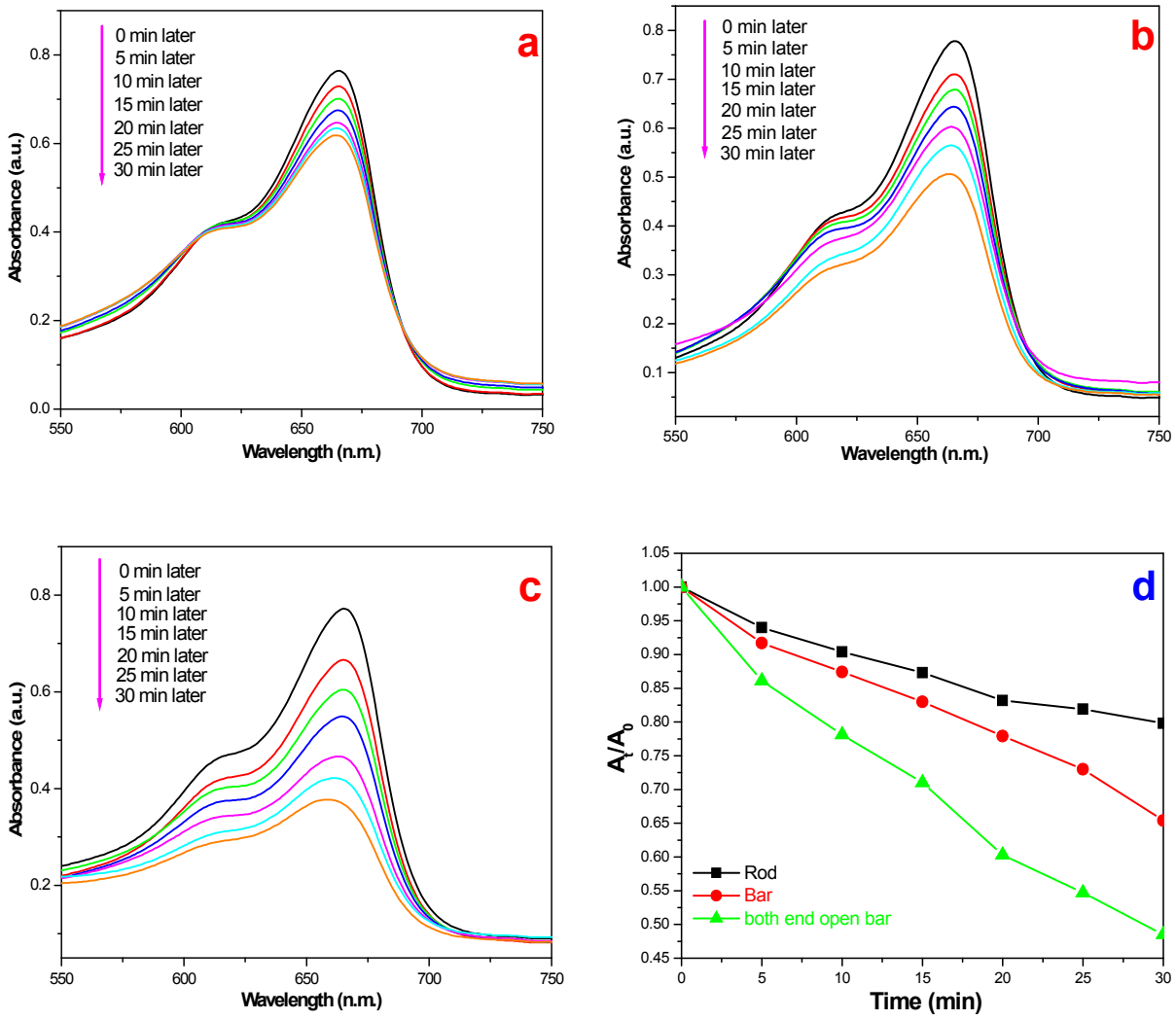

Figure 6.6: UV-Vis photo bleaching study of MB in presence of the synthesized hexagonal ZnO (a) rod (Sample-A), (b) bar (Sample-B) and (c) both end open bar (Sample-C) like microcrystals. d) Kinetics of photo bleaching of MB in presence of various ZnO micro structures.

It can be seen that the absorption peak at 665nm are reduced significantly, indicating the degradation of the dye molecules. The photo degradation of MB can be considered as a pseudo-first order reaction [41] at the initial stage and its kinetics can be expressed by the following equation.

$$A_t = A_0 e^{-kt}$$

where 'k' is the degradation constant and A_0 is the absorbance of MB in absence of UV exposure and A_t is the absorbance of MB under UV exposure at different time 't'. It is shown in fig.6.6d that the photocatalytic performance of ZnO microcrystals is changed significantly with the change in morphology. In general, the photocatalytic activity of ZnO for the degradation of pollutants is related to its band gap. The catalytic capacity of different ZnO microstructures is associated with the actual surface areas because of the size and shape effect. On the basis of the morphological features, it can easily be recognized that the arrays with both end open ZnO microstructures represent the largest effective surface area of all the investigated nanostructures herein. It is therefore not surprising that this structure enhances the photocatalytic capacity to some degree, when compared to other investigated structures. Photo oxidations occur according to the following pathway involving hydroxyl radicals as the oxidizing intermediate.

$$ZnO + h\nu(UV) \rightarrow ZnO(e^-_{CB} + h^+_{VB})$$

$$h^+_{VB} + H_2O \rightarrow {}^{\bullet}OH + H^+$$

$${}^{\bullet}OH + MB \rightarrow LMB$$

The degraded product is Leuco Methylene Blue (LMB). It has been observed that hydroxyl radical has little selectivity for attacking dye molecules and are able to oxidize the pollutants due to their high oxidative capacity (reduction potential of ${}^{\bullet}OH$ is 2.8 V). In case of hexagonal rod and bar like ZnO micro crystals, it can get much more time to excitonic hole-electron

recombination than to form $^{\bullet}OH$ to degrade the MB. Therefore our observe increase rate of catalytic oxidation is in accordance with the increase surface area of ZnO microparticles.

6.4. Conclusions

Present article addresses a simple but novel solution phase, one step synthesis of hexagonal rod, bar and both end open bar like ZnO microcrystal. SEM study shows the homogeneous morphology in all the three cases. Sharp and intense X-ray absorption peaks of ZnO and the absence of other impurities suggests that the present synthesis route is capable of producing pure hexagonal ZnO microstructures. One of our synthesized ZnO microstructures exhibits strong blue emission which is very rarely observed from ZnO nano or microstructures. The catalytic efficiency of all the ZnO nanostructures were evaluated by studying the degradation of Methelyne blue (MB) under UV irradiation. It has been observed that hexagonal both end open bar like ZnO microparticles have highest photo catalytic activity, whereas hexagonal bar like ZnO microparticles shows a little higher activity than the ZnO micro rod. It is nicely correlated with the increased effective surface area from ZnO rod to ZnO bar to both end open ZnO bar like microstructures.

References:

[1] R. Viswanatha, P.K. Santra, C. Dasgupta, D.D. Sarma, *Phys. Rev. Lett.,* 98, **2007**, 255501

[2] D. Banerjee, S.H. Jo, Z.F. Ren, *Adv. Mater*. 22, **2004**, 2028

[3] J. Zhou, Y.D. Gu, Y.F. Hu, W. J. Mai, P.H. Yeh, G. Bao, A.K. Sood, D.L. Polla, Z.L.Wang, *Appl. Phys. Lett.*, 94, **2009**, 191103.

[4] Y.F. Gao, M. Nagai, *Langmuir,* 22, **2006**, 3936

[5] R. Khan, A. Kaushik, P.R. Solanki, A.A. Ansari, M.K. Pandey, B.D. Malhotra, *Anal. Chim. Acta*, 616, **2008**, 207

[6] M.H. Huang, S. Mao, H. Feick, H.Q. Yan, Y.Y. Wu, H. Kind, E. Weber, R. Russo, P.D. Yang, *Science,* 292, **2001**, 1897

[7] H.Y. Xu, Y.C. Liu, R. Mu, C.L. Shao, Y.M. Lu, D.Z. Shen, X.W. Fan, *Appl. Phys. Lett.*, 86, **2005**, 123107.

[8] S.S. Mao, S. Shen, L. Guo, *Progress in Natural Science: Materials International,* 22, **2012**, 522

[9] M. Raula, M.H. Rashid, T.K. Paira, E. Dinda, T.K. Mandal, *Langmuir,* 26, **2010**, 8769

[10] S. Sarkar, A. Makhal, S. Baruah, M.A. Mahmood, J. Dutta, S.K. Pal, *J. Phys. Chem. C,* 116, **2012**, 9608

[11] S.Y. Yu, H.J. Zhang, Z.P. Peng, L.N. Sun, W.D. Shi, *Inorg. Chem.* 46, **2007**, 8019

[12] A. Asthana, K. Momeni, A. Prasad, Y.K. Yap, R.S. Yassar, *Appl. Phys. A*, 105, **2011**, 909

[13] M. Bechelany, A. Amin, A. Brioude, D. Cornu, P. Miele, *J. Nanopart. Res.,* 14, **2012**, 980

[14] J. Liu, L. Xu, B. Wei, W. Lv, H. Gao, X. Zhang, *Cryst. Eng. Comm.*, 13, **2011**, 1283

[15] W. Feng, J. Chen, C. Hou, *Appl. Nanosci.*, 4, **2014**, 15

[16] A. Kamalianfar, S.A. Halim, M.G. Naseri, M. Navasery, F. Ud Din, J.A.M. Zahedi, K.P. Lim, E.B. Saion, C.K. Chen, A.L. Monfared, *Int. J. Electrochem. Sci.*, 8, **2013**, 7724

[17] S. Pyne, G.P. Sahoo, D.K. Bhui, H. Bar, P. Sarkar, S. Samanta, A. Maity, A. Misra, *Spectrochim. Acta Part A*, 93, **2012**, 100

[18] P.S. Kumar, P. Paik, A.D. Raja, D. Mangalaraj, D. Nataraj, A. Gedanken, S. Ramakrishna, *Appl. Surf. Sci.*, 258, **2012**, 6765

[19] S. Kar, A. Dev, S. Chaudhuri, *J. Phys. Chem. B*, 110, **2006**, 17848

[20] F. Waltz, G. Wibmann, J. Lippke, A.M. Schneider, H.C. Schwarz, A. Feldhoff, S. Eiden, P. Behrens, *Crys. Growth Des.*, 12, **2012**, 3066

[21] N. Sadananda Kumar, K.V. Bangera, G.K. Shivakumar, *Appl. Nanosci.*, 4, **2014**, 209

[22] J. Sarkar, M. Ghosh, A. Mukherjee, D. Chattopadhyay, K. Acharya, *Bioprocess. Biosyst. Eng.*, 37, **2014**, 165

[23] C. Panatarani, I.W. Lenggoro, K. Okuyama, *J. Nanopart. Res.,* 5, **2003**, 47

[24] A. Khorsand Zak, W.H.abd. Majid, H.Z. Wang, R. Yousefi, A.M. Golsheikh, Z.F. Ren, *Ultrason. Sonochem.,* 20, **2013**, 395

[25] N.F. Hamedani, A.R. Mahjou, A. Ali Khodadadi, Y. Mortazavi, *Sens. Actuators, B*, 156, **2011**, 737

[26] G.R. Li, C.R. Dawa, B. Qetal, *J. Phys. Chem. C,* 111, **2007**, 1919

[27] J.X. Duan, X.T. Huang, E.K. Wang, *Mater. Lett.,* 60, **2009**, 1918

[28] M. Sabbaghan, A.A. Firooz, V.J. Ahmadi, *J. Mol. Liq.,* 175, **2012**, 135

[29] Y.X. Wang, J. Sun, X.Y. Fan, X. Yu, *Ceram. Int.*, 37, **2011**, 3431

[30] M.H. Sarvari, H. Sharghi, *J. Org. Chem.*, 69, **2004**, 6953

[31] X. L. Xu, X. Duan, Z. G. Yi, Z. W. Zhou, X.M. Fan, Y. Wang, *Catal. Commun.*, 12, **2010**, 169

[32] G. Zhang, X. Shen, Y. Yang, *J. Phys. Chem. C*, 115, **2011**, 7145

[33] F.M. Moghaddam, H. Saeidian, *Mater. Sci. Engg. B*, 2–3, **2007**, 265

[34] J. Strunk, K. Kahler, X. Xia, M. Muhler, *Surf. Sci.,* 10-12, **2009**, 1776

[35] Z. Mirjafary, H. Saeidian, A. Sadeghi, F.M. Moghaddam, *Catal. Commun.*, 2, **2008**, 299

[36] M. Sabbaghan, A. Ghalaei, *J. Mol. Liq.,* 193, **2014**, 116

[37] K. Govender, D.S. Boyle, P.B. Kenway, P. O'Brien, *J. Mater. Chem.*, 14, **2004**, 2575

[38] W.H. Zhang, J.L. Shi, L.Z. Wang, D.S. Yan, *Chem. Mater.*, 12, **2000**, 1408

[39] B.X. Lin, Z.X. Fu, Y.B. Jia, *Appl. Phys. Lett.*, 79, **2001**, 943

[40] H. Zeng, G. Duan, Y. Li, S. Yang, X. Xu, W. Cai, *Adv. Func. Mater.*, 20, **2010**, 561

[41] D. Chu, Y. Masuda, T. Ohji, K. Kato, *Langmuir,* 26, **2010**, 2811

Chapter VII

Microwave-assisted synthesis of fluorescent N-doped carbon nanodots and its potential use as sensor for Fe (III) ions

*A part of this chapter has been communicated in the article, **Sadhan Samanta**, Ajay Misra, **Sensors and Actuators B**

Microwave-assisted synthesis of fluorescent N-doped carbon nanodots and its potential use as sensor for Fe (III) ions

7.1. Introduction:

Presently, a newly emerged fluorescent nanomaterials, carbon dots (CDs) have become very interesting in the nanocarbon family due to their potentiality in wide range of applications including bioimaging [1], chemical sensing [2], biosensing [3], drug delivery [4], photocatalysis [5], electrocatalysis [6], LED [7] etc. The unique characteristics of CDs compared to conventional semiconductor quantum dots, such as chemically non-toxicity, abundance of inexpensive starting material, simple preparation, facile functionalization, excellent photostability, good biocompatibility, strong and tunable fluorescence emission allow them for versatile applications.

In recent years, synthesis of heteroatom doped such as N-doped CDs (N-CDs) has been reported and those N-CDs exhibit improved electronic and fluorescence properties compared to that of the undoped CDs. There are a few reports on the synthesis methods of N-CDs such as hydrothermal method [8], ultrasonication method [9] and microwave (MW) assisted synthesis method [10] by using an apparent carbon precursor in the presence of a nitrogen source. Various research groups used different combinations of carbon precursor and nitrogen source such as Z.Ma et al [9] used glucose as carbon precursor and ammonium hydroxide as nitrogen source, Yan-Qing Zhang et al [11] used carbon tetrachloride as carbon precursor and $NaNH_2$ as nitrogen source, S.Dey et al [12] used glucose as carbon precursor and urea as nitrogen source, Minghan Xu et al [10] used calcium citrate and urea as carbon and nitrogen source respectively.

Herein, we report a facile one step MW assisted method using PEG-200 as carbon precursor and urea as nitrogen source to synthesize water soluble photo luminescent N-CDs with fluorescence quantum yield (QY) of 8.63%.

Many researchers have shown the application of CDs and N-CDs as sensors for different metal ions. For example, Sen Liu et al [13] reported detection of Cu (II) ion using N-CDs, Li Zhou et al [14] demonstrated detection of Hg^{2+} ion, S.N.A. Mohd Yazid et al [15] showed detection of Sn (II) ions using CDs.

Every living cell-whether plant or animal-contains iron. Iron plays some important roles in our body such as it helps red blood cells to transport oxygen to all parts of the body and helps many enzymes in our body cells in the process of energy release from food. Hence iron is essential for our body and we get it from food and drinking water. But getting too much iron from diet and drinking water causes 'iron overload' also referred to as 'hemochromatosis' and may exhibit warning signs which include joint pain, irregular heart rate, weight loss, abdomal pain and may lead to development of life-threatening complications like diabetes, cirrhosis, hepatocellular carcinoma, arthritis etc [16]. Therefore it is necessary to develop a facile sensor system which can detect iron qualitatively and quantitatively in drinking water. In this present work the as-prepared N-CDs contain distinctive –OH groups on their surfaces. Due to special response of –OH groups to Fe (III) ions, we demonstrate successfully the application of the as-prepared N-CDs as an effective fluorescent probe for selective detection of iron (III) in aqueous medium.

7.2. Experimental:

7.2.1. Chemicals and Materials:

Chemicals used in all the experiments were analytic reagent (AR) grade. Poly (ethylene glycol) (PEG-200) was purchased from Merck India Ltd. Urea was received from Avra Synthesis

Pvt. Ltd. $CuCl_2.2H_2O$, $HgCl_2$ and $CdCl_2.H_2O$ were purchased from Merck India Ltd. $CoCl_2.6H_2O$, $MnCl_2.4H_2O$ and $FeCl_3$ were purchased from SRL Pvt. Ltd. $ZnCl_2$ was purchased from Qualigens Fine Chemicals. Quinine Sulphate was received from Loba Chemicals. All chemicals were used as received without further purification. All solutions were prepared using triply distilled de-ionized water. Glasswares were cleaned thoroughly by aqua regia first and then washed with distilled water to remove any chance of contamination.

7.2.2. Synthesis of N-CDs:

Fluorescent N-CDs were prepared through a simple, convenient, one step MW assisted method using PEG-200 and urea. In a typical synthesis, 5 ml PEG-200 was mixed with 5 ml of water and a fixed amount of urea (0.5 g, 1g, 2g or 3g). After that, the resulting mixture was irradiated in a domestic MW oven at a fixed power level (300 W, 600W or 800W) for a regulated duration of time (5 min, 7 min or 10 min). A colour change from colourless to yellow/orange indicates the formation of N-CDs in the solution. After the reaction the resulting solution was cooled at room temperature before characterization and application as nanosensor probe.

7.2.3. Instrumentation and Characterization:

UV-Vis absorption spectroscopy was used to characterize optical properties of the synthesized N-CDs and was measured in a 1 cm quartz cuvette with the help of a Shimadzu UV-1800 spectrophotometer. The spectra were recorded at room temperature in the range from 200 nm to 600 nm at slit width 1 nm. The steady state fluorescence (FL) spectra of the samples were taken using a Hitachi F-7000 Fluorescence Spectrophotometer with both excitation and emission slit of 5 nm and 400 V PMT voltage. Quantum yield (QY) measurements were performed according to the previously established procedure [17]. Quinine sulphate dispersed in 0.1 M H_2SO_4 (QY 54%) was used as a standard as reported elsewhere [18]. The absorbance of N-CDs

and quinine sulphate was kept below 0.1 to minimize the chance of re-absorption by the N-CDs and quinine sulphate molecules. Samples were placed in a 10 mm optical path length quartz fluorescence cuvette. Fourier transform infrared spectroscopy (FT-IR) measurements were done using Perkin Elmer (Spectrum RX1) spectrophotometer.

7.3. Results and Discussions:

7.3.1. Optimization of synthetic conditions:

We have found that the fluorescent behaviour of N-CDs is affected by various factors such as PEG to urea ratio used, MW irradiation time, power level of MW used and PEG to water ratio. Therefore, it is necessary to optimize the synthetic conditions to achieve N-CDs having good fluorescent properties..

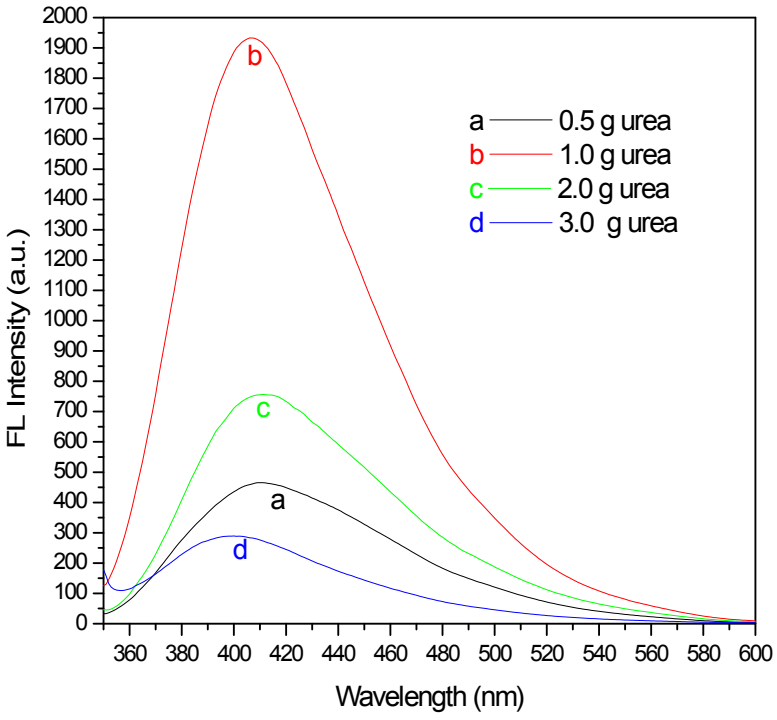

Figure 7.1: Effect of the amount of urea on FL emission intensity

Different amounts of urea (0.5 g, 1g, 2g and 3g) were added to the aqueous PEG-200 solution of constant concentration (5 ml PEG +5 ml water) at a fixed power level (300W) for a fixed time (5

min) of irradiation and the resulting sols are labelled as sample-a, b, c and d respectively. It was found that the FL intensity reaches maximum when 1g urea (10 %, w/v) was used (fig.7.1).This can be explained by the fact that when the amount of urea increases from 0.5 g to 1g more and more nitrogen would be doped into the carbon dots and thereby increases FL intensity. But as the amount of urea is further increased there is a possibility of blocking the passivated surface defects by the excess nitrogen.

The effect of MW irradiation time on the FL intensity of the as-synthesized N-CDs (sample-b) is demonstrated in fig.7.2. This time 1g urea was mixed with aq. PEG-200 solution and irradiated with MW at 300 W for varying duration (5 min, 7 min and 10 min).

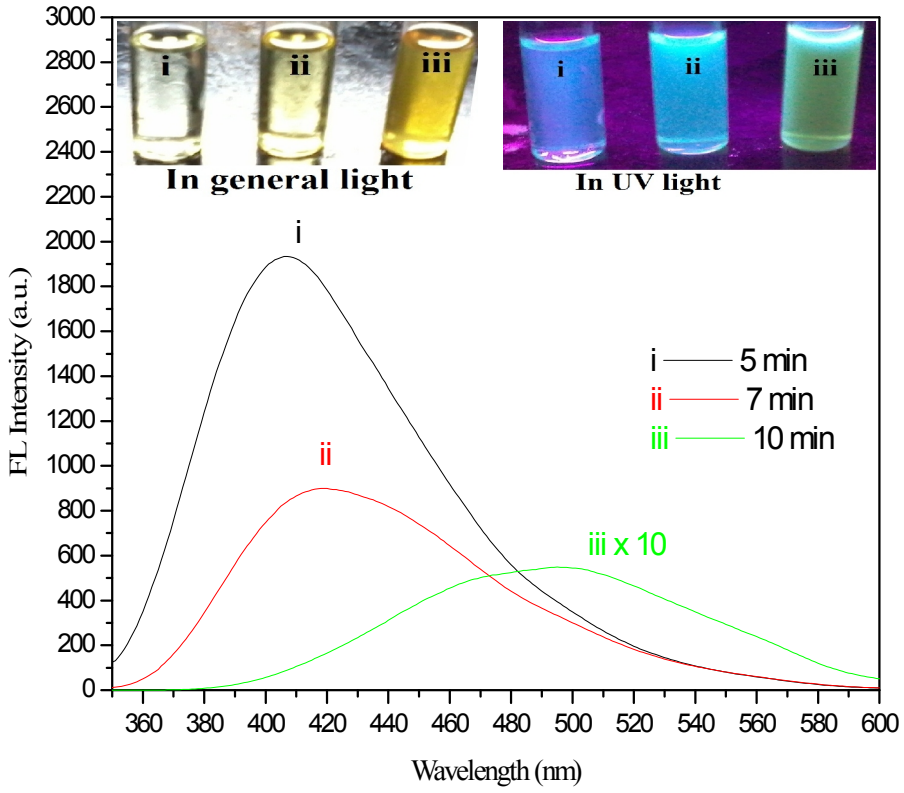

Figure 7.2: Effect of MW irradiation time on FL emission intensity. Inset shows the colour of the synthesized N-CDs

It is clearly observed that the 5 min irradiation time yield maximum FL intensity and increasing irradiation results decreasing intensity and red shift of the PL spectra (fig.7.2). Agglomeration of

N-CDs takes place to form larger size particles with increasing irradiation time and it is reflected in the decreasing intensity and red shift in the PL spectra.

PL intensity decreases 60 % and 95% from its initial value (intensity after 5 min irradiation) respectively as the MW irradiation time increases to 7 min and 10 min respectively. On the other hand the maximum of the PL spectra shifted from 400 nm to 430 nm to 500 nm as the irradiation takes place from 5 to 7 to 10 min. This red shift and decreasing intensity of PL spectra have been explained agglomeration of N-CDs to form larger aggregates upon prolonged irradiation time.

The effect of power level on the FL intensity and hence quantum yield was also examined. Sample-b was irradiated with MW for 5 min at different power levels (300 W, 600 W and 800 W). The results clearly demonstrate that the FL intensity is maximum at 300 W power level (fig. 7.3). This has been explained that as the power level is set to high, the rate of carbonization from C-source (PEG-200) becomes faster and hence larger sized N-CDs formation occurs. The formation of larger size N-CDs are reflected in the red shift and decreasing intensity of PL spectra.

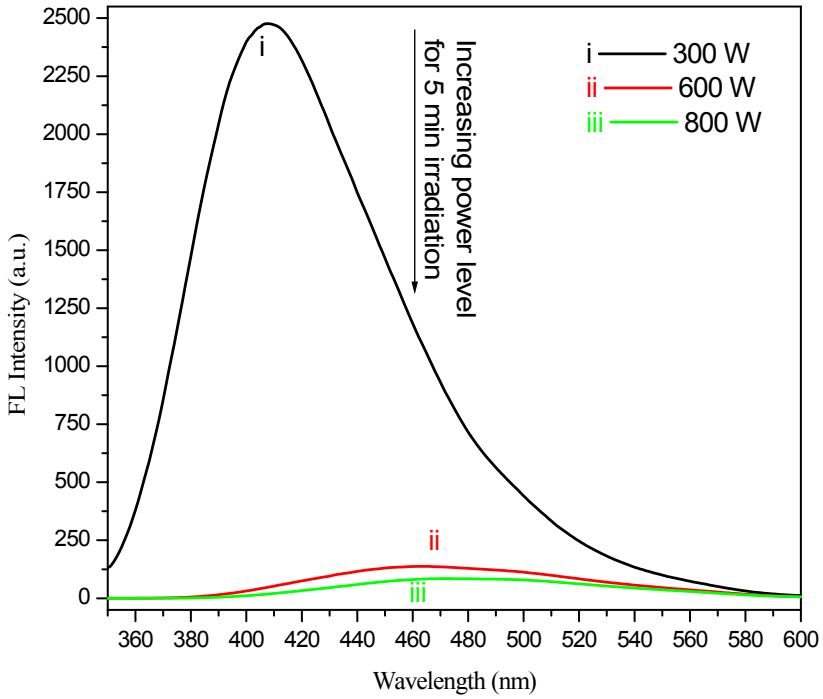

Figure 7.3: Effect of MW power level on FL emission intensity

We have also studied the effect of PEG to water ratio on PL intensity. It is observed that 1:1 PEG to water ratio show the highest PL intensity compared to others as shown in fig.7.4.

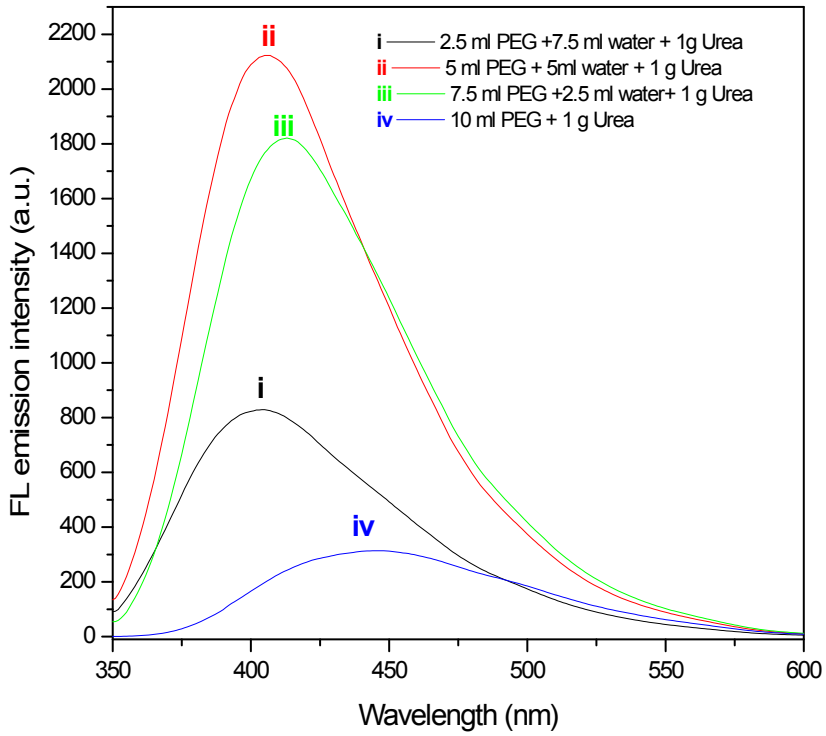

Figure 7.4: Effect of PEG to water ratio on FL emission intensity

Therefore, in brief the optimum experimental conditions using aq. PEG solution are as follows: 10% (w/v) urea, 5 min MW irradiation and 300 W power level of microwave oven and 1:1 ratio of PEG to water. It is worthy to mention that we have used these optimized conditions for the synthesis of N-CDs for further studies.

7.3.2. FL Emission spectroscopy study:

Fig.7.5 shows the PL emission spectra (down-conversion) of the synthesized N-CDs at various excitation wavelengths (340 to 440 nm). It is observed that the FL emission intensity is highest at 340 nm excitation with emission maxima centred at 407 nm.

As the excitation wavelength is changed from 340 nm to 440 nm the intensity of emission maxima decreases gradually along with regular red shifting of the maxima (fig.7.5a).

Therefore, the synthesized N-CDs show excitation wavelength dependent FL emission feature which is consistent with the previous reports [11, 19]. Inset (left side) of fig.7.5a shows the excitation spectra where emission is monitored at 410 nm and the observed maxima is at 340 nm. This excitation wavelength dependent emission maxima and intensity is due to π-π* transitions in

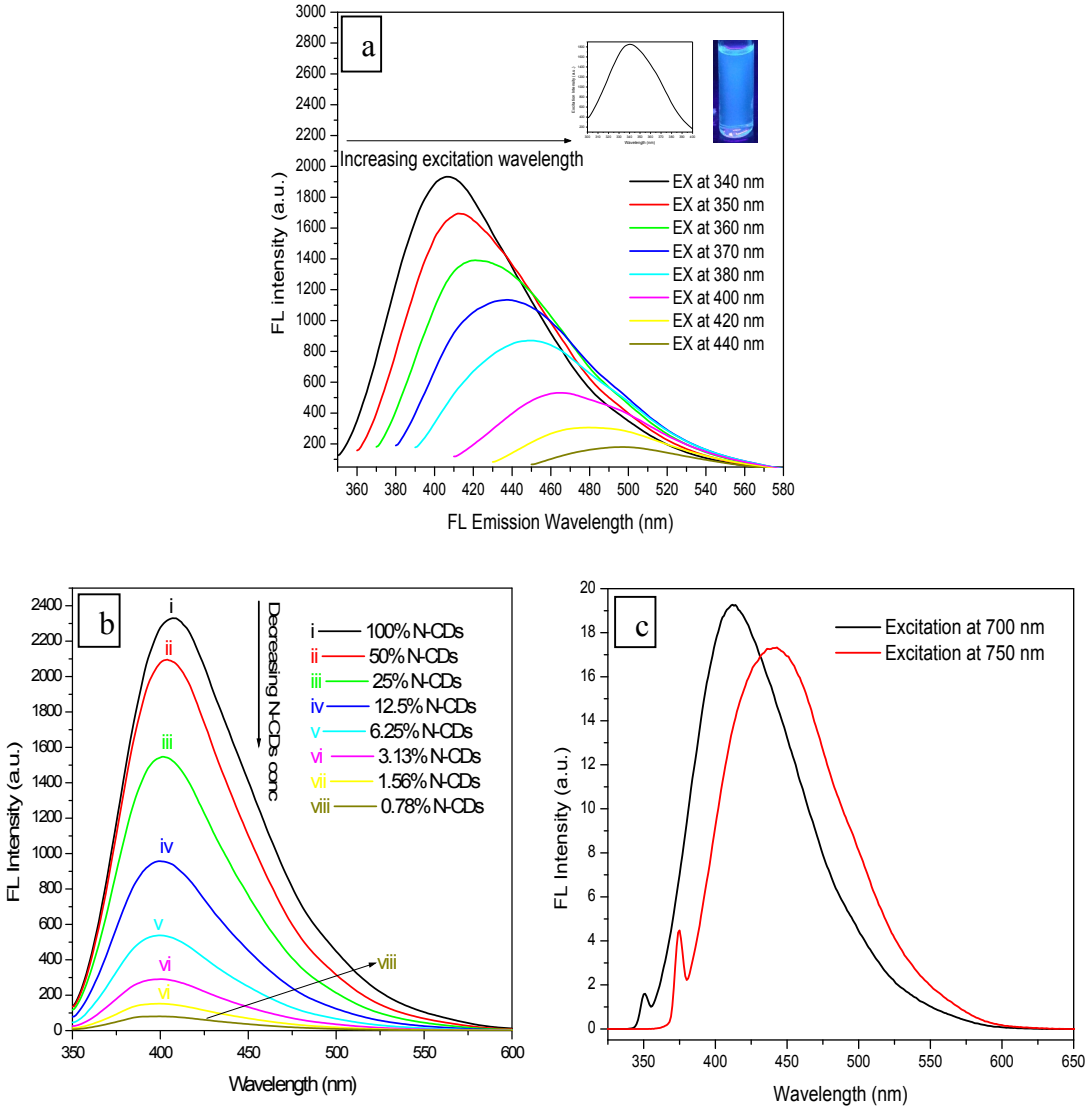

Figure 7.5: (a) FL emission spectra of synthesized N-CDs at various excitation wavelengths. Insets show excitation spectra at 410 nm emission (left side) and colour of the synthesized N-CDs upon UV light irradiation at 365 nm (right side), (b) FL emission intensity of the N-CDs in different volume percentage of water, (c) Up-conversion of FL spectra of the N-CDs

different emissive traps on the N-CDs surface or non-homogeneity in the sizes of the synthesized N-CDs (quantum effect) [20]. It is found that bright blue light is emitted (right side inset of fig.7.5a) when N-CDs are irradiated with UV light (365 nm). **C**hanges in PL emission intensity of the as prepared N-CDs in different volume percentage of water are shown in (fig.7.5b). The figure illustrates that the FL intensity decreases with the increasing volume percentage of water. This decrease of FL intensity of N-CDs is due to dilution effect.

The synthesized N-CDs also demonstrated up-conversion (emission maxima at shorter wavelength compared to the excitation wavelength) of FL emission which is displayed in fig.7.5(c). There are two different types of popular mechanisms for the up-conversion emission of CDs: the multiphoton active mechanism and anti-Stokes photoluminescence mechanism [21]. Considering that the energy difference between the excitation radiation and the emission radiation in the up-conversion process is not a constant value, the multiphoton active process is probably more suitable for explaining up-conversion FL emission of the present N-CDs. It is found that the intensity of up-converted FL spectra are comparatively low than the down-converted spectra.

7.3.3. UV-Vis absorption spectroscopy study:

Fig.7.6 shows the UV-Vis absorption spectra of dilute aq. solutions of synthesized N-CDs at room temperature. It shows a peak at ~ 217 nm and a broad absorption band ~ from 250 nm to 350 nm which can be ascribed to the presence carbonic core centre and it is similar to the earlier reports [10, 12, 22] of UV-Vis spectra of N-CDs.

It may be noted that the excitation wavelength for the highest FL emission intensity in our study (340 nm) is not the same to the maxima wavelength in UV-Vis absorption spectra. This is supported by the previous reports which revealed that excitation wavelength of maximum emission intensity may or may not be the same [23, 13] to the absorption maximum wavelength of UV-Vis absorption spectra of CDs.

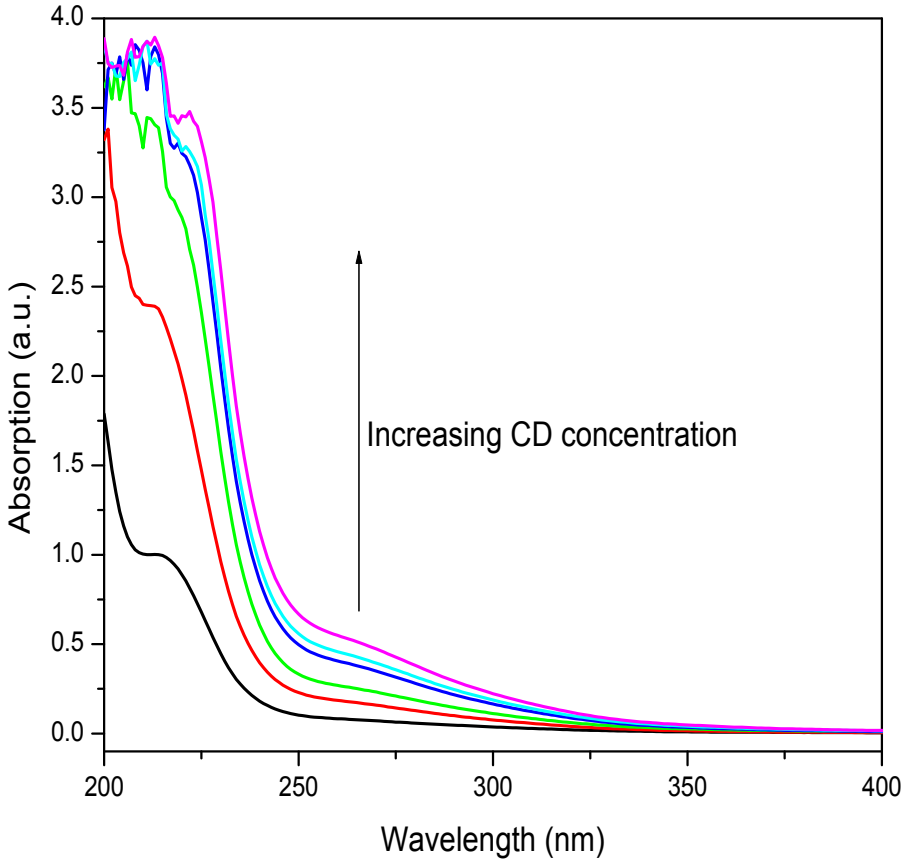

Figure 7.6: UV-Vis absorption spectra of dilute aq. solutions of synthesized N-CDs

7.3.4. Determination of Quantum Yield (QY):

The fluorescence quantum yield (QY) of the synthesized N-CDs was determined by calibrating against quinine sulphate as standard in 0.1 M H_2SO_4. The fluorescence QY of quinine sulphate in 0.1 M H_2SO_4 is 54%. QY was measured according to an established procedure [13] using the following formula:

$$Q = Q_R \times (m/m_R) \times (n/n_R)^2$$

Where Q is the quantum yield, m is the slope of the straight line obtained by plotting integrated fluorescence intensity *vs* absorbance and n is the refractive index of the medium. The subscript R refers to the reference fluorophore, quinine sulphate solution. We have calculated QY at 349 nm excitation wavelength. The values m = 436173 and m_R = 2727660 was obtained from the plot of integrated fluorescence intensity *vs* absorbance (fig.7.7). The quantum yield of N-CDs was

calculated to be 8.63%. Although the QY value is not very high but it is higher than some reported QY values of N-CDs [12].

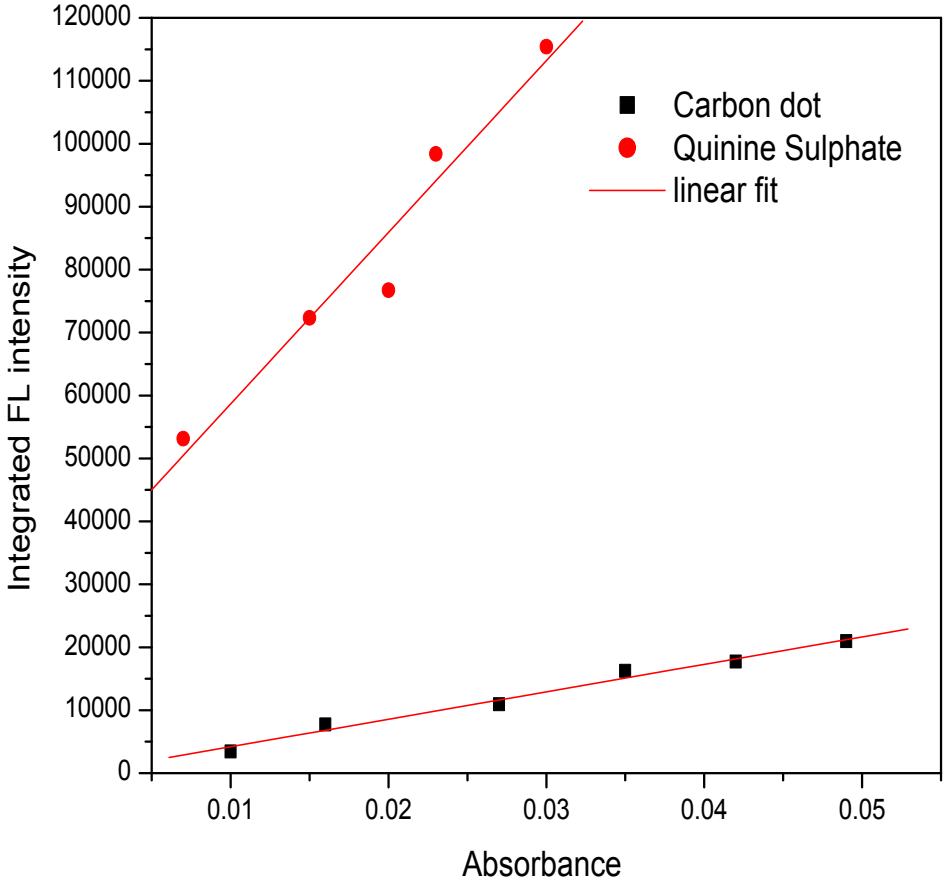

Figure 7.7: Integrated fluorescence intensity *vs* absorbance of N-CDs and Quinine sulphate

7.3.5. FT-IR spectroscopy study:

Fig.7.8 shows the FT-IR spectrum of the synthesized N-CDs. The bands in the region of 3200 - 3500 cm^{-1} can be ascribed to the characteristic absorption bands of O-H and N-H stretching vibration mode. The band at 2873 cm^{-1} is attributed to the C-H stretching vibration which is originated from the $–CH_2$ moieties for PEG-200. The peaks at 1715 cm^{-1} and 1611 cm^{-1} can be assigned to the stretching vibrations of C=O and C=C groups. The bands at 1240 - 1320 cm^{-1} corresponds to the C-O stretching vibration mode. The band at 1030 - 1130 cm^{-1} appears due

to the stretching of C-N vibration. Presence of these functional groups improves the stability and hydrophilcity of the N-CDs in aqueous environment.

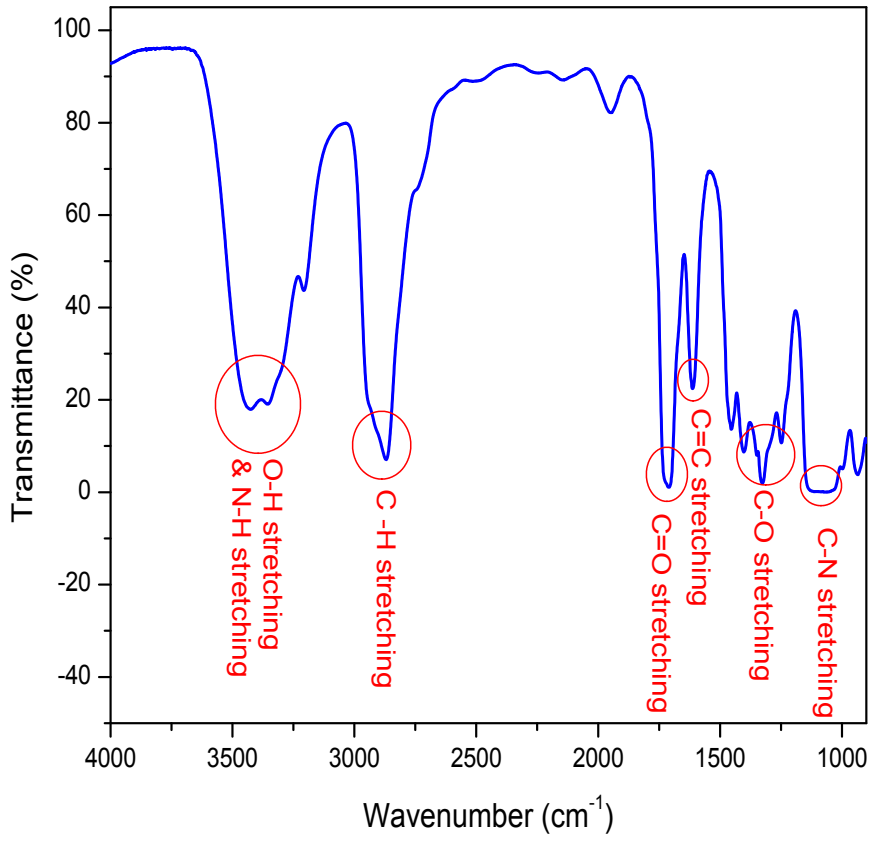

Figure 7.8: FT-IR spectrum of the synthesized N-CDs

7.3.6. Fluorescence detection of Fe^{3+}:

The sensitivity of Fe^{3+} was performed by control experiment at room temperature. 0.5 ml of as prepared N-CDs (sample-b) was added to 1.4 ml distilled water and then 100 µL aq. 10^{-2} (M) various metal salt solution having same anion (chloride) was mixed homogeneously. Concentration of the metal salts in resulting solutions was 500 µM. The FL response of the N-CDs solution containing various metal ions is given in fig.7.9 (a).

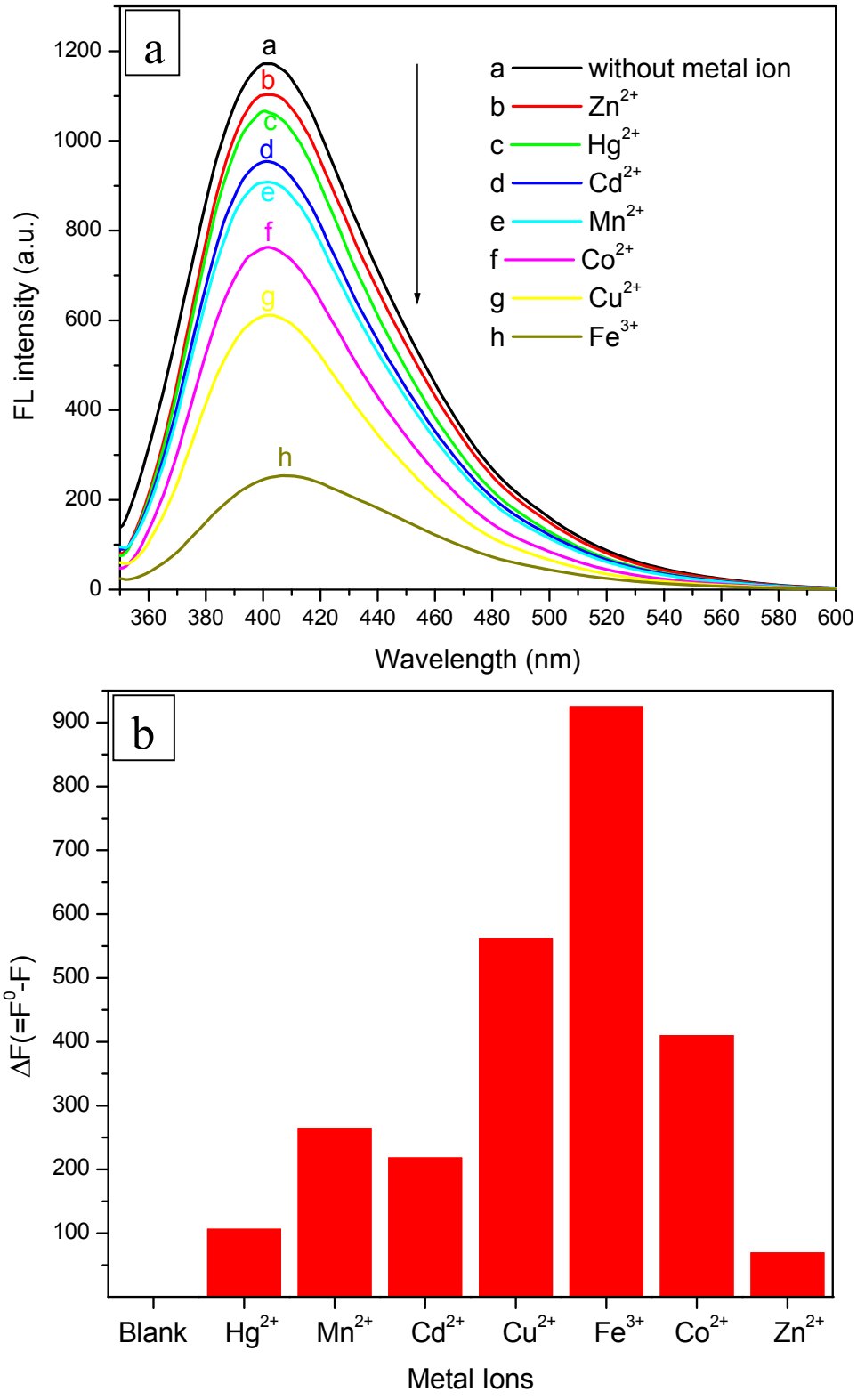

Figure 7.9: (a) FL response of the N-CDs solution containing various metal ions, (b) FL quenching effect ($\Delta F = F^0-F$) of different metal ions where F^0 and F are the FL emission intensity of N-CDs in absence and presence of metal ion respectively.

It is noticeable that only Fe^{3+} induces a substantial decrease in FL intensity which implies that the prepared N-CDs could be used to detect of Fe^{3+} in aq. solution. The sensitivity of N-CDs to Fe^{3+} may be attributed to the fact that the interaction between Fe^{3+} and the N-CDs' surface groups makes N-CDs close to each other, which accelerates the non-radiative recombination of the excitons through an effective electron transfer process, leading to a substantial decrease of the FL intensity of N-CDs.

We used ΔF for FL quenching effect as an indicator for the detection of Fe^{3+} where $\Delta F = F^0 - F$. F^0 and F are the FL emission intensity of N-CDs in absence and presence of metal ion respectively. As demonstrated in fig.7.9(b) the highest FL quenching effect was observed with addition of 500 μM Fe^{3+} while that of other metal ions was comparatively low, except Cu^{2+} and Co^{2+}. Among the added metal ions Fe^{3+} has the highest charge/radius ratio and it makes Fe^{3+} as an efficient electron acceptor to quench PL intensity of N-CDs.

We also examined the quenching kinetics of N-CDs using 500 μM Fe^{3+} by recording the FL emission spectra at different time (fig.7.10).

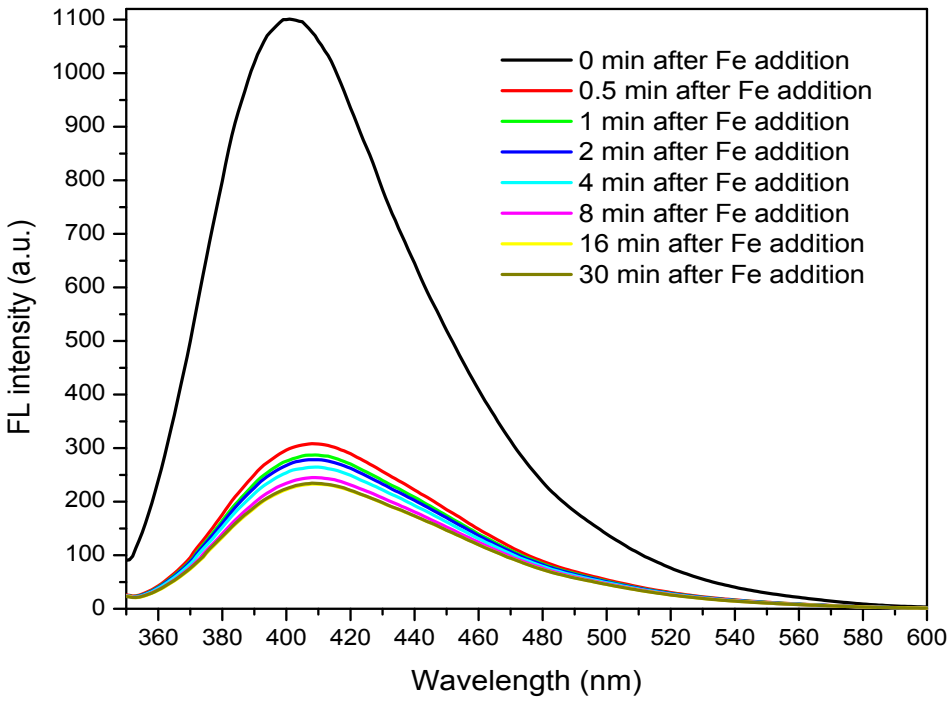

Figure 7.10: FL emission spectra at different time after addition of Fe(III) solution in N-CDs.

It was observed that the FL emission intensity decreased sharply upon the addition of $Fe^{3+,}$ and the fluorescence intensity did not decrease after ~ 16 min, indicating that the quenching kinetics was fairly fast. The results also confirm that Fe^{3+} induced FL quenching of N-CDs can be attributed to the close proximity of N-CDs which is induced by the chelation of Fe^{3+} with the surface groups. This surface binding of Fe^{3+} with N-CDs accelarates the non-radiative recombination of excitons via the charge transfer process and causing to the FL quenching of N-CDs.

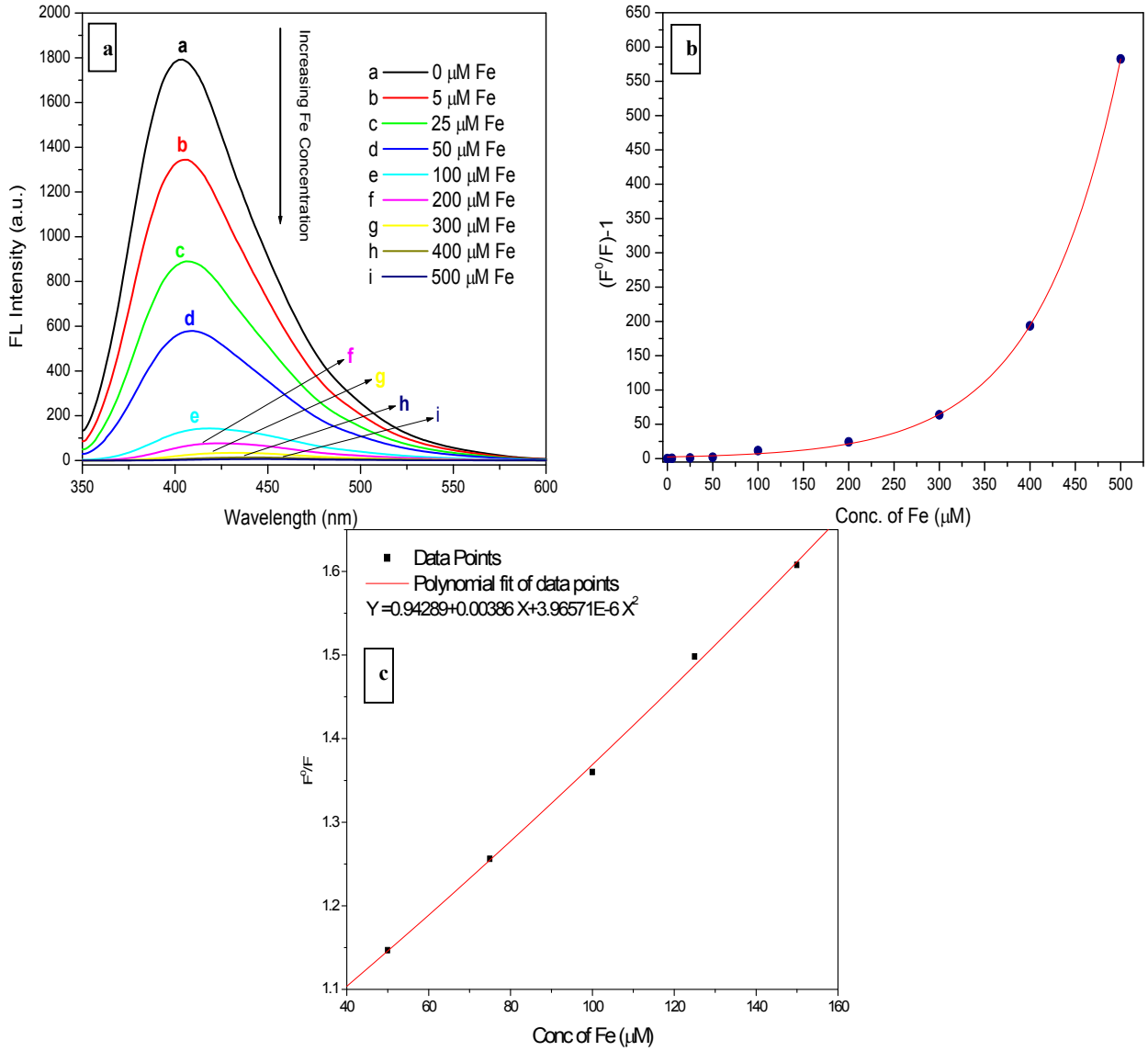

Figure 7.11: (a) FL response of N-CDs with increasing Fe (III) concentration, (b) Stern-Volmer plot, (c) Modified Stern-Volmer plot

The sensitivity of N-CDs to Fe^{3+} was also assessed. It is observed that the quenching of the N-CDs FL emission intensity is a linear function of Fe^{3+} concentration i.e. with the increase in the concentration of Fe^{3+} the FL intensity of N-CDs decreases gradually (fig.7.11a). We also determined detection limit of Fe (III) metal ions using the formulae [24]:

$$\text{detection limit} = 3\sigma/k$$

where σ is the standard deviation of blank measurement, and k is the slope of the calibration curve obtained from linear dynamic plot of fluorescence intensity versus concentration of Fe^{3+}. The calculated detection limit is 7.5 μM.

To get insight into the FL quenching mechanism, the FL quenching data were analyzed using the Stern–Volmer equation. The Stern–Volmer plot shown in fig.7.11 (b) does not fit to the conventional linear Stern–Volmer equation in the whole concentration range, indicating both dynamic and static quenching processes occur in this FL quenching processes. The following modified Stern–Volmer plot should then be used when static and dynamic quenching occurs simultaneously. $F^0/F = 1 + (K_D + K_S)[Q] + K_D K_S [Q]^2$ where K_D and K_S are dynamic and static quenching constant, F^0 and F are FL intensity in absence and presence of quencher, Q. This modified equation was used to fit our experimental data (fig.7.11 c). From the fitted curve it is found that the values of K_D and K_S are 1.93×10^{-3} and 2.05×10^{-3} respectively. Therefore, dynamic and static quenching occurs with almost same proportion.

7.4. Conclusions

We have developed a convenient, fast and low cost microwave irradiation method for the synthesis of fluorescent N-CDs using the aq. solution of PEG-200 and urea. The prepared N-CDs show excellent stability and fluorescence properties. As-synthesized N-CDs show prominent down-conversion and up-conversion fluorescence spectra. This method provides a simple fluorescent turn-off tool for the detection of Fe^{3+} ions. We found that quenching kinetics is fairly

fast. It is also observed that both dynamic and static quenching processes occur in this sensor system and both quenching constants are of comparable values.

References:

[1] X. Zhang, S. Wang, C. Zhu, M. Liu, Y. Ji, L. Feng, L. Tao and Y. Wei, *J. Colloid Interface Sci.,* 397, **2013**, 39-44.

[2] Y. Dong, R. Wang, G. Li, C. Chen, Y. Chi, G. Chen, *Anal. Chem.,* 84, **2012**, 6220

[3] R. Zhang, W. Chen, *Biosens. Bioelectron.,* 55, **2014**, 83

[4] C.-W. Lai, Y.-H. Hsiao, Y.-K. Peng, P.-T. Chou, *J. Mater. Chem.,* 22, **2012**, 14403

[5] Y. Han, H. Huang, H. Zhang, Y. Liu, X. Han, R. Liu, H. Li, Z. Kang, *ACS Catal.,* 4, **2014**, 781

[6] C. Z. Zhu, J. F. Zhai, S. J. Dong, *Chem. Commun.,* 48, **2012**, 9367

[7] F. Wang, Y. Chen, C.Y. Liu, D.G. Ma, *Chem. Commun.,* 47, **2011**, 3502

[8] Y.Q. Zhang, D.K. Ma, Y. Zhuang, X. Zhang, W. Chen, L.L. Hong, Q.X. Yan, K. Yu, S.-M. Huang, *J. Mater. Chem.,* 22, **2012**, 16714

[9] Z. Ma, H. Ming, H. Huang, Y. Liu, Z. Kang, *New J. Chem.,* 36, **2012**, 86

[10] M. Xu, G. He, Z. Li, F. He, F. Gao, Y. Su, L. Zhang, Z. Yang, Y. Zhang, *Nanoscale,* 6**, 2014**, 10307

[11] Y.-Q. Zhang, D.-K. Ma, Y. Zhuang, X. Zhang, W. Chen, L.-L. Hong, Q.-X. Yan, K. Yu, S.-M. Huang, *J. Mater. Chem.,* 22, **2012**, 16714

[12] S. Dey, P. Chithaiah, S. Belawadi, K. Biswas, C.N.R. Rao, *J. Mater. Res.,* 29, **2014**, 383

[13] S. Liu, J. Tian, L. Wang, Y. Zhang, X. Qin, Y. Luo, A.M. Asiri , A.O. Al-Youbi, X. Sun, *Adv. Mater.*, 24, **2012**, 2037

[14] L. Zhou, Y. Lin, Z. Huang, J. Ren, X. Qu, *Chem. Commun.,* 48, **2012**, 1147

[15] Siti Nur Akmar Mohd Yazid, Suk Fun Chin, Suh Cem Pang, Sing Muk Ng, *Microchim Acta,* 180, **2013**, 137

[16] Bruce R. Bacon, Paul C. Adams, Kris V. Kowdley, Lawrie W. Powell, Anthony S. Tavill, *Hepatology*, 54, **2011**, 328

[17] Xinyun Zhai, Peng Zhang, Changjun Liu, Tao Bai, Wenchen Li, Liming Daic, Wenguang Liu, *Chem. Commun.,* 48, **2012**, 7955

[18] D. Sun, R. Ban, P.-H. Zhang, G.-H. Wu, J.-R. Zhang, J. J. Zhu, *Carbon,* 64, **2013**, 424

[19] P.-C. Hsu, Z.-Y. Shih, C.-H. Lee, H.-T. Chang, *Green Chem.,* 14, **2012**, 917

[20] A. Bhattacharya, S. Chatterjee, R. Prajapati, T.K. Mukherjee, *Phys. Chem. Chem. Phys.,* 17, **2015**, 12833

[21] J.H. Shen, Y.H. Zhu, C. Chen, X.L. Yang, C.Z. Li, *Chem. Commun.,* 47, **2011**, 2580

[22] C. Wang, X. Wu, X. Li, W. Wang, L. Wang, M. Gu, Q. Li, *Mater. Chem.,* 22, **2012**, 15522

[23] Y. Guo, Z. Wang, H. Shao, X. Jiang, *Carbon,* 52, **2013**, 583

[24] L. Wang, W. Qin, X. Tang, W. Dou, W. Liu, Q. Teng, X. Yao, *Org. Biomol. Chem.* 8, **2010**, 3751

LIST OF PUBLICATIONS

*[1] Microwave-assisted synthesis of fluorescent N-doped carbon nanodots and its potential use as sensor for Fe (III) ions, **Sadhan Samanta**, Ajay Misra, **Sensors and Actuators B (Communicated)**

[2] Highly Selective Turn-On Fluorogenic Chemosensor for Robust Quantification of Zn(II) Based on Aggregation Induced Emission Enhancement Feature, Milan Shyamal, Prativa Mazumdar, Samir Maity, **Sadhan Samanta**, Gobinda P. Sahoo, Ajay Misra, **ACS Sensors 1 (2016) 739−747**

[3] Morphology directing synthesis of 1-aminopyrene microstructures and its super quenching effect towards nitro aromatics, Ashim Maity, Prativa Majumdar, **Sadhan Samanta**, Debasish Das, Milan Shyamal, Gobinda P. Sahoo, Ajay Misra, **Journal of Molecular Liquids 221(2016) 358-367**

*[4] Hydrothermal synthesis of hexagonal ZnO microstructures in HPMC polymer matrix and their catalytic activities, Gobinda Prasad Sahoo, **Sadhan Samanta**, Dipak Kumar Bhui, Santanu Pyne, Ashim Maity, Ajay Misra, **Journal of Molecular Liquids 212 (2015) 665–670**

[5] Microwave-assisted synthesis of anisotropic gold nanocrystals in polymer matrix and their catalytic activities, Gobinda Prasad Sahoo, Samita Basu, **Sadhan Samanta** and Ajay Misra, **Journal of Experimental Nanoscience, 10 (2015) 690-702**

[6] Photochemical synthesis of Ag nanobars and their potential application as catalyst, Santanu Pyne, **Sadhan Samanta,** Ajay Misra, **Solid State Sciences 26 (2013) 1-8**

*[7] Synthesis of silver nanodiscs and triangular nanoplates in PVP matrix: Photophysical study and simulation of UV–vis extinction spectra using DDA method, **Sadhan Samanta,** Priyanka

Sarkar, Santanu Pyne, Gobinda Prasad Sahoo, Ajay Misra, **Journal of Molecular Liquids 165 (2012) 21–26**

[8] Enhanced photocatalytic activity of metal coated ZnO nanowires, Santanu Pyne, Gobinda Prasad Sahoo, Dipak Kumar Bhui, Harekrishna Bar, Priyanka Sarkar, **Sadhan Samanta,** Ashim Maity, Ajay Misra, **Spectrochimica Acta Part A 93 (2012) 100– 105**

[9] Synthesis and photo physical properties of star shaped gold nanoparticles, Gobinda Prasad Sahoo, Harekrishna Bar, Dipak Kumar Bhui, Priyanka Sarkar, **Sadhan Samanta**, Santanu Pyne, Sankarlal Ash, Ajay Misra, **Colloids and Surfaces A: Physicochem. Eng. Aspects 375 (2011) 30–34**

[10] Solution-phase synthesis of silver nanodiscs in HPMC-matrix and simulation of UV–vis extinction spectra using DDA based method, Priyanka Sarkar, Santanu Pyne, Gobinda P. Sahoo, Dipak K. Bhui, Harekrishna Bar, **Sadhan Samanta,** Ajay Misra, **Spectrochimica Acta Part A 82 (2011) 368– 374**

[11] DDA-Based Simulation of UV–vis Extinction Spectra of A, Nanorods Synthesized Through Seed-Mediated Growth Process, Priyanka Sarkar, Dipak K. Bhui, Harekrishna Bar, Gobinda P. Sahoo, **Sadhan Samanta,** Santanu Pyne, Ajay Misra, Plasmonics **6 (2011) 43–51**

*[12] Synthesis of silver nanostructures of varying morphologies through seed mediated growth approach, **Sadhan Samanta,** Santanu Pyne, Priyanka Sarkar, Gobinda P. Sahoo, Harekrishna Bar, Dipak Kr. Bhui, Ajay Misra, **Journal of Molecular Liquids 153 (2010) 170–173**

[13] Synthesis and characterization of gold nanoparticles adsorbed in methyl cellulose micro fibrils, Gobinda Prasad Sahoo, Dipak Kumar Bhui, Harekrishna Bar, Priyanka Sarkar, **Sadhan Samanta,** Santanu Pyne, Ajay Misra, **Journal of Molecular Liquids 155 (2010) 91–95**

[14] Aqueous-Phase Synthesis of Silver Nanodiscs and Nanorods in Methyl Cellulose Matrix: Photophysical Study and Simulation of UV–Vis Extinction Spectra Using DDA Method, Priyanka Sarkar, Dipak Kumar Bhui, Harekrishna Bar, Gobinda Prasad Sahoo, **Sadhan Samanta,** Santanu Pyne, Ajay Misra, **Nanoscale Res Lett. 5 (2010) 1611–1618**

* Marked are included in this thesis